

MINISTÉRIO DA EDUCAÇÃO
UNIVERSIDADE FEDERAL DO RIO GRANDE DO SUL
PROGRAMA DE PÓS-GRADUAÇÃO EM ENGENHARIA MECÂNICA

IMPROVED CORRELATIONS FOR PREDICTING HOT GAS LAYER
TEMPERATURE IN A PRE-FLASHOVER COMPARTMENT FIRE CONSIDERING
HEAT SOURCE LOCATION

por

Calisa Katiuscia Lemmertz

Dissertação para obtenção do Título de
Mestre em Engenharia

Porto Alegre, Março de 2019.

IMPROVED CORRELATIONS FOR PREDICTING HOT GAS LAYER
TEMPERATURE IN A PRE-FLASHOVER COMPARTMENT FIRE CONSIDERING
HEAT SOURCE LOCATION

por

Calisa Katuscia Lemmertz
Bacharel em Engenharia Mecânica

Dissertação submetida ao Programa de Pós-Graduação em Engenharia Mecânica, da Escola de Engenharia da Universidade Federal do Rio Grande do Sul, como parte dos requisitos necessários para obtenção do Título de

Mestre em Engenharia

Área de Concentração: Energia

Orientador: Prof. Dr. Felipe Roman Centeno

Aprovada por:

Prof. Dr. Alexandre Landesmann, COPPE/UFRJ

Prof. Dr. Guilherme Henrique Fiorot, DEMEC/UFRGS

Prof. Dr. Luiz Alberto Oliveira Rocha, PROMEC/UFRGS

Prof. Dr. Fernando Marcelo Pereira
Coordenador do PROMEC

Porto Alegre, 25 de Março de 2019.

ACKNOWLEDGEMENTS

I would like to express my deep gratitude to my advisor, Professor Felipe Roman Centeno, not only for his guidance, but also for his friendship and inspiration.

I would also like to thank my partner in life, Cristiano da Luz Fabricio, by his support, comprehension and love along these past ten years.

I wish to thank my colleagues and friends from the Federal University of Rio Grande do Sul, Specially my friends Roger Mazurek da Silva and Larissa Domingues Lemos, for being always there helping and supporting me.

Last but not least, I wish to thank my parents for their support and encouragement throughout my education.

This research has been developed with assistance of the National Center for Supercomputing (CESUP), of the Federal University of Rio Grande do Sul (UFRGS).

This study was financed in part by the Coordenação de Aperfeiçoamento de Pessoal de Nível Superior - Brasil (CAPES) - Finance Code 001.

RESUMO

Este estudo tem como objetivo analisar a influência da localização da fonte de calor (fogo) na temperatura da camada de gases quentes (HGL) em incêndios pré-flashover em compartimentos, e baseado nestes resultados desenvolver correlações melhoradas para prever esta temperatura, considerando a localização (transversa, longitudinal e vertical) em que se encontra o fogo. Os dados para esta análise e desenvolvimento das correlações foram obtidos através de um código CFD chamado Fire Dynamics Simulator (FDS). Uma análise de malha foi realizada para assegurar a qualidade dos resultados, e o modelo numérico foi validado comparando os resultados obtidos aos dados experimentais descritos por Steckler et al., 1982a, 1982b, 1984a, 1984b, apresentando boa concordância. Este estudo foi baseado em 294 simulações, reproduzindo a mesma geometria estudada no experimento de Steckler. Primeiramente, 15 posições de fogo no nível do piso foram testadas para determinar sua influência nos resultados de temperatura. Foi observado que as posições transversal e longitudinal (eixos x e y) não afetam consideravelmente os resultados, exceto quando o fogo encontra-se próximo a uma parede ou canto. Em uma segunda análise, a influência da elevação do fogo foi testada, e demonstrou um importante efeito sobre os resultados. À medida que a fonte de calor era elevada, a temperatura da camada de gases quentes e a máxima temperatura no interior da sala aumentavam, assim como a altura de interface da camada de gases quentes. Portanto, foi possível concluir que a posição do fogo, especialmente sua elevação, é um importante parâmetro a ser considerado na análise de incêndios pré-flashover no interior de compartimentos. Uma breve análise da influência da proximidade do fogo junto às paredes e cantos também foi realizada. A partir dos dados gerados, e baseando-se em um balanço de energia na HGL, seis novas correlações para prever a temperatura da camada de gases quentes em incêndios pré-flashover em compartimentos foram desenvolvidas. Três delas para incêndios no nível do piso (longe de paredes, próximo às paredes e próximo aos cantos) e outras três semelhantes para incêndios em posições elevadas. Os resultados obtidos através de todas as correlações foram comparados aos dados numéricos e a diferentes conjuntos de dados experimentais disponíveis na literatura, apresentando uma boa concordância. Portanto, pode-se concluir que estas correlações melhoradas são capazes de prever a temperatura da camada de gases quentes para diferentes cenários de incêndio pré-flashover, considerando o local onde o fogo se inicia.

Palavras-chave: Incêndios pré-flashover; Incêndios em compartimentos; Posição da fonte de calor; Temperatura da camada de gases quentes; FDS.

ABSTRACT

This study aims to analyze the influence of the fire heat source location on the hot gas layer (HGL) temperature in pre-flashover compartment fires, and based on the findings develop improved correlations to predict the HGL temperature considering the fire source location (transversal, longitudinal and vertical). The data for the analysis and correlations were obtained through a CFD code called Fire Dynamic Simulator (FDS). A mesh resolution analysis was performed to ensure the quality of numerical results, and the numerical model was validated comparing the obtained results to experimental data described by Steckler et al., 1982a, 1982b, 1984a, 1984b, showing a good agreement. The present study was based on 294 simulations reproducing the room geometry applied on Steckler's experiment. Firstly, 15 fire heat source positions at the ground level were tested to determine their influence on the temperature results. It was found that the transversal and longitudinal fire positions (x and y axes) do not affect considerably the results, except when the fire is placed near a wall or corner. In a second analysis the fire source elevation influence was tested, and showed an important effect on the results. As the fire source was elevated from the ground, the hot gas layer and the maximum temperatures augmented, as well as the interface layer height. So, it was concluded that the fire source location, primarily its elevation, is an important parameter to be considered during the pre-flashover compartment fire analysis. A brief wall and corner vicinity influence was also assessed. With all the numerical data generated, and based on an energy balance on the upper layer, six new correlations were developed to predict the HGL temperature in pre-flashover compartment fires. Three correlations were fit for fires at the ground level (away from walls, near a wall and near a corner), and other three for fires in elevated positions (for those same wall-vicinity positions). The results obtained for all correlations were compared to the numerical data and several sets of experimental data available on literature, showing a good agreement. So, we can conclude that these improved correlations are able to predict the HGL temperature for different pre-flashover fire scenarios, considering the place where the fire started.

Keywords: Pre-flashover fires; Compartment fires; Heat source location; Upper layer temperature; FDS.

INDEX

1	INTRODUCTION	1
1.1	Research Justification	2
1.2	Objectives	2
1.2.1	Main Objective	2
1.2.2	Specific Objectives	2
1.3	Work Contributions	3
1.4	Work Structure.....	3
2	LITERATURE REVIEW	5
3	THEORETICAL BACKGROUND	15
3.1	Natural Turbulent Diffusion Flames.....	15
3.2	Compartment Fires and Hot Gas Layer Formation	16
3.3	Compartment Fire Stages	19
3.4	Compartment Fire Model (Two-zone Model)	20
3.5	Conservation Equations in Compartment Fires	23
3.6	The MQH Method	25
4	FIRE DYNAMICS SIMULATOR MATHEMATICAL MODEL.....	28
4.1	Numerical Grid	29
4.2	Fundamental Equations	29
4.3	Simplifying Assumptions	30
4.4	Combustion Model	32
4.5	Radiation Model	32
4.6	Large Eddy Simulation Model (LES).....	34
4.6.1	Deardorff Model	34
4.7	Time Step and Solution Procedure	35
5	METHODOLOGY	36
5.1	Steckler’s Experiment.....	36
5.2	FDS Simulations	38
5.2.1	Initial and Boundary Conditions.....	40
5.3	Mesh Resolution	41
5.4	Comparison with Experimental Data.....	44
5.5	Data Correlation.....	49

6	RESULTS AND DISCUSSIONS.....	51
6.1	Fire Source Position Influence (ground level).....	51
6.2	The Heat Release Rate Influence.....	54
6.3	Ventilation Factor Influence.....	55
6.4	Fire Source Position Influence (vertical position).....	56
6.5	Wall and Corner Vicinity Influence.....	62
6.6	Correlations to Predict Upper Layer Temperature at the Ground Level.....	68
6.7	Correction Term for Elevated Fire Sources.....	72
6.8	Comparison Between Experimental Data and Correlation Predictions.....	76
6.8.1	Comparison of the Results.....	76
7	CONCLUSIONS.....	81
7.1	Future Works.....	82
	REFERENCES.....	83

LIST OF FIGURES

Figure 3.1	Height of jet flames as a function of nozzle velocity, showing transition to turbulence [Hottel and Hawthorne, 1949]	15
Figure 3.2	(a) Plume-ceiling interaction, (b) Ceiling jet-wall interaction and (c) Hot gas layer formation and growth [adapted from Cooper, 2002].....	18
Figure 3.3	Compartment fire stages [adapted from Drysdale, 2011]	20
Figure 3.4	Two layer zone modelling (adapted from Quintiere, 2002).....	22
Figure 5.1	Room geometry and thermocouple tree position	36
Figure 5.2	Room opening configurations	37
Figure 5.3	Fifteen studied fire source ground positions	38
Figure 5.4	Fire source elevations.....	39
Figure 5.5	Comparison of the mesh sizes ($\delta x = 6$ cm, 5 cm, 4 cm and 3 cm) tested during the mesh resolution analysis.....	42
Figure 5.6	Mesh sensitivity analysis (Steckler's case 14)	43
Figure 5.7	Temperature profiles for fire source at the center of the room (position A).....	46
Figure 5.8	Temperature profiles for fire source at the corner of the room (position B).....	47
Figure 5.9	Temperature profiles for fire source at the back wall of the room (position C)	48
Figure 6.1	Average upper layer temperature in each fire source position on the ground level	52
Figure 6.2	Heat Release Rate influence on the upper layer temperature	55
Figure 6.3	Ventilation factor influence on the upper layer temperature	56
Figure 6.4	Relation between fire source elevation and upper layer temperature for fires away from walls (ground position A)	57
Figure 6.5	Relation between fire source elevation and upper layer temperature for fires near corner (ground position B)	58
Figure 6.6	Relation between fire source elevation and upper layer temperature for fires along walls (ground position C)	59
Figure 6.7	Reduction on the air entrainment area when the fire source is elevated (a) $z=0$ m (b) $z=0.6$ m (c) $z=1.2$ m.....	60
Figure 6.8	Temperature profiles for different fire source elevation in ground position A (center).....	61

Figure 6.9 Temperature profiles for different fire source elevation in ground position B (corner).....	61
Figure 6.10 Temperature profiles for different fire source elevation in ground position C (wall).....	62
Figure 6.11 Wall vicinity influence on HGL temperature analysis scheme.....	62
Figure 6.12 Corner vicinity influence on HGL temperature moving along the backwall analysis scheme.	63
Figure 6.13 Corner vicinity influence on HGL temperature moving away from both walls analysis scheme.	63
Figure 6.14 Influence of the wall vicinity in the upper layer temperature.	64
Figure 6.15 Lateral view of flame and backwall interaction (a) $\Delta x = 0cm$ (b) $\Delta x = 20cm$ (c) $\Delta x = 40cm$ and (d) $\Delta x = 60cm$	64
Figure 6.16 Influence of the corner vicinity moving the fire source along the back wall.....	65
Figure 6.17 Front view of flame and sidewall interaction (a) $\Delta y = 0cm$ (b) $\Delta y = 20cm$ (c) $\Delta y = 40cm$ and (d) $\Delta y = 60cm$	65
Figure 6.18 Influence of the corner vicinity moving the fire source diagonally to the center of the room.....	66
Figure 6.19 Flame and walls interaction (a) front view $\Delta x = \Delta y = 0cm$ (b) (a) lateral view $\Delta x = \Delta y = 0cm$ (c) front view $\Delta x = \Delta y = 20cm$ (d) lateral view $\Delta x = \Delta y = 20cm$ (e) front view $\Delta x = \Delta y = 40cm$ (f) lateral view $\Delta x = \Delta y = 40cm$ (g) front view $\Delta x = \Delta y = 70cm$ and (h) lateral view $\Delta x = \Delta y = 70cm$	67
Figure 6.20 Dimensionless temperatures as a function of the dimensionless groups (X1 and X2) showing a power relation	69
Figure 6.21 Dimensionless temperature logarithm as a function of the dimensionless groups logarithm showing a linear behaviour (linearized data applied to the multiple linear regression)	69
Figure 6.22 Comparison between predicted upper layer temperature and numerical data for fire sources away from walls.	70
Figure 6.23 Comparison between predicted upper layer temperature and numerical data for fire sources along walls	71
Figure 6.24 Comparison between predicted upper layer temperature and numerical data for fire sources near corners	72

Figure 6.25 Fitting of the correction term for elevated fire sources away from walls (center).	73
Figure 6.26 Fitting of the correction term for elevated fire sources near a wall.	73
Figure 6.27 Fitting of the correction term for elevated fire sources near a corner.	73
Figure 6.28 Comparison between predicted upper layer temperature and numerical data for elevated fire sources away from walls.	74
Figure 6.29 Comparison between predicted upper layer temperature and numerical data for elevated fire sources near a wall.	75
Figure 6.30 Comparison between predicted upper layer temperature and numerical data for elevated fire sources near a corner.	75
Figure 6.31 Comparison between upper layer temperature for fire away from walls at the ground level predicted by Equation 6.13 and experimental data	77
Figure 6.32 Comparison between upper layer temperature for fire along walls or near obstructions at the ground level predicted by Equation 6.14 and experimental data	78
Figure 6.33 Comparison between upper layer temperature for fire near corners at the ground level predicted by Equation 6.15 and experimental data	78
Figure 6.34 Comparison between upper layer temperature for fires away from walls or obstructions and above the ground level ($z > 0$) predicted by Equation 6.18 and experimental data	79
Figure 6.35 Comparison between upper layer temperature for fires along walls or obstructions and above the ground level ($z > 0$) predicted by Equation 6.19 and experimental data	80
Figure 6.36 Comparison between upper layer temperature for fires near corners and above the ground level ($z > 0$) predicted by Equation 6.20 and experimental data	80

LIST OF TABLES

Table 5.1	Compartment wall and ceiling properties.....	37
Table 5.2	List of openings and HRRs employed in the simulations	39
Table 5.3	Values of D^* and $D^*/\delta x$ for meshes 6 cm, 5 cm, 4 cm and 3 cm	42
Table 5.4	Mesh sensitivity analysis and computational time	43
Table 5.5	MTR for mesh $\delta x = 5$ cm	44
Table 5.6	Comparison between numerical (FDS, present study) and experimental (Steckler's) results.....	45
Table 6.1	Upper layer temperature as a function of the vertical position (ground position A)	57
Table 6.2	Upper layer temperature as a function of the vertical position (ground position B)	58
Table 6.3	Upper layer temperature as a function of the vertical position (ground position C)	59
Table 6.4	Experimental data sets compared to correlation results	76

LIST OF ABBREVIATIONS AND ACRONYMS

ASTM	American Society for Testing and Materials
CAPES	Coordenação de Aperfeiçoamento de Pessoal de Nível Superior
CESUP	National Center for Supercomputing
CFAST	Consolidated Fire and Smoke Transport
CFD	Computational Fluid Dynamics
CFL	Courant-Friedrichs-Lewy Criterion
CPU	Central Processing Unit
CV1	Control Volume 1
CV2	Control Volume 2
EDC	Eddy Dissipation Concept
EF	Entrainment Factor
FDS	Fire Dynamics Simulator
FVM	Finite Volume Method
HGL	Hot Gas Layer
HRR	Heat Release Rate
LES	Large-Eddy Simulation
MPI	Message Passing Interface
MQH	McCaffrey, Quintiere and Harkleroad correlation
MTR	Measure of Turbulence Resolution
NIST	National Institute of Standards and Technology
RadCal	Narrow-band model for radiation calculations in a combustion environment
RANS	Reynolds Averaged Navier-Stokes
RTE	Radiation Transfer Equation
SGS	Subgrid-Scale
SPSS	Statistical Package for the Social Sciences
U.S.	United States of America
VTT	Technical Research Centre of Finland

LIST OF SYMBOLS

Latin Letters

A	Area, m ²
A_o	Opening area, m ²
$A_o\sqrt{H_o}$	Ventilation factor
A_T	Total area of the compartment surface, m ²
B	Emission source term
c	Specific heat of the compartment wall, J/kgK
C_d	Orifice constriction coefficient
C_p	Specific heat of gas, J/kgK
C_V	Deardorff model constant
D	Characteristic diameter (usually the diameter of the fuel bed), m
D^*	Characteristic fire diameter, m
D_α	Diffusion coefficient of species α
e	Specific internal energy, J/kg
f_b	Drag force exerted by subgrid scale particles and droplets, N
F_n	View factor
Fr	Froude number
g	Gravity acceleration, m/s ²
h	Specific enthalpy, J/kg
h_k	Effective heat transfer coefficient, W/(m ² K)
h_s	Specific Sensible enthalpy, J/kg
H	Compartment height, m
H	Height of the computational domain, m
H_o	Opening height, m
I	Total radiation intensity, W/(m ² .sr)
I_b	Blackbody radiation intensity, W/(m ² .sr)
$I_{b,n}$	Fraction of blackbody radiation, W/(m ² .sr)
I_n	Radiation intensity integrated all over the band n, W/(m ² .sr)

I_λ	Radiation intensity at wavelength λ . W/(m ² μm.sr)
k	Thermal conductivity of the wall material, W/mK
k_{SGS}	Subgrid kinetic energy, m ² /s ²
L	Compartment length, m
\dot{m}_a	Mass flow rate of air into the opening, kg/s
\dot{m}_f	Mass burning rate of the fuel, kg/s
\dot{m}'''_F	Mean chemical source term for fuel, (kg/s)/m ³
\dot{m}_g	Mass flow rate of gases out the opening, kg/s
\dot{m}_p	Rate of air entrainment into the plume, kg/s
\dot{m}'''_b	Mass source term, (kg/s)/m ³
$\dot{m}'''_{b,\alpha}$	mass production rate per unit volume of species α by evaporating droplets/particles, (kg/s)/m ³
\dot{m}'''_α	Mass production rate per unit volume of species α by chemical reactions, (kg/s)/m ³
M_a	Mach number
p	Pressure, Pa
\bar{p}	Background pressure, Pa
\tilde{p}	perturbation
p_∞	Ambient pressure, Pa
\dot{q}'''	Heat release rate per unit volume, W/m ³
\dot{q}''	Conductive, diffusive and radiative heat fluxes, W/m ²
\dot{q}'''_b	Energy transferred to subgrid-scale droplets and particles, W/m ³
\dot{q}'''_r	Radiative heat flux, W/m ²
\dot{Q}	Heat release rate, W
\dot{Q}_L	Heat loss due to convection through openings, W
\dot{Q}_w	Heat loss due to conduction through boundaries, W
R	Universal gas constant, J/(molK)
s	Direction vector of the intensity
s	Stoichiometric coefficient for air
Sc_t	Schmidt number
t	Time of exposure, s

t_p	Thermal penetration time, s
T	Temperature, K
T_L	Lower layer temperature, K
T_U	Upper layer temperature or hot gas layer temperature, K
T_∞	Ambient temperature, K
\mathbf{u}	Velocity vector $u = (u, v, w)$
$\bar{u}, \bar{v}, \bar{w}$	Filtered velocity components at length scale Δ
$\tilde{u}, \tilde{v}, \tilde{w}$	Resolved LES velocity components
$\tilde{\tilde{u}}, \tilde{\tilde{v}}, \tilde{\tilde{w}}$	Weighted average of velocity components over the adjacent cell
U	Velocity of the gas, m/s
V_C	Cell volume, m ³
\bar{W}	Molecular weight of the gas mixture
w_α	Molecular weight of the primitive species α
W	Compartment width, m
W_o	Opening width, m
x, y, z	Cartesian coordinates
x^*	Dimensionless length
X_1	Dimensionless group representing the ratio of energy released to the energy convected
X_2	Dimensionless group representing the energy loss divided by the energy convected
y^*	Dimensionless width
Y_i	Species mass fraction
z	Height of the fire source, m
z^*	Dimensionless height
Z_{int}	Interface layer height, m
Z_A	Mass fraction of air
Z_F	Mass fraction of fuel
Z_N	Height of the neutral plane, m
Z_α	Species α mixture

Greek letters

δ	Thickness of the compartment wall, m
δ_t	Time step, s
$\delta_x, \delta_y, \delta_z$	Dimensions of the mesh cell, m
Δh_c	Heat of combustion of the fuel vapor, J/kg
ΔT	Upper layer temperature rise, K
ΔT_p	Excess temperature over ambient in the plume, K
Δx	Distance between the backwall and the pool fire tangent, m
Δy	Distance between the sidewall and the pool fire tangent, m
κ	Local absorption coefficient, m^{-1}
κ_n	Mean absorption coefficient for band n, m^{-1}
μ	Dynamic viscosity, Pa.s
μ_t	Turbulent viscosity
∇	Nabla operator
ρ	Density, kg/m^3
ρ_f	Fuel density, kg/m^3
ρ_w	Compartment wall material density, kg/m^3
ρ_0	Background density, kg/m^3
ρ_∞	Ambient air density, kg/m^3
σ	Stefan-Boltzmann constant
$\bar{\tau}$	Viscous stress tensor
τ_{ij}^{SGS}	Subgrid scale stress
τ_{min}	Time scale for mixing, s

1 INTRODUCTION

To adequately design and manage fire safety systems, it is necessary to properly understand fire dynamics and the conditions resulting from a compartment fire.

Compartment fires are extremely complex phenomena. A compartment fire depends mainly on the compartment geometry (walls, ceiling and floor dimensions), the ventilation (doors and windows) and the fuel (type, amount, surface area and position).

In a pre-flashover compartment fire, hazardous gases and heat are accumulated in the upper portion of the room, which is then denominated as hot gas layer (HGL), and its composition influences on visibility and hazards for occupants. Therefore, the HGL interface height and temperature are considered the most important parameters in pre-flashover fire safety [Johansson, 2016].

The hot gas layer temperature in a pre-flashover compartment fire is related to the occurrence of hazardous conditions for people, to the fire spread to combustible items far from the fire source and to the occurrence of flashover (when the entire room is involved by the fire) [Dusso et al., 2016]. The HGL temperature is considered the main indicator to assess the hazardous conditions to people, property and structural damage [Karlsson and Quintiere, 2000].

According to Karlsson and Quintiere, 2000, the rapid progress in the understanding of fire processes and their interaction with buildings has resulted in the development of a wide variety of models that are used to simulate fires in compartments, among them the computational fluid dynamics (CFD) models, also known as Field models, the zone models and the hand-calculation models.

Computational Fluid Dynamics (CFD), particularly Large Eddy Simulation (LES) codes, provide an efficient tool to predict large-scale effects, such as plume characteristics, combustion product dispersion, and heat effects to adjacent objects [Ryder et al., 2004]. These CFD models solve the Navier–Stokes equations and the fundamental conservation equations.

Although CFD methods are considered very efficient, the hand-calculation methods are still widely applied, since they are time-efficient compared to numerical simulations and in general can provide a rough, but useful first estimative of the result.

Both, HGL temperature and interface height can be assessed through analytical equations (hand-calculation methods) or computational models (zone models or CFD).

The McCaffrey, Quintiere and Harkleroad correlation (known as MQH correlation) is considered the most established hand-calculation method to predict hot gas layer temperatures

in pre-flashover compartment fires. However, this correlation was designed for fires positioned at the center of the room and on the ground level. Nowadays, several other hand-calculation methods are available to predict fire safety parameters, but none of them takes into account the fire source location to determine the hot gas layer temperature.

1.1 Research Justification

The main justification for choosing this topic was the necessity of improvement on the hand-calculation methods applied to obtain pre-flashover compartment fire parameters, to allow the fire safety engineers to obtain rapidly, more reliable data to design fire safety systems.

The pre-flashover stage was chosen once the concern of this work is the safety of the enclosure occupants. During the pre-flashover stage the fire can still be controlled, applying suppression methods, and it is during this stage that the enclosure must be evacuated. After the flashover the room is completely on fire and the concern changes for firefighters safety and structural safety, once the fire can no longer be easily controlled and the structure can collapse.

Knowing the HGL temperature helps engineers to predict the onset of flashover and to design fire suppression and smoke detection/extraction systems, which give occupants more time to leave the fire compartment, saving lives.

1.2 Objectives

1.2.1 Main Objective

This research has the main goal of developing easy-to-apply correlations to predict the average hot gas layer temperature in a pre-flashover compartment fire, taking into account the fire source location.

1.2.2 Specific Objectives

This work has the following specific goals:

- a) Considering the experimental data reported by Steckler et al., 1982a, 1982b, and, Steckler et al., 1984a, 1984b, concerning compartment fires, implement on a CFD software (Fire Dynamics Simulator - FDS) 40 fire scenarios (see Table 5.6) in order to validate the numerical code towards a reliable/accurate prediction of upper layer temperature in a compartment fire;
- b) Run 195 compartment fire simulations, combining four different heat release rates, 10 ventilation factor and 15 ground positions, to generate numerical data of the hot gas layer temperature in pre-flashover compartment fires;
- c) Analyse the obtained data to determine the influence of the fire source location on the ground level (longitudinal, transversal) on the hot gas layer temperature;
- d) Select some relevant ground positions to run new simulations considering the fire source at different vertical locations, allowing to analyse the influence of the vertical fire source location on the upper layer temperature;
- e) Develop easy-to-apply correlations to predict the average hot gas layer temperature in a pre-flashover compartment fire taking into account the heat source location;
- f) Verify these new correlations comparing to different experimental data from literature.

1.3 Work Contributions

Six new and improved correlations were developed to predict hot gas layer temperatures in pre-flashover compartment fires, considering the fire source location. The fire source location has not been considered in the correlations available in the literature, but the study developed in this research showed its importance and great influence on temperature results. Most correlations are designed to predict the temperature for fires occurring in a central position, on the floor and away from obstructions, e.g. pieces of furniture, which results in the lowest possible temperatures. So, as a matter of safety, these new correlations can provide better results, allowing estimating the upper layer temperature considering the influence of the air entrainment restriction caused by the proximity of walls and furniture or elevation of the fire source.

1.4 Work Structure

This work has been divided in seven chapters. After introduction in the first chapter, the second chapter presents a literature review on fire dynamics and fire safety research. This

chapter brings the development of important concepts as plume theory and zone models and a review of the works which studied fire location influence and developed correlations to predict fire parameters.

The third chapter describes the main concepts and theories that are important for a basic understanding of the fire phenomena and comprehension of this work.

The fourth chapter presents the mathematical model and main assumptions applied by the software Fire Dynamics Simulator (FDS).

The fifth chapter explains the methodology applied in this research and describes the cases studied, as well as the mathematical model verification and mesh resolution analysis.

The sixth chapter presents the results obtained for the fire source location influence analysis and the development process of the six new correlations, as well as the verification of its agreement to numerical and experimental results.

The seventh chapter brings the conclusions of this research as well as suggestions for future researches.

2 LITERATURE REVIEW

This chapter brings chronologically the development of important concepts in fire dynamics and a review of the works which studied fire location influence and developed correlations to predict fire parameters.

Fire dynamics have been intensively studied for the past decades, and one of the pioneers on the study of compartment fires was Dr. Kunio Kawagoe from the Building Research Institute in Tokyo, Japan. Kawagoe, 1958, described a decade's work in fully developed fires (post-flashover). The fuel applied was waste timber, allowed to burn until extinction. Temperature and pressure gradients were measured inside the room and thermal radiation flux, gas velocity and compositions were measured at the opening. The results confirmed that the temperature inside the room can be considered uniform and that the theoretical expression for air flow into small openings, known as the ventilation factor, was correct [Thomas, 2004]. Vent flow was computed based on stagnant hot and cold gas reservoirs on either sides of the vent, assuming a uniform temperature in the compartment for fully developed fires. This work by Kawagoe, 1958, seems to be the first time that the concept of a compartment fire presenting homogeneous properties appeared in the literature.

At this same decade Morton et al., 1956, in their study about turbulent gravitation convection in maintained and instantaneous sources developed a theory using methods which are applied to stratified body fluids with any variation of density with height. Their analysis was applied to the atmosphere and predictions were made of the height to which smoke plume from typical sources of heat should rise in a still, stable stratified atmosphere under various conditions. Their findings are known today as the Classical Plume Theory.

Professor Howard Wilson Emmons is known today as the "Father of the modern fire engineering science" for his contributions to the understanding of the fire dynamics, field where he started his researches in the mid-1950's. Petersen and Emmons, 1961, published an article about the theory of laminar flame fronts, which has been a reference for fire engineering until today. Later that same year Lee and Emmons, 1961, published a theoretical and analytical study on the behaviour of natural convection plumes above a line fire. This was one of the first analytical treatments of the fire dynamics problem using viscous fluid dynamics theory. This work considered a turbulent plume above a steady two-dimensional finite source of heated fluid in a uniform ambient fluid, applying a lateral entrainment assumption. Experimental data was obtained and compared to analytical results showing an excellent agreement.

Gross and Robertson, 1965, presented results of experimental measurements for mass burning rates, temperatures, and gas compositions for fully developed fire compartments. The burning rate was found to be generally proportional to the ventilation factor. A characteristic change in the pattern and flaming in ventilation-limited model enclosures resulted in a pronounced shift in the mass burning rate. They concluded that burning rate data in geometrically similar enclosures may generally be correlated in terms of the ventilation parameter normalized by the square of the linear-scale ratio.

The late 1950's and the 1960's seem to be the starting point of the fire engineering science, when qualitative descriptions of the phenomena and some basic concepts were carved. Later in the 1970's the fire safety research started to grow, when several studies and fire models based on empirical data and theory were developed.

Prahl and Emmons, 1975, gave an important step to comprehend pre-flashover compartment fires. The buoyantly driven flow of fire gases out through an opening of a burning room was calculated for a constant density hot gas layer. An experimental model was developed to test the validity of the theory. The results indicated that the theory, with flow coefficients determined from the experiment could adequately predict the behaviour, while the theory discussed failed to predict the room layer depth at low inflow rates. Flow formulas useful for practical calculations were presented.

Rockett, 1976, extended the concept designed by Kawagoe, 1958, by considering the gas in the enclosure to be composed of a hot upper and a cold lower layer with homogeneous properties. In this work a small fire in a large room was considered. He developed generalizations of the Kawagoe's expressions for the window air flow and the height of the neutral plane and applied them to rationalize previously unexplained features of Gross and Robertson's enclosure fire data. This work is extremely important for fire dynamics, once it provided the well-established equation for mass flow rate out through an opening.

McCaffrey and Rockett, 1977, measured some enclosure fire static pressure and compared with the present hydraulics-orifice flow model for fire induced flows into and out of enclosures. They found out that the vertical pressure differential (enclosure to ambient) followed the expected hydrostatic distribution quite well and accurately reflected the doorway inflow and outflow gas velocities. Measurements of ceiling and floor differential pressure using different quantities of gas burners illustrated how the neutral plane and layer interface vary with upper gas temperature. They also observed the variation of pressure and temperature due to fire location within the room. Observing that, the upper gas temperature is

significantly hotter for corner burner than for center burner. They argued that this might be explained by the plume entrainment.

Zukoski, 1978, developed a simple analytical model to determine the time required for a room to fill with products of combustion from a small fire. The room was a compartment with small openings at either the floor or ceiling level, and was assumed that the leak was large enough to allow the transient pressure term in the energy equation to be neglected. Products of combustion were assumed to occupy an upper layer and the developed model predicted the growth of the thickness and the mean density of this layer as a function of time. The analysis showed that times required to fill a typical room were small. The time required to fill a room and the mean density of ceiling layer were determined in terms of fire size, room geometry, leak position, fire elevation and geometry.

Heskestad and Delichatsios, 1979, studied the physical modelling of the initial fire environment generated by fire in an enclosure. They investigated experimentally the validity of modelling relations, proposed by Alpert, 1975, for the convective flow generated by "power-law" fires. Temperatures and velocities were measured in the hot gas layer. The data showed a good correlation to dimensionless variables of the modelling theory. Analytical expressions for the dimensionless temperature and velocity fields were established. It was found that the local gas velocity in the hot gas layer can be related directly to the local temperature rise and ceiling clearance, regardless of fire growth rate and time from ignition. Later, Heskestad and Delichatsios, 1989, published a brief update of the previous work, they updated the correlations based on the actual heat of combustion of wood. In addition, the correlations were generalized to include combustibles with a significantly different convective fraction of total heat release rate than wood.

Thomas et al., 1980, described how various factors affected the thermal instability caused by the energy generation rate of aggregated energy losses, which can result in flashover, and demonstrated a quasi-steady approach that can be used to explain fire growth in enclosures. They found out that there are three equilibria and two instabilities (ignition and extinction) and that the ignition leads to a "jump" increase in the mean equilibrium temperature, suggesting that this is the basis of the flashover. Based on that, a critical compartment gas temperature can be computed, provided approximations can be made for describing the thermal feedback.

Zukoski et al., 1981, described a new technique for measurement of mass flow rate in buoyant fire plumes. A transition in the dependence of flame height on heat input and burner size was observed when the flame height was about four times the burner diameter. The mass

flow rate in the region of the plume was correlated by the use of a simple plume model (plume theory), which is widely applied until today. It was found that at the early stages of a fire in a building, the rate of production of hot gas by a fire and the temperature of this gas depends very strongly on the rate of entrainment in the fire plume and in the flame itself. In building fires the interesting region of the plume is located very close to the origin, in these regions it was expected that the size of the fire source, the effects of large density differences and the presence of heat release due to combustion would greatly influence the entrainment process. The results shown that the simple plume model can be used to make remarkably good estimates of entrainment rates, when the top of the visible flame lies below the interface between hot gas layer and cooler layer near the floor.

McCaffrey et al., 1981, developed a well-established correlation (called MQH) to estimate room temperatures and the likelihood of flashover for pre-flashover compartment fires based on the heat release rate of the fire, the room ventilation, and the geometry and thermal properties of the enclosure. Their correlation was derived considering an energy balance on the well-stirred gas layer in the upper portion of the room and 112 experimental data were used to fit the correlation, with the fire source positioned at the center of the room. This correlation holds for compartment upper layer gas temperatures up to approximately 600°C (onset of flashover), it is not applicable to rapidly developing fires in large enclosures, it requires a suitable estimation of the heat release rate, and the characteristic fire grow time and thermal penetration time must be determined to specify the effective heat transfer coefficient. The location of the fuel array must be factored into any judgment, once the correlation was designed for fires at the center of the room and on the floor.

Steckler et al., 1982a, 1982b, reported 55 full-scale steady-state experiments conducted to study the flow induced by a pool fire in a pre-flashover compartment fire. The mass flow rate through the door or window opening and fire plume entrainment rate are presented as a function of opening geometry, fire strength, and fire location. The characteristics of the measured opening flow rates were explained by a simple hydrostatic model based on temperature distribution. A good correlation between the measured results and the idealized flows, taking into account the complete temperature distribution, was demonstrated. This experimental data is considered one of the most complete and reliable available in the literature, and has been extensively used to verify different mathematical models. The results of these experiments have been applied to verify the CFD solution in the present study. As a continuity of the previous work, Steckler et al., 1984a, 1984b, reported a theoretical study of steady-state fire-induced flows through openings. A static-pressure flow

model was used to establish ideal orifice flows. The opening and ideal flow results were combined to form room-opening flow coefficients as a function of fire energy release rate, opening geometry, and fire location. An irrotational jet model for the flow coefficients was developed and found to be in reasonable agreement with experimental data.

Quintiere et al., 1984, examined fluid dynamic models and concepts without concern for the energy transport models. The energy transport information required by the fluid mechanic models was derived from experimental data. A line fire along a wall was considered, it was assumed that a theoretical entrainment rate, derived from a line-source turbulent wall plume solution would be sufficiently accurate for this analysis, so no specific entrainment rate checks were made. New experimental data was presented consisting of vent flow rates for various vent geometries and wall line fires. Theoretical computations based on the “simple” flow model, which in turn is based on the vent flow and fire plume air entrainment, assuming an ambient lower layer and no wall or vent mixing effects were compared to the experimental data. It was found that this “simple” model consisting of a hot upper layer and ambient cold layer predicts vent flow rates and layer positions to within 50% accuracy. The temperature profiles can be approximated, but the lower layer can be significantly hotter than the ambient temperature, due to the vent mixing.

Hasemi and Tokunaga, 1984, measured the temperature distribution and visible flame height on the fire plumes from square burners in a semi-infinite space, against a wall and in a corner of walls. They concluded that the existence of walls near a fire source is thought to suppress the growth of eddy scale in the plume.

Mowrer and Williamson, 1987, noticed that fires in corners and along walls have a restricted air entrainment and it results in higher layer temperatures than those predicted by the MQH correlation. So, they developed modification factors to adjust that correlation and extend its applicability to wall and corner burning geometries.

Tran and Janssens, 1991, reported the results of several full-scale wall and corner experiments performed in an ASTM room. Six wood materials having different flame spread indices were applied. Only heat release rates, smoke release, selected temperatures, and heat fluxes were reported. Later, Tran and Janssens, 1993, conducted steady-state experiments to characterize the corner ignition source used in the proposed ASTM room fire standard at two heat release rates (40 kW and 160 kW). Flame height, heat flux to wall, temperature, velocity, mass and enthalpy flux, and flame structure were measured primarily in the flaming region.

Dembsey et al., 1995, conducted twenty experiments and compared their results with zone models (CFAST and FIRST). The compartment was a 2.5 m × 3.7 m × 2.5 m

compartment room with a single doorway of 0.76 m × 2.0 m. The gas burner was placed in two different locations (center of the room and sidewall), always elevated 0.61 m from the floor. The heat release rates tested were 330, 630 and 980 kW. CFAST predicted HGL temperatures 150-260°C hotter than the measurements, while FIRST predicted temperatures slightly cooler than the measured ones.

Takahashi et al., 1997, studied experimentally the relationship between air entrainment and flame/plume behavior, when a fire source was placed in and near a corner of vertical walls. Observation of flame height and measurements of temperature and upward velocity around a corner were carried out. The heat release rate and the separation distance from the wall were varied as well as the burner size.

Matsuyama et al., 1998, proposed simple predictive equations for the room fire behaviour in post-flashover fires. These equations were obtained applying the method for pre-flashover compartment fires proposed by McCaffrey et al., 1981, to ventilation controlled fire. The results obtained applying these equations were compared with the results of a more detailed computer model, showing a good agreement.

Poreh and Garrad, 2000, presented measurements of flame heights and mass fluxes in fires burning away from walls, close to a wall and in a corner. The measurements confirmed that adjacent walls decrease the mass flux of plumes (entrainment) and increase the mean and peak flame heights. Based on the experimental data, an approximate, simple model for describing the effect of walls on the mass flux above the flaming region was offered. This model provided a good agreement with measurements, when used with an assumption by Hansell, 1993, that the reduction of the air entrainment into the plume is equal to the ratio of the open to the total perimeters of the trays. Two similar models for predicting the effects of walls on the mean flame height were also presented. These models overestimated the measured values of the mean flame height above fuel trays close to a wall and in a corner by approximately 15-30%, respectively.

Azhakesan et al., 2003, undertook an experimental study of liquid pool fires in corner and center fire geometries. They correlated the measured well-mixed ceiling gas temperature and energy release rate with two dimensionless groups, as used in the MQH correlation. In an initial interrogation they found out that the modifications to MQH correlation suggested by Mowrer and Williamson, 1987, are reasonable.

Xiaojun et al., 2005, developed a multi-layer zone fire growth model to predict the fire behavior in a single room. The fire room volume was divided into an arbitrary number of horizontal layers, in which the temperature and other physical properties were assumed to be

uniform. The principal equations for each layer were derived from the conservation equations of mass and energy. The implemented fire sub-models for combustion, fluid flow and heat transfer models were introduced. The results obtained were compared with the experimental data and in general, a good agreement was found.

Hamins et al., 2006, conducted experiments in a compartment with $7.04 \text{ m} \times 21.7 \text{ m} \times 3.82 \text{ m}$, designed to represent a realistic-scale compartment in a nuclear power plant. The studied compartment had a door opening of $2.0 \text{ m} \times 2.0 \text{ m}$. The fire source was placed at the center of the room or near a wall at the ground level and the heat release rate was tested for 350 kW, 1 MW and 2 MW. This study was carried out with the objective of producing experimental data for validation of fire simulations.

Wang and Quintiere, 2009, developed a mathematical study to compute the doorway flow behavior due to fire in a room. Two approaches were taken, first a model attempting to include the effect of fire entrainment and vent mixing; second was a model based on an ideal point source plume fire (both in the zone model concept). The results were compared to available flow data, and an approximate formula was developed to predict the doorway mass flow rate to within 20% for a wide range of fire conditions. As a continuity of this work, Quintiere and Wang, 2009, developed a new correlation for fire-induced wall vent flow rate extended to include window flows. A theoretical model based on an ideal point source fire plume is used to guide the form of the empirical correlation. The results of the correlation were compared to available flow data and shown to be within 15% accuracy for a wide range of fire conditions.

Delichatsios et al., 2009 presented a new correlation for predicting enclosure gas temperature based on the energy balance for adiabatic conditions, an estimate of the heat flux imposed on the enclosure boundary and the transient thermal response of the boundary. This correlation was verified, being able to predict enclosure gas temperature in both well- and under-ventilated fires.

Wang et al., 2012, investigated the accuracy of predictions of fire-induced flow into a compartment by Fire Dynamics Simulator (FDS), a follow-up study was explored by comparing with the Steckler's experimental data.

Zhang et al., 2012, presented an experimental study on smoke filling in closed compartments with elevated fire sources. The mass loss rate, the light extinction coefficient, the oxygen concentration and the gas temperature profile were measured. The results presented a distinctive smoke filling process and a distinct stratification phenomenon, being the interface of the stratification at the fuel surface level. As a continuity of the previous

work, Zhang et al., 2013, investigated experimentally the impact of the elevation on fires in a ceiling vented compartment. Similar parameters were measured. It was observed that for a higher elevated fire, the average fuel loss rate and the overall light extinction coefficient were smaller, the oxygen concentration was higher and the gas temperature was lower. In addition, the smoke descending was slower. These results point to less hazardous fire scenario when fire was elevated, which is totally different from what is observed in elevated fires in closed compartments.

Gao et al., 2014, investigated experimentally the influence of sidewall restriction on the maximum ceiling gas temperature of buoyancy-driven thermal flow in a reduced scale tunnel model. Results shown that, until a certain distance from the sidewall the maximum temperature was basically independent of this parameter, but as this distance decreased the maximum temperature increased significantly. A correlation for the maximum ceiling gas temperature was proposed, taking the heat release rate, distance to the nearest sidewall, and effective ceiling height into account. The results obtained by the proposed formula were compared with experimental data and shown a good agreement.

Ji et al., 2015, conducted a set of experiments on sidewall fires in a small-scale corridor-like structure. The mass loss rate, ceiling jet flame length and maximum ceiling jet temperature were investigated by correlating with the distance between fire source and ceiling. The results showed that as the effective ceiling height decreases, the mass loss rate increases due to the enhanced radiation heat feedbacks from the ceiling and ceiling jet flame to the fuel surface. The mass loss rates are higher for the pans with long edge attaching sidewall compared to those with short edge attaching sidewall, due to the enhanced sidewall confinement effect. A simplified equation for predicting the mass loss rate per unit area was developed involving the dimensionless effective ceiling height and the length ratio of pan edges attached and perpendicular to the sidewall. A modified correlation for the maximum ceiling jet temperature by taking into account the effect of the pan layout and the aspect ratio of the pan edges was also proposed.

Johansson et al., 2015, compared predictions of the hot gas layer temperature obtained through two hand-calculation methods, to experimental data from a multi-room reduced-scale compartment fire. Two different room configurations were tested and the openings between the rooms and to the outside were also varied. The fire source was placed at the center of the inner room at the ground level and different heat release rates were tested. The first method compared was an empirical method (being the MQH method applied to the fire room and a similar method applied to the adjacent room), and the second method consisted of several

calculation steps in order to solve a simple energy balance. Generally the temperature predictions with the two hand-calculations methods were within the bounds of the experimental uncertainty, for both fire and adjacent room.

Li and Hertzberg, 2015, conducted two series of tests in three different scaling rooms (full, medium and small) to investigate the scaling of internal wall temperatures. The fire source was placed both at the center of the room and near a corner. The measured time-dependent internal wall temperatures, incident heat fluxes, and gas temperatures in different scales were presented. They concluded that the proposed scaling method was able to scale the internal wall temperatures (temperatures inside the walls) and incident heat fluxes well, especially in medium scale.

Tili et al., 2015 analyzed the impact of the roof shape on the hot gases evacuation process for three heat source ground locations (center of the room, at the corner and near the doorway) inside the room. Two typical roof shapes were tested, a pyramidal roof and a domed one. The obtained results were compared with those obtained with the basic model (flat roof). They concluded that for all roof shapes the lowest exhaust gas temperature is recorded for a source placed in the room center, in addition, regardless of the heat source position, the dome-shaped roof allows to have a lower temperature within the fire room and for a source placed at the center, the temperature inside the room is higher for a flat roof compared with the other forms.

Tili et al., 2016 conducted a series of numerical investigations of fire induced by flow in a compartment, in order to examine the effect of the source location on the thermal flow field and the mass flow rate at the exit doorway. The results shown that, the height of the heat source has a significant influence on the temperature field and the stratification interface of the buoyant layer, comparing to transversal and longitudinal positions. With these results they developed a mathematical correlation linking the ventilation mass flow rate and the three dimensional coordinates.

Gao et al., 2016, presented an experimental investigation to explore the effect of tunnel sidewall on flame characteristics and air entrainment factor of methanol pool fires with decreasing distance to the sidewall. The results showed that due to the confinement effect of sidewall, the flame height increases with the decrease of fire-sidewall distance. Especially for fire immediately against sidewall, the air entrainment process is confined to the largest extent and the flame height increases significantly. Correlations of the flame height with difference distances to the sidewall are obtained based on dimensionless analysis and experimental data. The Entrainment Factor (EF) was also estimated for different fire locations.

Zeinali et al., 2018, investigated the fire growth in a corner configuration MDF panels (combustible walls) to provide a set of experimental data, but first, test results with inert calcium silicate panels (non-combustible wall) were discussed for three values of HRR, allowing to address the main physics involved. A new correlation for mean flame height was introduced, using the hypotenuse of the triangle as characteristic length for entrainment of air into the fire plume, and expressing that the flame height increases proportional to the square root of the fire heat release rate.

Węgrzyński and Konecki, 2018, presented results of CFD simulations and scale modelling of the flow of heat and smoke in a compartment fire. Both, location of the fire and the compartment size were analysed to verify its influence on the mass flow and the temperature of smoke that leaves the room. The results showed small influence of both parameters on the mass flow of smoke exiting the room. However, both of these parameters influenced the temperature of the smoke. In larger compartments lower average temperatures of the smoke layer, but higher maximum values were observed.

For the past 60 year, several researchers have been dedicating their efforts to understand fire dynamics and to predict the fire behaviour and its parameters, but none of them have developed correlations able to predict the hot gas layer temperature considering the fire source location, especially the vertical position of the fire.

3 THEORETICAL BACKGROUND

This chapter presents the main concepts and theories that are important for a basic understanding of the fire phenomena and comprehension of this work.

3.1 Natural Turbulent Diffusion Flames

A fire is usually described as a natural turbulent diffusion flame. The main characteristic of a diffusion flame is that the fuel and oxidizer (air) are initially separated, and the combustion process occurs in the region where the gases mix [Drysdale, 2011].

Flames associated with the burning of condensed fuels (i.e., solids and liquids) are dominated by buoyancy. If the fuel bed is less than 0.05 m in diameter, the flame will be laminar, with the degree of turbulence increasing with the increase of the fuel bed diameter, until achieving 0.3 m diameter, when buoyant diffusion flames with fully developed turbulence are observed [Drysdale, 2011].

Although fire is basically a natural buoyant flame, in pre-flashover compartment fire experiments is very usual to employ jet flames to represent the fire source, once these flames are easier to control and permit a constant HRR. According to Drysdale, 2011, in jet flames, turbulence first appears at the tip of the flame, extending further down towards the burner nozzle as the jet velocity is increased, although never reaching it (see Figure 3.1). The decrease observed in flame height from the maximum inside the laminar region to a constant value in the fully turbulent regime can be explained by the increased entrainment of air by eddy mixing, which results in more efficient combustion [Drysdale, 2011].

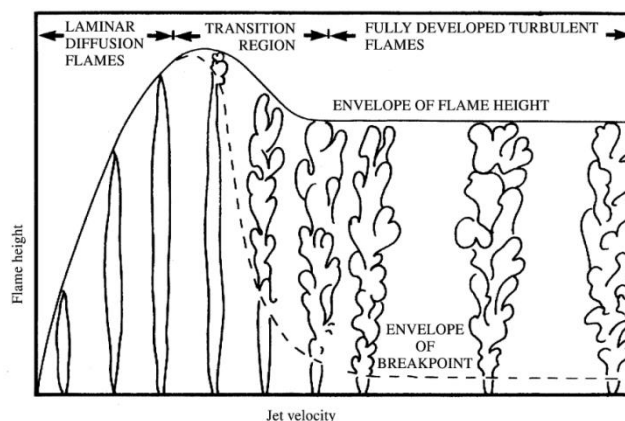


Figure 3.1 - Height of jet flames as a function of nozzle velocity, showing transition to turbulence [Hottel and Hawthorne, 1949]

The relative importance of momentum and buoyancy in a flame will determine the type of fire, and the Froude number (Fr) may be used as a mean of classification:

$$Fr = \frac{U^2}{gD} \quad (3.1)$$

where U is the velocity of the gases, D is a characteristic dimension (usually the diameter of the burner) and g is the gravity acceleration.

In natural fires or pool fires, the initial velocity of the gases cannot be measured, but it can be derived from the heat release rate (\dot{Q}).

$$U = \frac{\dot{Q}}{\Delta h_c \rho_f \left(\frac{\pi D^2}{4} \right)} \quad (3.2)$$

where Δh_c is the heat of combustion of the fuel vapor, ρ_f is the fuel density and D is the diameter of the fuel bed. For jet flames, the velocity is simply the fuel jet velocity.

Turbulent jet flames are associated to high Froude numbers, indicating that the momentum of the fuel stream is dominating the flame behaviour [Heskestad, 2002]. However, in natural fires or pool fires, buoyancy is the predominant driving force (low Froude numbers), so, these flames have a much less ordered structure and are more susceptible to external influences (such as air movement) than jet flames [Drysdale, 2011].

3.2 Compartment Fires and Hot Gas Layer Formation

Fire is a strongly interactive phenomenon, being its interactions non-linear and extremely complex to quantitatively estimate. The processes of interest in enclosure fires mainly involve mass and heat fluxes to and from the surroundings. When a fuel package is burned within a compartment, the environment conditions generated by the fire and the enclosure boundaries (walls, floor, ceiling) interact with the fuel, making predictions of fire growth extremely difficult [Karlsson and Quintiere, 2000].

The compartment can be described as any confined space that controls the ultimate air supply and thermal environment of the fire [Quintiere, 2006].

After fire ignition, the fire grows producing increasing amounts of energy, mostly due to the flame spread. Besides the energy release, this process produces a great variety of toxic and nontoxic gases and particulate (smoke). In the early stages the fire has little or no influence from the compartment, being described as fuel-controlled [Cooper, 2002; Karlsson and Quintiere, 2000; Walton and Thomas, 2002].

As the fuel burns, heat, light and combustion products (hot gases) are produced. These hot gases surrounded by colder gases (with a temperature close to ambient temperature), rise upward due to buoyancy. This buoyancy driven flux (including the flame itself) is called fire plume [Cooper, 2002; Karlsson and Quintiere, 2000].

For the full height of the plume and its periphery, relatively quiescent and cold gases are entrained laterally and mixed to the plume as it keeps rising. This mixture of combustion products and entrained cold air impinge on the ceiling of the fire compartment and cause a layer of hot gases to be formed. It is important to highlight that only a small portion of the mass that reaches the ceiling originates from the combustion products, being the greatest portion originated from the cold air entrained [Cooper, 2002; Karlsson and Quintiere, 2000].

When the hot gases impinge the ceiling, they spread across it as a momentum-driven circular jet. As the hot jet moves outward under the ceiling surface, it entrains ambient air from below and transfers energy by conduction to the relatively cool adjacent ceiling surface and by convection to the entrained air. This ceiling jet is retarded by frictional forces from the ceiling surface above, and by turbulent momentum transfer to the entrained air from below. As a result of all this flow and heat transfer activity, the ceiling jet continuously decreases in temperature, smoke concentration and velocity, and increases in thickness with increasing radius (Figure 3.2a) [Cooper, 2002; Karlsson and Quintiere, 2000].

This ceiling jet eventually reaches the walls of the enclosure and is forced to move downward along the wall. The downward wall jet is of higher temperature and lower density than the ambient air into which it is being driven. This wall jet is retarded in its downward descent by buoyancy and frictional forces at the wall surface, and at some point its movement downward is halted. The wall jet is cooled by conductive/convective heat transfer to relatively cool wall surfaces. The now upward-moving flow entrains ambient air in a manner which is reminiscent of entrainment into the original fire plume. Eventually, a relatively quiescent upper gas layer is formed below the ceiling. (Figure 3.2b) [Cooper, 2002; Karlsson and Quintiere, 2000].

The gases in the ceiling and wall jets redistribute themselves across the upper volume of the room. Eventually, a relatively quiescent, high temperature upper layer of uniform

thickness is formed below the ceiling. As the thickness of this layer grows, it eventually submerges the flows generated by the ceiling jet-wall interactions. The bottom of this layer is defined by a distinctive interface, which separates the lower ambient air from the upper hot gases. With increasing time the level of the smoke layer interface continues to drop, and the temperature and smoke concentration of the upper layer continue to rise (Figure 3.2c) [Cooper, 2002; Karlsson and Quintiere, 2000; Walton and Thomas, 2002].

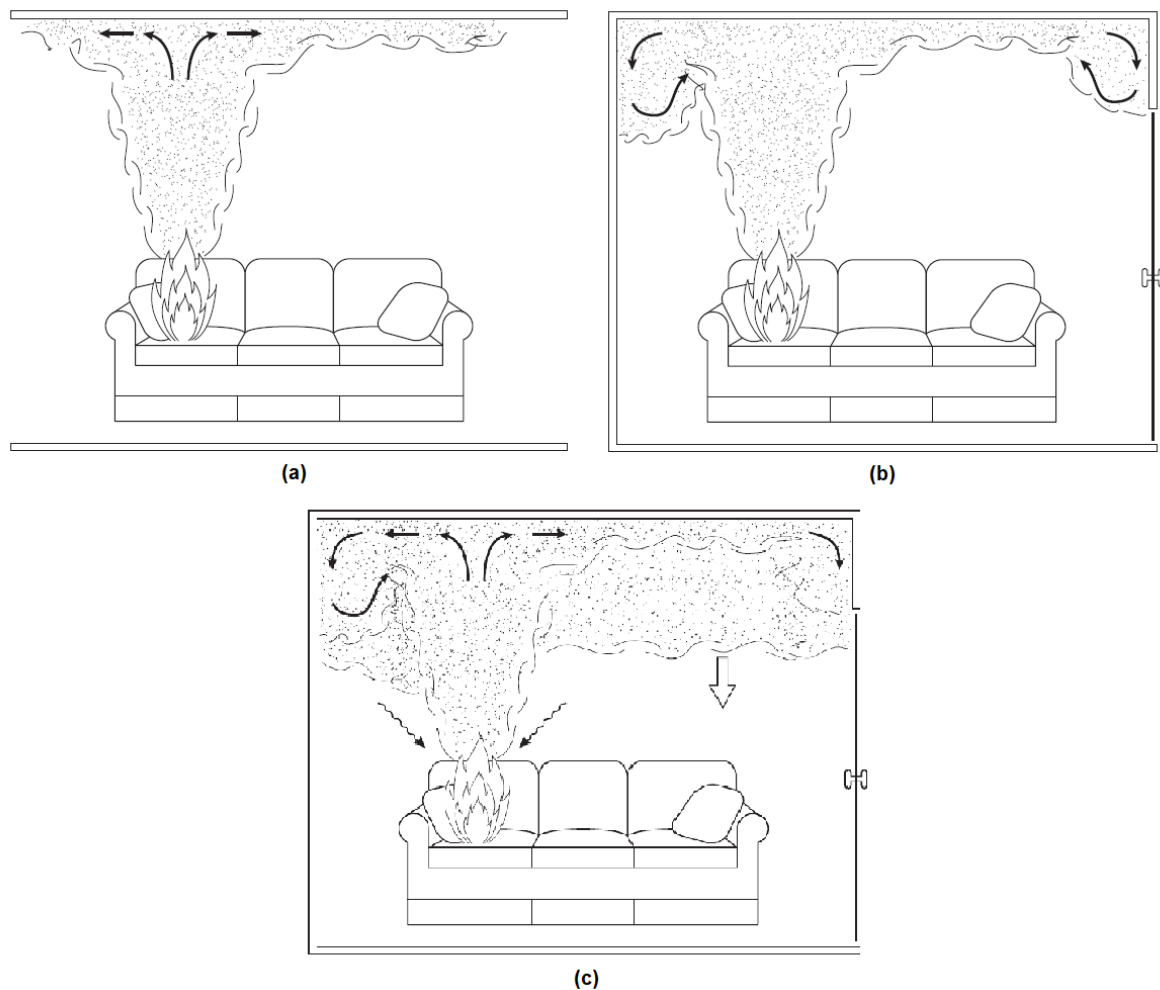


Figure 3.2 - (a) Plume-ceiling interaction, (b) Ceiling jet-wall interaction and (c) Hot gas layer formation and growth [adapted from Cooper, 2002]

If there is an opening (door or window) that allows the gases to flow out/into the compartment, smoke flows out through it, as soon as the hot layer reaches the top of the opening. Often, the increasing heat in the enclosure causes the breakage of windows and thereby create an opening [Karlsson and Quintiere, 2000].

As the HGL grows in volume and temperature, heat is transferred by radiation and convection from the hot gas layer to the ceiling and walls that are in contact with the hot

gases. Heat from the hot layer is also radiated towards the floor and the lower walls, and some of the heat is absorbed by the air in the lower layer (participant medium). Heat is also transferred by radiation from the hot gases and the hot enclosure boundaries to the fuel bed, which leads to an increase in the burning rate of the fuel and the heating up of other fuel packages in the enclosure. As a result, the hot gas layer keeps growing in temperature and may become extremely hot. Consequently, there may be a stage where all the combustible material in the enclosure is ignited, with a very rapid increase in energy release rates. This very rapid and sudden transition from a growing fire to a fully developed fire is called flashover [Karlsson and Quintiere, 2000].

3.3 Compartment Fire Stages

A fire analysed by the temperature point of view can be divided in five stages [Walton and Thomas, 2002]:

- a) Ignition;
- b) Growth (pre-flashover);
- c) Flashover;
- d) Fully developed fire (post-flashover);
- e) Decay.

Ignition is the period during which the fire begins. This stage is followed by the growth stage, when the fire growth is initially a function of the fuel (fuel-controlled), with little or no influence from the compartment. If sufficient fuel and oxidant are available, the fire keeps growing, causing a temperature rising inside the compartment. High temperatures inside the compartment may lead to a stage when all the combustible material in the enclosure is ignited, which is called flashover [Drysedale, 2011; Karlsson and Quintiere, 2000; Walton and Thomas, 2002].

Flashover is usually defined as the transition from a growing fire to a fully developed fire. During the fully developed fire, the heat release rate (HRR) and temperatures are the highest. During this stage more fuel is pyrolyzed than can be burned with the available oxygen, so this stage is called ventilation-controlled. If there are openings the unburned fuel will leave the compartment with the hot gas flow and may burn outside the compartment. That is why the appearance of flames through the openings is usually an indicator that the fire

is fully developed and flashover has occurred. As the fuel becomes consumed and the heat release rate declines the fire reached its last stage, the decay. During this stage the fire may change from ventilation-controlled to fuel-controlled [Drysdale, 2011; Karlsson and Quintiere, 2000; Walton and Thomas, 2002].

Figure 3.3 presents the temperature as a function of the time and indicates the five stages of a ventilated (with openings) compartment fire. It is important to note that not all fires reach the flashover stage, either by fuel or oxidant shortages. These cases are represented as the dashed line in Figure 3.3.

In this particular study, only fires in stage pre-flashover (growth stage) and with constant heat release rate (HRR) will be dealt with.

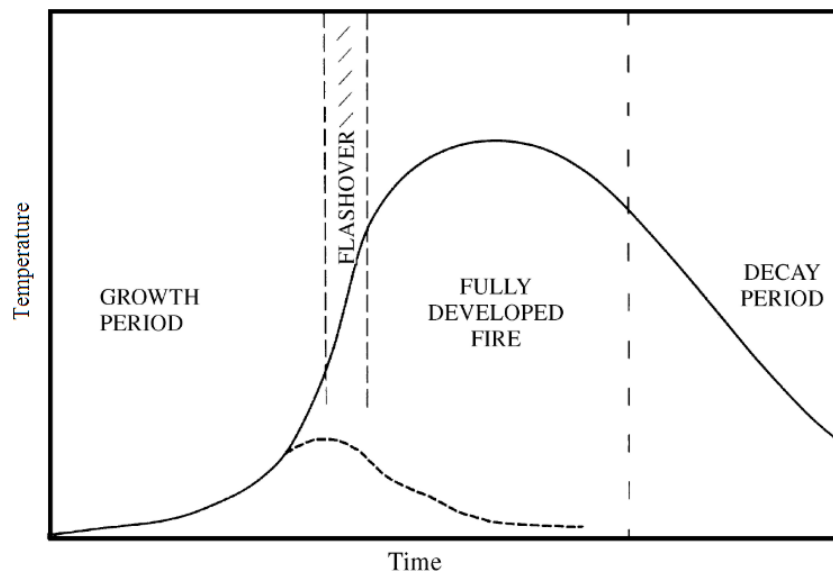


Figure 3.3 - Compartment fire stages [adapted from Drysdale, 2011]

When the fire is on pre-flashover stage the emphasis in fire safety engineering design is on the safety of humans, through parameters like visibility, gas toxicity and hot gas layer temperature. When the fire reaches the post-flashover stage the objective changes for structural stability and safety of fire fighter [Johansson, 2016; Karlsson and Quintiere, 2000]. Ideally provisions should be taken to prevent fires from reaching large proportions, characteristic from post-flashover stage, such as the use of non-combustible lining materials and fire suppression systems.

3.4 Compartment Fire Model (Two-zone Model)

In order to predict temperatures in a compartment fire a model of the fire phenomena must be applied.

According to Quintiere, 2002, an approach to predict several aspects of fire phenomena in compartments is known as the zone modelling, being it based on a conceptual representation of the compartment fire process, and it is an approximation to reality.

The two-zone model consists in assuming two distinct zones (regions) inside the compartment formed by the thermal stratification (hot gas upper layer and cold gas lower layer). The temperature and composition are assumed as uniform spatially in each zone. Kawagoe, 1958, was the first researcher to prove that the temperature has a uniform behaviour in each zone within a compartment.

It is important to note that this assumption may be less valid for large enclosures, such as shopping malls and supermarkets or long narrow spaces, such as corridors and shafts [Walton and Thomas, 2002].

In the two-zone model conservation equations are applied to each zone and serve to embrace various transport and combustion processes. The fire is represented as a source of mass and energy, manifesting itself as a fire plume which acts as a pump for the mass from the lower zone to the upper zone through a process called entrainment [Quintiere, 2002]. The zone model concept can be applied for both computer models, such as CFAST, and hand-calculation.

According to Quintiere, 2002, a control volume, CV1 in Figure 3.4, is defined to enclose the gas in the upper layer and the fire plume. The interface between layers moves with the control volume such that no mass is transferred across this thermally stratified region. The velocity of the control volume along this interface, \bar{w} , is equal to the fluid velocity, \bar{V} . The lower layer (zone) which includes all the remaining gas in the room is delineated by a second control volume, CV2. It has been assumed in zone modelling that the volume of the fire plume is small relative to the gas layer or zone volumes, and therefore its effect can be ignored. The properties of the upper and lower zones are assumed to be spatially uniform, but can vary with time. Thus, temperature, T , and species mass concentration, Y_i , are properties associated with ideal upper and lower homogeneous gas layers. Other assumptions in the application of the conservation laws to the zones are listed below:

- 1) The gas is treated as ideal;
- 2) Exchange of mass at free boundaries is due to pressure differences or shear mixing effects;

- 3) Combustion is treated as a source of mass and energy;
- 4) The plume instantly arrives at the ceiling, once transport times are not explicitly accounted for in zone modelling;
- 5) The mass or heat capacity of room contents is ignored compared to the enclosure wall, ceiling, and floor elements;
- 6) The horizontal cross section of the enclosure is a constant area, A ;
- 7) The pressure in the enclosure is considered uniform in the energy equation, since the enclosure pressure, p , is much greater than the variations due to hydrostatics;
- 8) Mass flow into the fire plume is due to turbulent entrainment. Entrainment is the process by which the surrounding gas flows into the fire plume as a result of buoyancy;
- 9) Fluid frictional effects at solid boundaries are ignored.

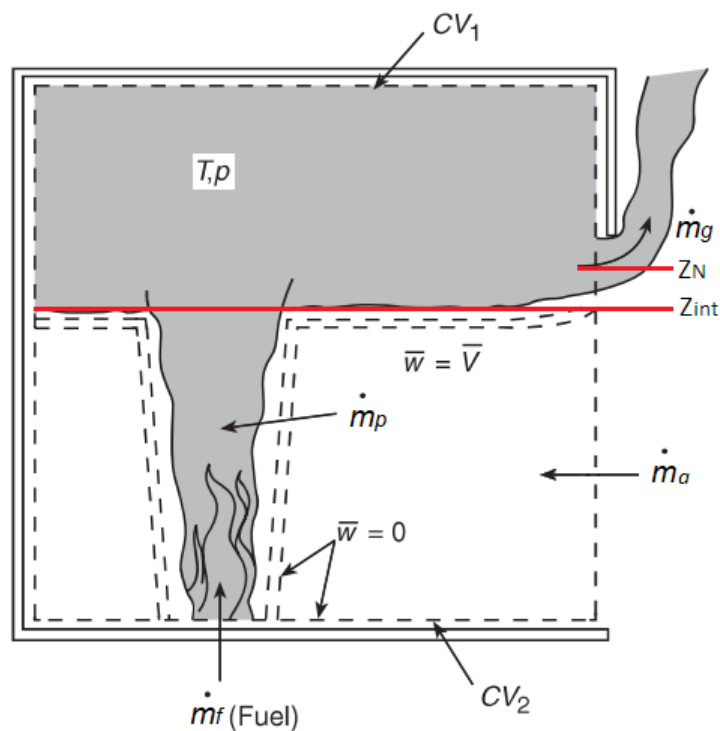


Figure 3.4 - Two layer zone modelling (adapted from Quintiere, 2002)

The description of the two-zone modelling is important for the present work, once its concepts will be applied to the analysis of the FDS results to obtain the hot gas layer temperature and to the development of the correlations to predict the hot gas layer temperature.

3.5 Conservation Equations in Compartment Fires

According to Walton and Thomas, 2002, the basic principle used to calculate the temperature in a compartment fire is the conservation of energy. The conservation of energy applied to the hot upper layer can be simply stated as follows: the energy added to the hot upper layer by the fire equals the energy lost from the hot layer plus the time rate of change of energy within the hot upper layer. From the time rate of change of energy within the hot layer, the temperature of the layer can be computed. Since the volume of the upper layer changes with time, and mass flows in and out of the upper layer, conservation of mass must be used along with the conservation of energy.

It is important to note that the fire process is transient but for this analysis the steady-state equations are applied.

The energy generated by the fire has probably the most important influence on the temperature in a compartment. The rate of energy release is equal to the mass loss rate of the fuel times the heat of combustion of the fuel [Walton and Thomas, 2002]:

$$\dot{Q} = \dot{m}_f \Delta h_c \quad (3.3)$$

where \dot{Q} is the energy release rate (kW), \dot{m}_f is mass burning rate of the fuel (kg/s) and Δh_c is the effective heat of combustion of the fuel (kJ/kg). The effective heat of combustion considers an incomplete combustion, once fires usually have this characteristic.

The amount of energy released by the fire which enters the hot upper layer is a function of the fire, layer conditions, and geometry [Walton and Thomas, 2002]. Only about 35% of the energy released by the fire leaves the fire plume as radiation [De Ris, 1979]. The majority of the remaining energy released by the fire is convected into the upper layer by the plume. As a first approximation, it can be assumed that all of the energy generated by the fire is transported to the upper layer [Walton and Thomas, 2002].

The mass conservation can be described by the equation:

$$\dot{m}_g = \dot{m}_a + \dot{m}_f \quad (3.4)$$

where \dot{m}_f is the mass burning rate of the fuel (kg/s), \dot{m}_g is the mass flow rate of hot gases out of the opening (kg/s) and \dot{m}_a is the mass flow rate of air into the opening (kg/s).

The mass flow rate out through an opening (\dot{m}_g) is given by Rockett, 1976:

$$\dot{m}_g = \frac{2}{3} C_d W_0 \rho_\infty \left[2g \frac{T_\infty}{T_U} \left(1 - \frac{T_\infty}{T_U} \right) \right]^{\frac{1}{2}} (H_0 - Z_N)^{\frac{3}{2}} \quad (3.5)$$

where, C_d is the orifice constriction coefficient (typically ≈ 0.7), W_0 is the opening width (m), ρ_∞ is the ambient air density (kg/m^3), g is the gravity (m/s^2), T_∞ is the ambient temperature (K), T_U is the hot gas layer temperature (K), H_0 is the opening height (m) and Z_N is the height of the neutral plane (m), which is the height where the pressure difference across the opening is zero.

The mass flow rate in through an opening (\dot{m}_a) is given by:

$$\dot{m}_a = \frac{2}{3} C_d W_0 \rho_\infty \left[2g \left(1 - \frac{T_\infty}{T_U} \right) \right]^{\frac{1}{2}} (Z_N - Z_{int})^{\frac{1}{2}} \left(\frac{Z_N + Z_{int}}{2} \right) \quad (3.6)$$

where, Z_{int} is the interface layer height (m).

The expressions for mass flow in (\dot{m}_a) and mass flow out (\dot{m}_g) cannot be solved directly to solve the hot gas layer temperature (T_U), since both the height of the neutral plane (Z_N) and the interface layer height (Z_{int}) are unknown.

However, if the mass burning rate of the fuel (\dot{m}_f) is small compared with the mass flow rate of air into the compartment (\dot{m}_a), we can neglect \dot{m}_f and assume:

$$\dot{m}_a = \dot{m}_g \quad (3.7)$$

The conservation of energy applied at the upper layer is described by:

$$\dot{Q} = \dot{Q}_W + \dot{Q}_L \quad (3.8)$$

where \dot{Q}_W is the heat loss due to conduction through the boundaries and \dot{Q}_L is the heat loss due to convection through the openings, so the expressions can be rewritten as:

$$\dot{Q} = h_k A_T (T_U - T_\infty) + \dot{m}_g C_p (T_U - T_\infty) \quad (3.9)$$

where h_k is the effective heat transfer coefficient (kW/(m²·K)), A_T is the total area of the compartment enclosing surface (m²) and C_p is the specific heat of gas (kJ/(kg·K)).

The effective heat transfer coefficient can be determined using a steady-state approximation, when the time of exposure, t , is greater than the thermal penetration time, t_p :

$$h_k = \frac{k}{\delta} \quad t > t_p \quad (3.10)$$

Or using an approximation based on conduction in a semi-infinite solid, when the time of exposure, t , is smaller or equal to the thermal penetration time, t_p :

$$h_k = \left(\frac{k \rho_w c}{t} \right)^{\frac{1}{2}} \quad t \leq t_p \quad (3.11)$$

where k is the thermal conductivity of the wall material (kW/mK), ρ_w is the density of the wall material (kg/m³), c is the specific heat of the wall (kJ/kgK) and t is the exposure time (s).

The thermal penetration time is defined as:

$$t_p = \left(\frac{\rho_w c}{k} \right) \left(\frac{\delta}{2} \right)^2 \quad (3.12)$$

where δ is the thickness of the compartment wall (m).

3.6 The MQH Method

This conservation energy expression, Equation 3.9, and a correlation to data have been applied by McCaffrey et al., 1981, to obtain an approximation of the upper layer temperature in a compartment. Their method is known as the MQH method.

Rearranging Equation 3.9, the dimensionless temperature rise is obtained in terms of two dimensionless groups:

$$\frac{\Delta T}{T_{\infty}} = \frac{\dot{Q}/(C_P T_{\infty} \dot{m}_g)}{1 + h_k A_T / (C_P \dot{m}_g)} \quad (3.13)$$

where ΔT is the upper layer temperature rise above ambient ($T_U - T_{\infty}$) (K).

The mass flow rate of hot gases through an opening can be rewritten from Equation 3.5:

$$\dot{m}_g = \frac{2}{3} C_d W_0 H_0^{\frac{3}{2}} \rho_{\infty} \left[2g \frac{T_{\infty}}{T_U} \left(1 - \frac{T_{\infty}}{T_U} \right) \right]^{\frac{1}{2}} \left(1 - \frac{Z_N}{H_0} \right)^{\frac{3}{2}} \quad (3.14)$$

According to McCaffrey et al., 1981, since Z_N depends basically on T_U , \dot{Q} , and the ventilation factor, \dot{m}_g may be replaced by $\sqrt{g} \rho_{\infty} A_0 \sqrt{H_0}$, without losing generality, once the effects of T_U and \dot{Q} were incorporated into the correlation via other terms.

Based on the correlation of the data from eight sets of experiments (112 experiments), the Equation 3.13 can be written as a power relationship [McCaffrey et al., 1981]:

$$\frac{\Delta T}{T_{\infty}} = 1.6 \left(\frac{\dot{Q}}{\sqrt{g} C_P \rho_{\infty} T_{\infty} A_0 \sqrt{H_0}} \right)^{\frac{2}{3}} \left(\frac{h_k A_T}{\sqrt{g} C_P \rho_{\infty} A_0 \sqrt{H_0}} \right)^{-\frac{1}{3}} \quad (3.15)$$

This correlation was obtained from data including both steady-state and transient fires in cellulosic and synthetic materials, and gaseous hydrocarbon fuels and its limitations are:

1. It holds for compartment upper layer temperatures up to approximately 600 °C;
2. It can be applied for both, steady-state or transient fires;
3. It cannot be applied to rapidly developing fires in large enclosures, in which significant fire growth has occurred before the hot gases have exited the enclosure;
4. This correlation does not include data from extensive ventilation-controlled fires nor combustible walls or ceilings;
5. The data corresponds to fire sources at the center of the room.

Several other hand-calculation methods can be applied to approximate upper layer temperature (see Walton and Thomas, 2002), but these methods do not take into account the fire source position. However, Mowrer and Williamson, 1987, developed modification factors

to adjust the MQH correlation and extend its applicability to wall and corner burning geometries, obtaining a reasonable agreement.

4 FIRE DYNAMICS SIMULATOR MATHEMATICAL MODEL

Fire Dynamics Simulator (FDS), is a computational fluid dynamics (CFD) model of fire-driven fluid flow. It is a free and open source code in Fortran, developed by the National Institute of Standards and Technology (NIST) and VTT Technical Research Centre of Finland. It solves numerically the Navier-Stokes equations adapted for low-speed ($Ma < 0.3$), thermally-driven flow with an emphasis on smoke and heat transport from fires.

Some of the major features of the model are according McGrattan et al., 2017a:

- Low Mach, large-eddy simulation (LES);
- Explicit, second-order, kinetic-energy-conserving numerics;
- Structured, uniform, staggered grid;
- Simple immersed boundary method for treatment of flow obstructions;
- Generalized “lumped species” method (simplified chemistry using a reaction progress variable);
- Deardorff eddy viscosity subgrid closure;
- Constant turbulent Schmidt and Prandtl numbers;
- Eddy dissipation concept (fast chemistry) for single-step reaction between fuel and oxidizer;
- Gray gas radiation with finite volume solution to the radiation transport equation;

FDS is described as a “fire model” because it incorporates source terms and boundary conditions that describe the turbulent combustion of gaseous fuel and oxygen, the transport of thermal radiation through hot, soot-laden gases, the thermal decomposition of real materials, the activation of sprinklers and smoke detectors, the transport of water and liquid fuel droplets, and a variety of other features that describe fires inside and outside of buildings [McGrattan et al., 2017a].

This chapter presents the governing equations of Fire Dynamic Simulator (FDS), the applied models and assumptions, and its solution procedures:

4.1 Numerical Grid

FDS was designed to simulate buoyant-driven flows within buildings (compartment fires), so its numerical grid is rectilinear by simplicity. In addition, for LES models uniform meshing is always preferred and a staggered grid is employed to avoid “checker-boarding” in pressure-velocity coupling by naturally representing the pressure cell velocity divergence.

The governing equations are approximated using second-order accurate finite differences on a collection of uniformly spaced three-dimensional grids.

4.2 Fundamental Equations

The set of equations which describe the fire phenomenon is composed by the Mass conservation equation (Equation 4.1), the Energy conservation equation (Equation 4.2), the Momentum conservation equation (Equation 4.3) and the equation of state (Equation 4.4).

$$\frac{\partial \rho}{\partial t} + \nabla \cdot (\rho \mathbf{u}) = \dot{m}_b''' \quad (4.1)$$

$$\frac{\partial}{\partial t} (\rho h_s) + \nabla \cdot (\rho h_s \mathbf{u}) = \frac{D\bar{p}}{Dt} + \dot{q}''' + \dot{q}_b''' - \nabla \cdot \mathbf{q}'' \quad (4.2)$$

$$\frac{\partial(\rho \mathbf{u})}{\partial t} + \rho(\mathbf{u} \cdot \nabla) \mathbf{u} = -\nabla p + \rho \mathbf{g} + \mathbf{f}_b + \nabla \cdot \bar{\tau} \quad (4.3)$$

$$\bar{p} = \frac{\rho R T}{\bar{W}} \quad (4.4)$$

where ρ is the density, t is the time, \mathbf{u} is the velocity vector, \dot{m}_b''' is the source term of mass, h_s is the sensible enthalpy, \bar{p} is the background pressure, \dot{q}''' is the heat release rate per unit volume from a chemical reaction, \dot{q}_b''' is the energy transferred to subgrid-scale droplets and particles and \mathbf{q}'' represents the conductive, diffusive, and radiative heat fluxes, p is the pressure, \mathbf{g} is the gravity, \mathbf{f}_b represents the drag force exerted by the subgrid-scale particles and droplets, $\bar{\tau}$ is the viscous stress tensor, T is the temperature, R is the universal gas constant, and \bar{W} is the molecular weight of the gas mixture.

4.3 Simplifying Assumptions

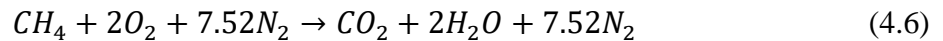
a) Lumped Species Approach

The lumped species approach reduces the computational burden of the full chemical system by combining species into groups that transport and react together, so the number of transport equations to be solved is reduced, which significantly increases the speed of the code [McGrattan et al., 2017a].

FDS assumes a single-step reaction, so only two transport equations must be solved explicitly (one for the fuel and one for the products) [McGrattan et al., 2017a]. In fire problems the primitive species are lumped into reacting groups and a simple reaction is expressed by:



So, in terms of primitive species, for methane, the fuel applied to this research, a one-step reaction may be written as:



The transport equation for each of the lumped species is expressed by Equation 4.7:

$$\frac{\partial}{\partial t}(\rho Z_\alpha) + \nabla \cdot (\rho Z_\alpha \mathbf{u}) = \nabla \cdot (\rho D_\alpha \nabla Z_\alpha) + \dot{m}'''_\alpha + \dot{m}'''_{b,\alpha} \quad (4.7)$$

where Z_α is the species mixture, \mathbf{u} is the velocity vector, D_α is the diffusion coefficient, \dot{m}'''_α is the mass production rate per unit volume of species α by chemical reactions and $\dot{m}'''_{b,\alpha}$ represents the addition of mass from evaporating droplets or other subgrid-scale particles.

According to McGrattan et al., 2017a, the diffusivity (D_α) is taken from the molecular and turbulent viscosities divided by the turbulent Schmidt number $((\mu + \mu_t)/Sc_t)$. The turbulent Schmidt number is constant with default value $Sc_t = 0.5$.

The mass density is obtained from $\rho = \sum(\rho Z)_\alpha$ and the summation of Equation 4.7 over all n species gives by the continuity equation (Equation 4.1).

b) Low Mach Number Approximation

According to the methodology described by Rehm and Baum, 1978, the spatially and temporally resolved pressure, p , can be decomposed into a “background” pressure, $\bar{p}(z, t)$, plus a perturbation, $\tilde{p}(x, y, z, t)$.

The background pressure is a function of the spatial coordinate in the direction of gravity (z), so the stratification of the atmosphere is included in the background pressure, while the perturbation, \tilde{p} , drives the fluid motion.

According to McGrattan et al., 2017a, the purpose of decomposing the pressure is that for low Mach number flows ($Ma < 0.3$), it can be assumed that the temperature and density are inversely proportional, and thus the equation of state can be approximated as:

$$\bar{p} = \rho T R \sum_{\alpha} \frac{Z_{\alpha}}{W_{\alpha}} \equiv \frac{\rho R T}{\bar{W}} \quad (4.8)$$

where T is the temperature, R is the universal gas constant, W_{α} is the molecular weight of gas species α and \bar{W} is the molecular weight of the gas mixture.

A consequence of the low Mach number approximation is that the internal energy, e , and enthalpy, h , may be related in terms of the thermodynamic (background) pressure: $h = e + \bar{p}/\rho$, so, the energy conservation equation may then be written in terms of the sensible enthalpy, h_s , according to Equation 4.2.

It is important to note that the Equation 4.2 is not solved explicitly by the FDS, but through the velocity divergence, instead:

$$\nabla \cdot \mathbf{u} = \frac{1}{\rho h_s} \left[\frac{D}{Dt} (\bar{p} - \rho h_s) + \dot{q}''' + \dot{q}_r''' + \dot{q}_b''' - \nabla \cdot \dot{\mathbf{q}}'' \right] \quad (4.9)$$

According to McGrattan et al., 2017a, once a low Mach number is assumed, the velocity divergence plays an important role in the overall solution scheme. This assumption has two purposes: filtering of acoustic waves, so the time step in the numerical algorithm is bound only by the flow speed as opposed to the speed of sound, and the reduction in the number of dependent variables in the system of equations by one.

4.4 Combustion Model

FDS addresses combustion reactions through the “mixed is burnt” assumption, which considers the mixing-limited, infinitely fast reaction of lumped species, so, the mean chemical source term for fuel is modelled using the Eddy Dissipation Concept (EDC) of Magnussen and Hjertager, 1977:

$$\dot{m}_F''' = -\rho \frac{\min(Z_F, Z_A/s)}{\tau_{min}} \quad (4.10)$$

where Z_F and Z_A are the mass fractions of the lumped species Fuel and Air, respectively, and s is the mass stoichiometric coefficient for Air. The quantity τ_{min} is a time scale for mixing which must be modelled.

4.5 Radiation Model

The radiative heat flux is calculated through the Radiative Transport Equation (RTE) for non-scattering gases. As the spectral dependence of the RTE cannot be resolved easily, the radiation spectrum is divided into bands and a separate RTE is derived for each band. The band specific RTE for a non-scattering gas is:

$$S \cdot \nabla I_n(x, s) = B_n(x) - \kappa_n(x) I_n(x, s), \quad n = 1 \dots N \quad (4.11)$$

where I_n is the intensity integrated over the band n , s is the direction vector of the intensity, κ_n is the appropriate mean absorption coefficient for the band and $B_n(x)$ is the emission source term for band n . When the intensities corresponding to the bands are known, the total intensity is calculated by summing over all the bands:

$$I(x, s) = \sum_{n=1}^N I_n(x, s) \quad (4.12)$$

The emission source term for radiation band n is given by:

$$B_n(x) = \kappa_n(x)I_{b,n}(x) \quad (4.13)$$

where $I_{b,n}$ is the fraction of the blackbody radiation at temperature $T(x)$:

$$I_{b,n}(x) = F_n(\lambda_{min}, \lambda_{max})\sigma [T(x)]^4 / \pi \quad (4.14)$$

and σ is the Stefan-Boltzmann constant and F_n is the view factor.

Even when a small number of bands are considered, solving multiple RTEs is very time consuming, so, for simplification, the Gray Gas assumption can be made. That is the approach employed in the current dissertation.

McGrattan et al., 2017a, state that, in most large-scale fire scenarios soot is the most important combustion product controlling the thermal radiation from the fire and hot smoke and as the radiation spectrum of soot is continuous, it is possible to assume that the gas behaves as a gray medium. The spectral dependence is then lumped into one absorption coefficient ($N = 1$) and the source term is given by the blackbody radiation intensity [Ludwig et al., 1973]:

$$I_b(x) = \frac{\sigma[T(x)]^4}{\pi} \quad (4.15)$$

The gas phase contribution to the radiative loss term in the energy equation is (considering the gray gas assumption):

$$\dot{q}_r''' \equiv -\nabla \cdot \dot{q}_r''(x) = \kappa(x)[U(x) - 4\pi I_b(x)] \quad ; \quad U(x) = \int_{4\pi} I(x, s') ds' \quad (4.16)$$

or, for N bands:

$$-\nabla \cdot \dot{q}_r''(x) = \sum_{n=1}^N \kappa(x)U_n(x) - 4\pi B_n(x) \quad ; \quad U_n(x) = \int_{4\pi} I_n(x, s') ds' \quad (4.17)$$

The mean absorption coefficient, κ , is obtained from a narrow-band model called RadCal and the radiation equation is solved using a Finite Volume Method (FVM), considering approximately 100 discrete angles which are updated over multiple time steps.

4.6 Large Eddy Simulation Model (LES)

The equations for large eddy simulation (LES) are derived by applying a low-pass filter, parameterized by a width (Δ), to the transport equations for mass, momentum and energy [McGrattan et al., 2017a]. In FDS, the filter width is taken to be the cube root of the cell volume, $\Delta = V_c^{\frac{1}{3}}$, $V_c = \delta_x \delta_y \delta_z$ and is a key parameter in the submodels for the turbulent viscosity and the reaction time scale.

The main goal of the LES is to evolve the cell mean values of mass, momentum and energy explicitly, while accounting for the subgrid transport and chemistry effects.

So, the LES momentum equation becomes:

$$\frac{\partial \bar{\rho} \tilde{u}_i}{\partial t} + \frac{\partial}{\partial x_j} (\bar{\rho} \tilde{u}_i \tilde{u}_j) = -\frac{\partial \bar{p}}{\partial x_i} - \frac{\partial \bar{\tau}_{ij}}{\partial x_j} - \frac{\partial \tau_{ij}^{sgs}}{\partial x_j} + \bar{\rho} g_i + \bar{f}_{d,i} + \overline{\dot{m}_b'''} \tilde{u}_{b,i} \quad (4.18)$$

where the subgrid scale stress, τ_{ij}^{sgs} , is given by:

$$\tau_{ij}^{sgs} \equiv \bar{\rho} (\tilde{u}_i \tilde{u}_j - \tilde{u}_i \tilde{u}_j) \quad (4.19)$$

According to McGrattan et al., 2017a, the ‘‘turbulence model’’ refers to the closure for SGS flux term and in FDS, gradient diffusion is the turbulence model used to close both the SGS momentum and scalar flux terms. Constant Schmidt number (for mass diffusivity) or Prandtl number (for thermal diffusivity) are applied to obtain the turbulent diffusivity.

In the present work, the turbulent viscosity (μ_t) is obtained through Deardorff model.

4.6.1 Deardorff Model

For this study the default FDS model was employed to obtain the turbulent viscosity, the Deardorff model [Deardorff, 1980]:

$$\mu_t = \rho C_V \Delta \sqrt{k_{sgs}}; k_{sgs} = \frac{1}{2} ((\bar{u} - \hat{u})^2 + (\bar{v} - \hat{v})^2 + (\bar{w} - \hat{w})^2) \quad (4.20)$$

where \bar{u} is the average value of u at the grid cell center and \hat{u} is a weighted average of u over the adjacent cells:

$$\bar{u}_{ijk} = \frac{\bar{u}_{ijk} + \bar{u}_{i-1,jk}}{2}; \hat{u}_{ijk} = \frac{\bar{u}_{ijk}}{2} + \frac{\bar{u}_{i-1,jk} + \bar{u}_{i+1,jk}}{4} \quad (4.21)$$

The terms \hat{v} and \hat{w} are defined similarly and the model constant is set to the value $C_V = 0.1$, in accordance to Pope, 2000.

4.7 Time Step and Solution Procedure

Once FDS applies the explicit schemes, stability criteria may often be understood in terms of using the time step (δt) to maintain conditions physically realizable [McGrattan et al., 2017a].

The time step is usually set automatically by dividing the size of a mesh cell by the characteristic velocity of the flow and during the calculation, it is adjusted to satisfy the CFL (Courant, Friedrichs, Lewy) condition. The default value of δt is $5(\delta x \delta y \delta z)^{\frac{1}{3}} / \sqrt{gH}$, where δx , δy , and δz are the dimensions of the smallest mesh cell, H is the height of the computational domain, and g is the acceleration of gravity (McGrattan et al., 2017b).

The Courant, Friedrichs, Lewy (CFL) constraint is given by:

$$CFL = \delta t \frac{\|u\|}{\delta x} \approx 1 \quad (4.22)$$

At the end of the first part of the explicit predictor-corrector time update, the time step is checked to ensure that it is within the appropriate stability bounds. If it is not, it is adjusted up or down by 10% (or until it is within limits) and the predictor part of the time step is re-run (McGrattan et al., 2017b).

The solution procedure advances the variables in time using an explicit second-order predictor/corrector scheme.

5 METHODOLOGY

This chapter describes the Steckler's Experiment (which was employed in the validation step of this work), the cases simulated in FDS, the mesh resolution analysis, the comparison between numerical and experimental data and the procedure employed to the data correlation.

5.1 Steckler's Experiment

Steckler et al. (1982a, 1982b, 1984a, 1984b) described the results of 55 full-scale steady-state experiments conducted to study the flow induced by a pool fire in a compartment under conditions characteristic of the developing fire period (pre-flashover). The room is a $2.8 \text{ m} \times 2.8 \text{ m} \times 2.13 \text{ m}$ compartment and its geometry can be seen in Figure 5.1.

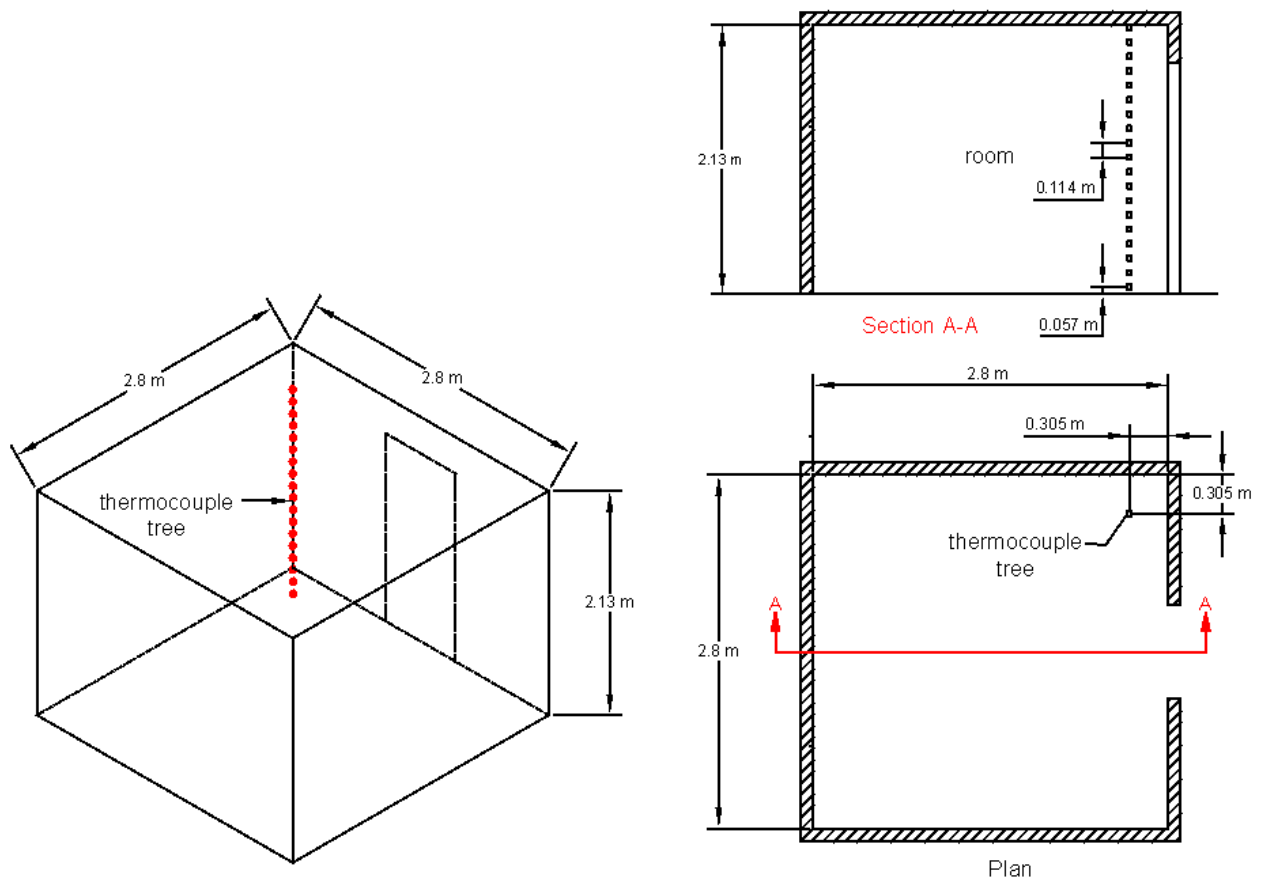


Figure 5.1 - Room geometry and thermocouple tree position

The compartment was built of light weighted walls and ceiling, which were covered with a 12.7 mm ceramic fiber insulation board to establish near-steady conditions within 30 minutes following ignition of the 30 cm diameter porous plate diffusion burner. That burner was supplied with methane at a fixed rate. Four constant heat release rates (HRR) were tested (31.6, 62.9, 105.3 and 158 kW). The compartment floor was composed of 19 mm calcium silicate board on top of 12.7 mm plywood on wood joists. The ceramic fiber insulation board properties can be found in Table 5.1.

Table 5.1 - Compartment wall and ceiling properties

Material	Density [kg/m ³]	Heat capacity [J/(kg·K)]	Thermal conductivity [W/(m·K)]
Ceramic fiber insulation board	260	1000	0.08

Ten door and window opening configurations (i.e., ten ventilation factors) were tested in these experiments. The configurations used in Steckler's experiments and reproduced in the present study can be observed in Figure 5.2.

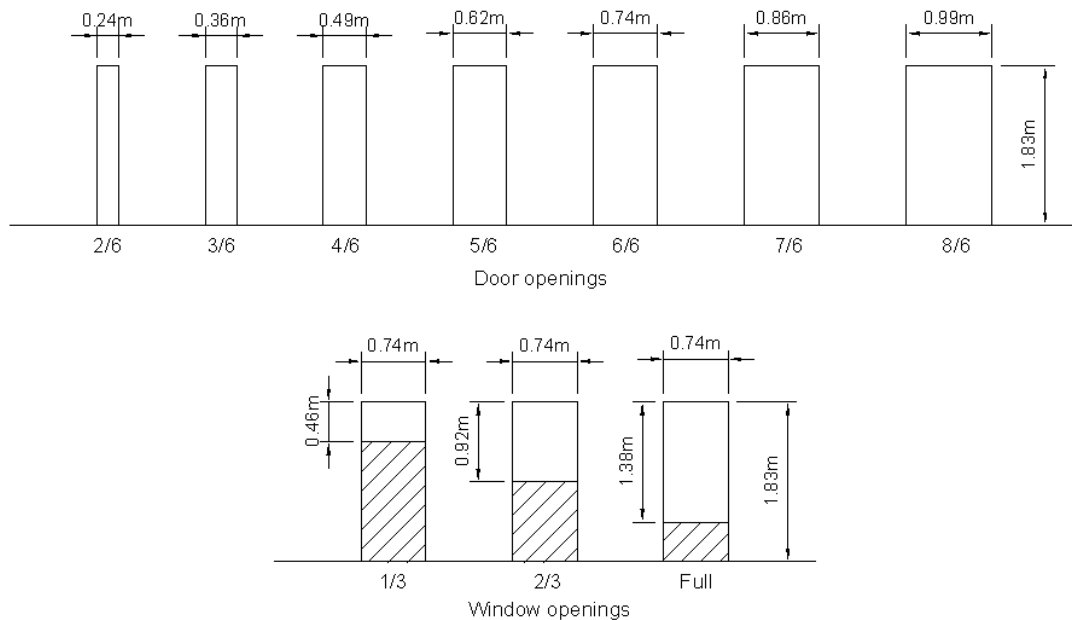


Figure 5.2 - Room opening configurations

Three heat source locations were analysed during the validation step: the center of the room (position A), the back wall (position C) and back left corner (position B) (positions shown in Figure 5.3). Therefore, 40 Steckler's cases have been considered for the validation step.

5.2 FDS Simulations

The CFD model called FDS was applied to generate data for pre-flashover compartment fires with different fire positions. These data were employed to fit the correlations developed to predict hot gas layer temperature. The version employed was the FDS 6.6.0.

The simulations have been run at the Cluster GAUSS located at the National Center for Supercomputing (CESUP) of the Federal University of Rio Grande do Sul (UFRGS). This Cluster consists of 64 processing units, with 64 GB of RAM and 2 dodecacore AMD Opteron processors each, resulting in 1536 processing cores and a theoretical performance of 24 TFlops (simple precision). The simulation domain was divided into nine meshes, so, the Cluster was set to work with nine nodes (one for each mesh) and two processors (cores) per node. This configuration was chosen through an efficiency study and presented the best results, which resulted in computational times of the order of fifty hours for each simulation.

Thirteen cases were simulated in each of the 15 ground positions shown in Figure 5.3. The studied cases are summarized in Table 5.2.

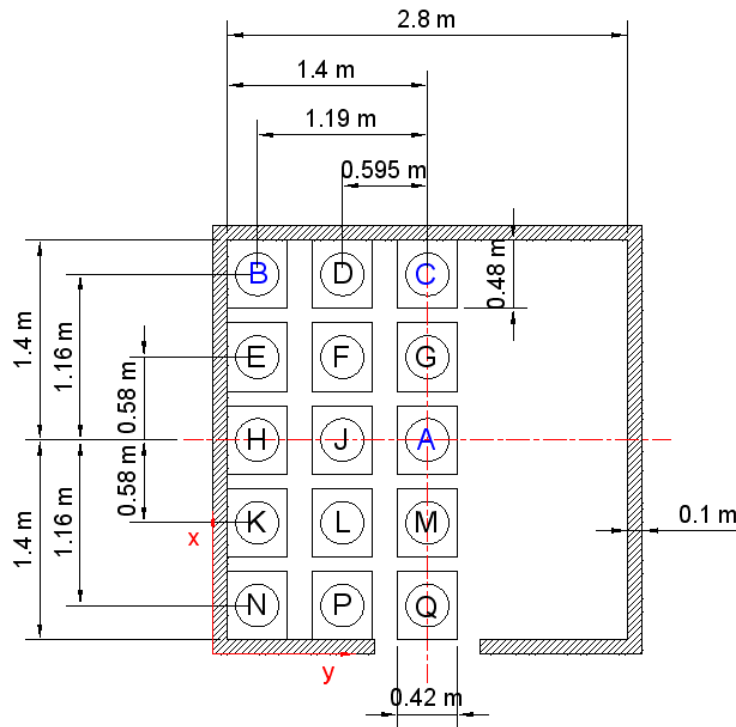


Figure 5.3 - Fifteen studied fire source ground positions

Table 5.2 - List of openings and HRRs employed in the simulations

#	Opening	HRR (kW)	T_{∞} (°C)
1	2/6 (0.24 × 1.83 m)	62.9	24
2	3/6 (0.36 × 1.83 m)	62.9	24
3	4/6 (0.49 × 1.83 m)	62.9	24
4	5/6 (0.62 × 1.83 m)	62.9	24
5	6/6 (0.74 × 1.83 m)	62.9	24
6	7/6 (0.86 × 1.83 m)	62.9	24
7	8/6 (0.99 × 1.83 m)	62.9	24
8	Full window (0.74 × 1.38 m)	62.9	24
9	2/3 window (0.74 × 0.92 m)	62.9	24
10	1/3 window (0.74 × 0.46 m)	62.9	24
11	6/6 (0.74 × 1.83 m)	31.6	24
12	6/6 (0.74 × 1.83 m)	105.3	24
13	6/6 (0.74 × 1.83 m)	158	24

Basing on the findings of the 15 fire positions on ground level, 19 different elevations on the positions A, B and C were simulated (Figure 5.4). A total of 195 fire scenarios were simulated for the ground fire analysis, and 57 fire scenarios were simulated for the elevated fire source analysis.

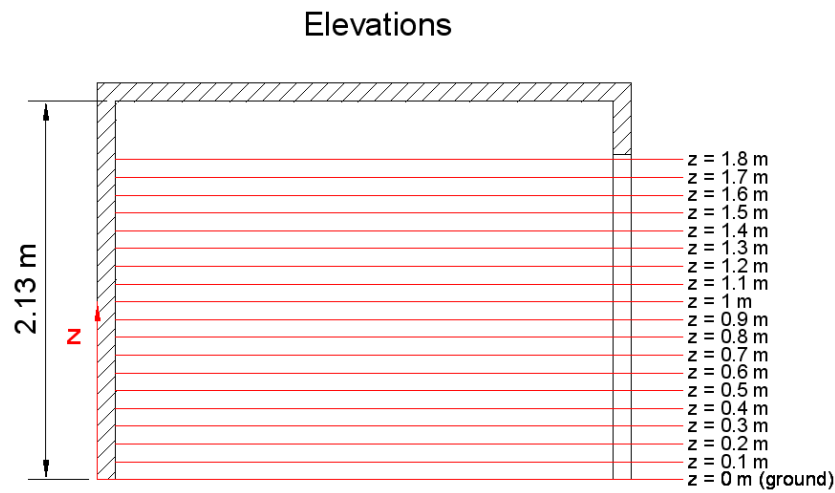


Figure 5.4 - Fire source elevations

A thermocouple tree of aspirated thermocouples in the front corner of the room measured the gas temperature profile. The hot gas layer temperature (T_U) was obtained through the average value of the temperature in the upper portion of the room, above the profile curve inflection (see Figures 5.7 to 5.9). The same method is applied to the lower layer

temperature (T_L). Then for the interface height (Z_{int}) the data reduction described by Janssens and Tran, 1992, was applied:

$$Z_{int} = \frac{T_L(I_1 I_2 - H^2)}{I_1 + I_2 T_L^2 - 2T_L H} \quad (5.1)$$

where

$$I_1 = (H - Z_{int})T_U + Z_{int}T_L = \int_0^H T(z) dz \quad (5.2)$$

and

$$I_2 = (H - Z_{int})\frac{1}{T_U} + Z_{int}\frac{1}{T_L} = \int_0^H \frac{1}{T(z)} dz \quad (5.3)$$

The thermocouples were modelled to represent the characteristics of the physical ones in the experiments. The thermocouple tree can be seen in Figure 5.1.

All cases were simulated for 900 s, and reached steady state. The temperature results were obtained through an average calculation from 800s to 900s, to compensate the oscillatory results caused by the LES turbulence model.

5.2.1 Initial and Boundary Conditions

For the validation step the initial ambient temperature (T_∞) was considered the same of the experiments, varying for each case, these values can be found in Table 5.6. However, for the cases run to generate data the initial ambient temperature was specified as 24 °C for all the cases, so the upper layer temperature could be analysed properly, once it depends on this initial condition. The initial and ambient pressure (p_∞) was specified as 101,325 kPa for all the cases.

The floor was considered as adiabatic, while walls and ceiling were modelled as 0.1 m thickness surfaces with the properties described in Table 5.1. These surfaces (walls and ceiling) have insulation characteristics of ceramic fiber boards, but still allow some conductive heat transfer.

The fuel applied to all cases was methane with a constant HRR, according to Table 5.2.

5.3 Mesh Resolution

As stated by Zhiyin, 2015, in LES simulations the computational mesh must be fine enough to resolve the smallest dynamically significant length-scale (the Kolmogorov micro-scale).

According to Gaitonde, 2008, generally, LES results are in better agreement with experimental evidence compared to RANS if a sufficiently fine grid is employed. However, without a prior knowledge of flow characteristics, it is difficult to verify the ‘sufficient’ resolution.

Three different methods were applied to ensure the mesh resolution. The first was the analysis of the non-dimensional parameter D^*/δ_x , the second was the comparison between results for different mesh sizes and the third was the Measurement of the Turbulence Resolution (MTR).

As suggested by McGrattan et al., 2017b, 2017c, for simulations involving buoyant plumes, the non-dimensional parameter D^*/δ_x is a good way to determine how well the flow field is resolved. D^* is the characteristic fire diameter expressed by Equation 5.4 and δ_x is the nominal size of a mesh cell.

$$D^* = \left(\frac{\dot{Q}}{\rho_\infty C_p T_\infty \sqrt{g}} \right)^{\frac{2}{5}} \quad (5.4)$$

where \dot{Q} is the HRR, ρ_∞ is the ambient air density, C_p is the specific heat of the air, T_∞ is the ambient temperature and g is the gravity acceleration.

According to McDermott et al., 2010, $D^*/\delta_x \approx 10$ has historically been considered an adequate grid resolution. The validation study sponsored by the U.S. Nuclear Regulatory Commission [Stroup and Lindeman, 2013], suggested D^*/δ_x values ranging from 4 to 16.

Table 5.3 presents the values of D^* and D^*/δ_x for four mesh sizes ($\delta_x = 6$ cm, 5 cm, 4 cm and 3 cm). These meshes are equally spaced in all directions x - y - z , and they are uniform all over the computational domain. As can be observed in Table 5.3, all meshes present D^*/δ_x

contained inside the recommended range. Figure 5.5 shows a representation of the tested meshes.

Table 5.3 - Values of D^* and D^*/δ_x for meshes 6 cm, 5 cm, 4 cm and 3 cm

HRR (kW)	D^*	D^*/δ_x			
		$\delta_x = 6 \text{ cm}$	$\delta_x = 5 \text{ cm}$	$\delta_x = 4 \text{ cm}$	$\delta_x = 3 \text{ cm}$
31.60	0.24	4.02	4.83	6.03	8.04
62.90	0.32	5.29	6.35	7.94	10.58
105.30	0.39	6.51	7.81	9.76	13.01
158.00	0.46	7.65	9.19	11.48	15.31

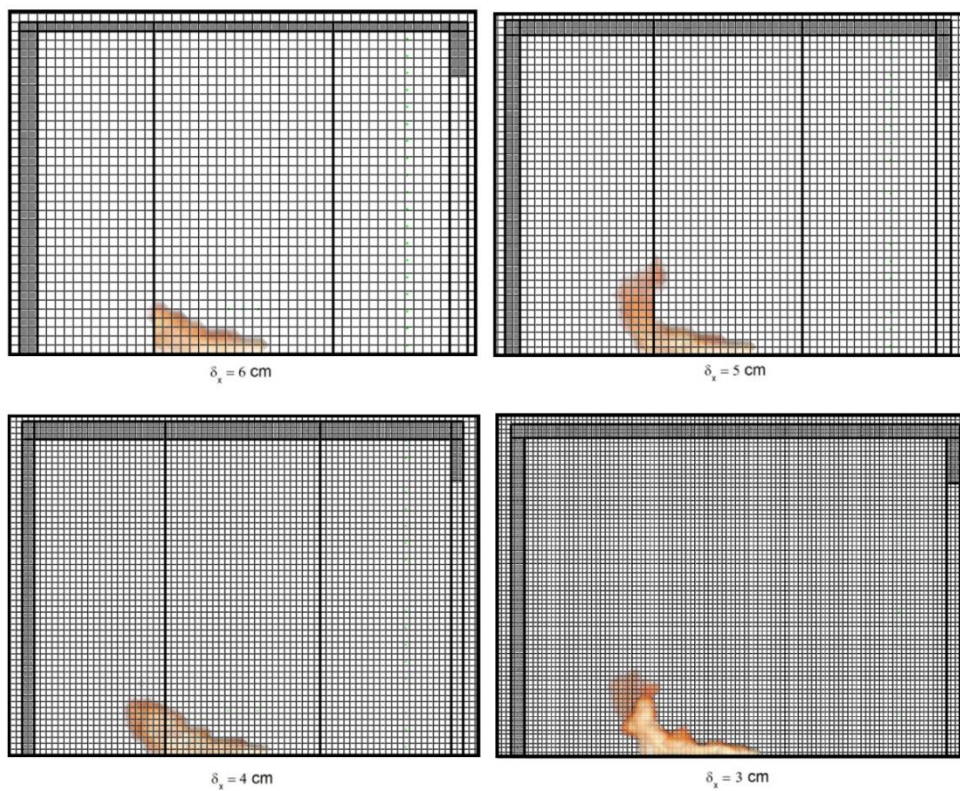


Figure 5.5 - Comparison of the mesh sizes ($\delta_x = 6 \text{ cm}$, 5 cm , 4 cm and 3 cm) tested during the mesh resolution analysis

Additionally, a mesh sensitivity analysis was performed. The temperature profiles, and the average hot gas layer temperature, average lower layer temperature and the computational time obtained for the four different meshes applied to Steckler's case 14 (see Table 5.6) are shown in Figure 5.6 and Table 5.4, respectively.

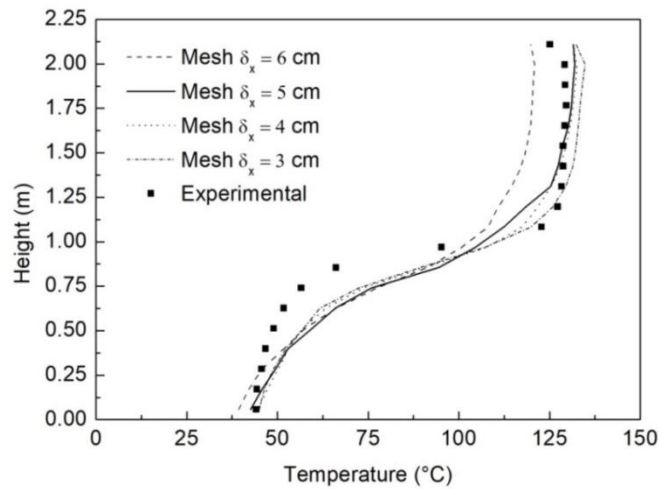


Figure 5.6 - Mesh sensitivity analysis (Steckler's case 14)

Table 5.4 - Mesh sensitivity analysis and computational time

Mesh size	T_U (°C)	T_L (°C)	Time (h)
$\delta x = 6$ cm	115.6	50.49	30.29
$\delta x = 5$ cm	124.82 (7.4%)	52.72	54.97
$\delta x = 4$ cm	126.29 (1.2%)	52.59	138.12
$\delta x = 3$ cm	128.55 (1.8%)	51.94	227.02

As can be observed, meshes $\delta_x = 5$ cm, 4 cm and 3 cm present similar results, all of them agreeing well with the experimental data. So, the mesh $\delta_x = 5$ cm has been chosen to be applied, as a matter of computational time and results stability.

To ensure the right selection of the mesh, the Measure of Turbulence Resolution (MTR) for the 5 cm mesh has been calculated, according to Equation 5.5:

$$MTR(x) = \frac{\langle k_{sgs} \rangle}{\langle TKE \rangle + \langle k_{sgs} \rangle} \quad (5.5)$$

where the resolved turbulent kinetic energy per unit mass (TKE) is given by:

$$TKE = \frac{1}{2} (\tilde{u}_i - \langle \tilde{u}_i \rangle) (\tilde{u}_i - \langle \tilde{u}_i \rangle) \quad (5.6)$$

\tilde{u}_i is the resolved LES velocity and can be obtained directly from FDS for each velocity component.

The subgrid kinetic energy (k_{sgs}) is estimated from Deardorff's eddy viscosity model previously presented in Equation 4.20, and its results are obtained from FDS.

The MTR value was calculated based on 15 points measured inside the flame. The results presented on Table 5.5 are the mean MTR values.

Table 5.5 - MTR for mesh $\delta x = 5$ cm

HRR (kW)	MTR (5 cm)
31.60	0.173
62.90	0.159
105.30	0.140
158.00	0.137

According to Pope, 2004, the MTR value has to be less or equal to 0.2, which corresponds to the resolution of 80% of the turbulent kinetic energy. So, as can be seen the selected mesh is capable to resolve more than 80% of the kinetic energy in the flow field. Additionally, as showed by McDermott et al., 2010, a MTR mean value near 0.2 provides satisfactory results for mean velocities and species concentrations in non-reacting, buoyant plumes.

More information about Measure of Turbulent Resolution can be found in McGrattan et al., 2017c.

5.4 Comparison with Experimental Data

To validate the numerical model, the results of hot gas layer temperature (T_U) and interface height (Z_{int}) are compared to experimental data presented by Steckler et al., 1982a, 1982b, and Steckler et al., 1984a, 1984b. The 40 fire scenarios described have been investigated. The description of the investigated scenarios and its results can be seen in Table 5.6. On experiments 160, 163 and 164 the fire sources are raised 0.3 m from the floor, while it is on the ground for the other experiments.

As can be observed in Table 5.6, the numerical model was validated, since for the upper layer temperature the maximum relative error found was 13.98% and the absolute average relative error was 3.17%, while the layer interface heights were predicted within the experimental uncertainty range.

The comparison between experimental temperature profiles and the ones obtained by FDS for fire source positions A, B and C can be seen in Figures 5.7, 5.8 and 5.9, respectively.

Table 5.6 - Comparison between numerical (FDS, present study) and experimental (Steckler's) results

Test ²	Opening ³	HRR (kW)	Fire position	T_{∞} [°C]	T_U (Exp) [°C]	T_U (FDS) [°C]	Relative Dif. [%]	Z_{int} (Exp) [m]	Z_{int} (FDS) [m]	ΔZ_{int} (Exp - FDS) [m]
10	2/6	62.9	A	26	190	203.61	-7.16	0.57 ±0.28	0.32	0.25
11	3/6	62.9	A	28	164	154.29	5.92	0.74 ±0.23	0.56	0.18
12	4/6	62.9	A	22	141	134.98	4.27	0.86 ±0.23	0.81	0.05
13	5/6	62.9	A	23	129	126.72	1.77	0.91 ±0.17	0.79	0.12
14	6/6	62.9	A	29	129	126.85	1.67	0.97 ±0.23	0.92	0.05
16	7/6	62.9	A	26	120	113.72	5.23	1.03 ±0.17	0.90	0.13
17	8/6	62.9	A	22	109	102.54	5.93	1.09±0.23	0.91	0.18
22	Full Win.	62.9	A	30	143	145.69	-1.88	0.74±0.34	0.47	0.27
23	2/3 Win.	62.9	A	26	177	181.43	-2.50	0.74±0.34	0.41	0.33
41	1/3 Win.	62.9	A	16	270	259.62	3.84	0.80±0.17	0.64	0.16
19	6/6	31.6	A	29	86	86.13	-0.15	0.97±0.11	0.88	0.09
20	6/6	105.3	A	35	183	187.78	-2.61	0.97±0.11	0.93	0.04
21	6/6	158	A	36	243	244.83	-0.75	0.91±0.17	0.80	0.11
160	6/6	62.9	Ar ¹	6	136	126.66	6.87	1.26±0.17	1.13	0.13
114	2/6	62.9	B	32	248	253.54	-2.23	1.14±0.17	0.99	0.15
144	3/6	62.9	B	30	216	215.36	0.30	1.14±0.17	1.12	0.02
212	4/6	62.9	B	24	194	193.87	0.07	1.31±0.12	1.21	0.10
242	5/6	62.9	B	29	197	192.48	2.29	1.31±0.23	1.21	0.10
410	6/6	62.9	B	21	181	177.71	1.82	1.37±0.17	1.23	0.14
240	7/6	62.9	B	29	179	173.51	3.07	1.43±0.23	1.30	0.13
116	8/6	62.9	B	29	172	167.29	2.74	1.49±0.17	1.30	0.19
122	Full Win.	62.9	B	28	194	199.64	-2.91	1.37±0.17	1.24	0.13
224	2/3 Win.	62.9	B	26	216	222.05	-2.80	1.37±0.17	1.31	0.06
220	6/6	31.6	B	26	118	120.94	-2.49	1.37±0.17	1.29	0.08
221	6/6	105.3	B	27	234	251.18	-7.34	1.31±0.23	1.23	0.08
163	6/6	62.9	Br ¹	6	190	183.35	3.50	1.49±0.17	1.48	0.01
514	2/6	62.9	C	9	209	204.73	2.04	1.03±0.17	0.87	0.16
544	3/6	62.9	C	7	173	163.15	5.69	1.09±0.23	1.18	-0.09
512	4/6	62.9	C	21	173	169.25	2.17	1.14±0.17	1.13	0.01
542	5/6	62.9	C	20	160	157.42	1.61	1.20±0.23	1.13	0.07
610	6/6	62.9	C	18	152	153.6	-1.05	1.26±0.17	1.23	0.03
540	7/6	62.9	C	14	140	135.28	3.37	1.26±0.17	1.23	0.03
517	8/6	62.9	C	15	134	131.76	1.67	1.31±0.11	1.36	-0.05
622	Full Win.	62.9	C	10	153	156.29	-2.15	1.26±0.17	1.26	0.00
524	2/3 Win.	62.9	C	9	178	175.88	1.19	1.14±0.17	1.14	0.00
541	1/3 Win.	62.9	C	8	288	265.58	7.78	1.09±0.23	1.13	-0.04
520	6/6	31.6	C	18	94	95.08	-1.15	1.26±0.17	1.22	0.04
521	6/6	105.3	C	14	207	207.79	-0.38	1.20±0.23	1.15	0.05
513	6/6	158	C	16	289	288.1	0.31	1.20±0.23	1.16	0.04
164	6/6	62.9	Cr ¹	7	161	138.5	13.98	1.37±0.17	1.25	0.12

¹ r represents the fire source locations raised 0.3 m from the floor level.

² Test numeration is in accordance with Steckler's reports.

³ Opening codes (e.g. 2/6, 3/6, 1/3, etc.) can be seen in Table 5.2

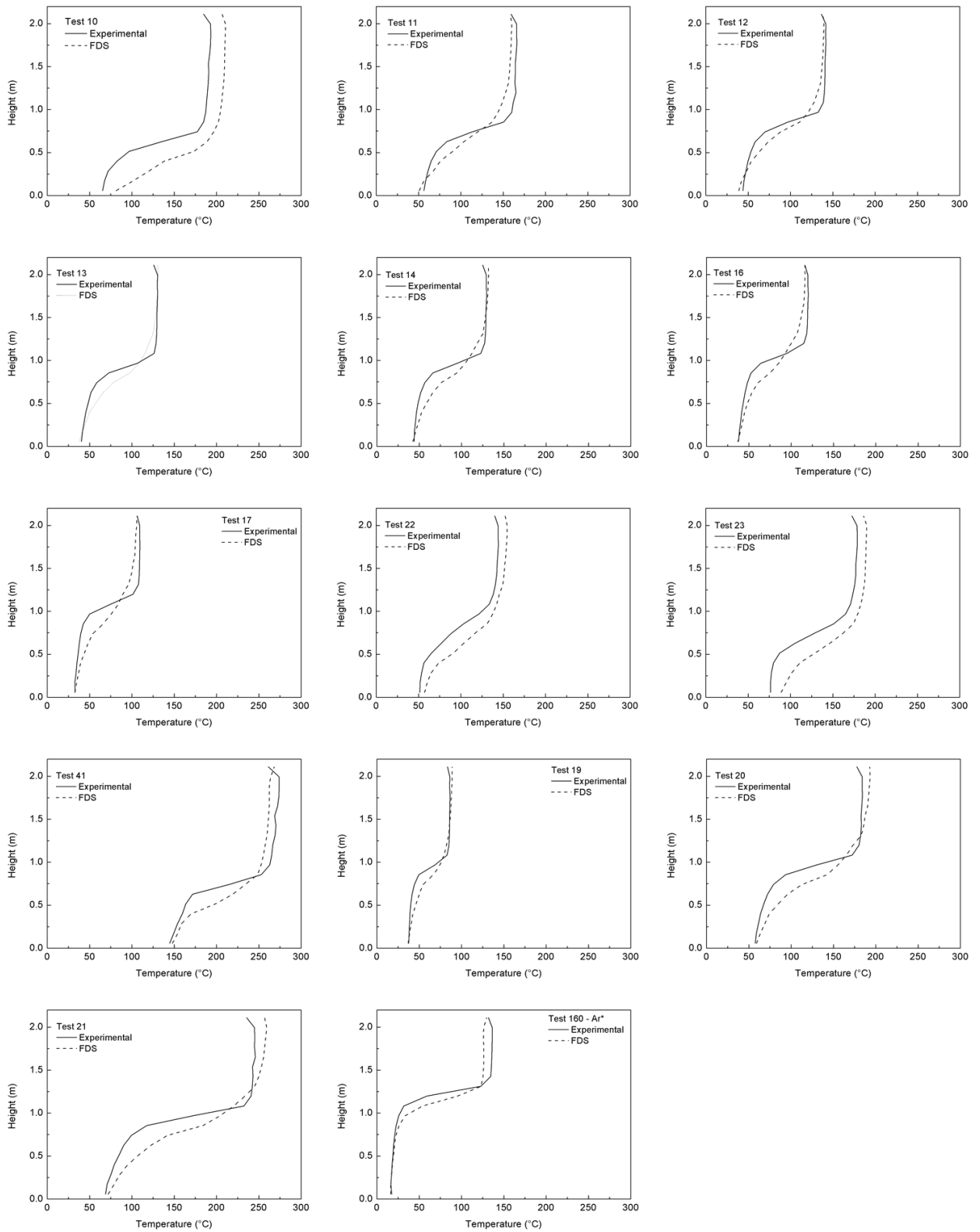


Figure 5.7 - Temperature profiles for fire source at the center of the room (position A)

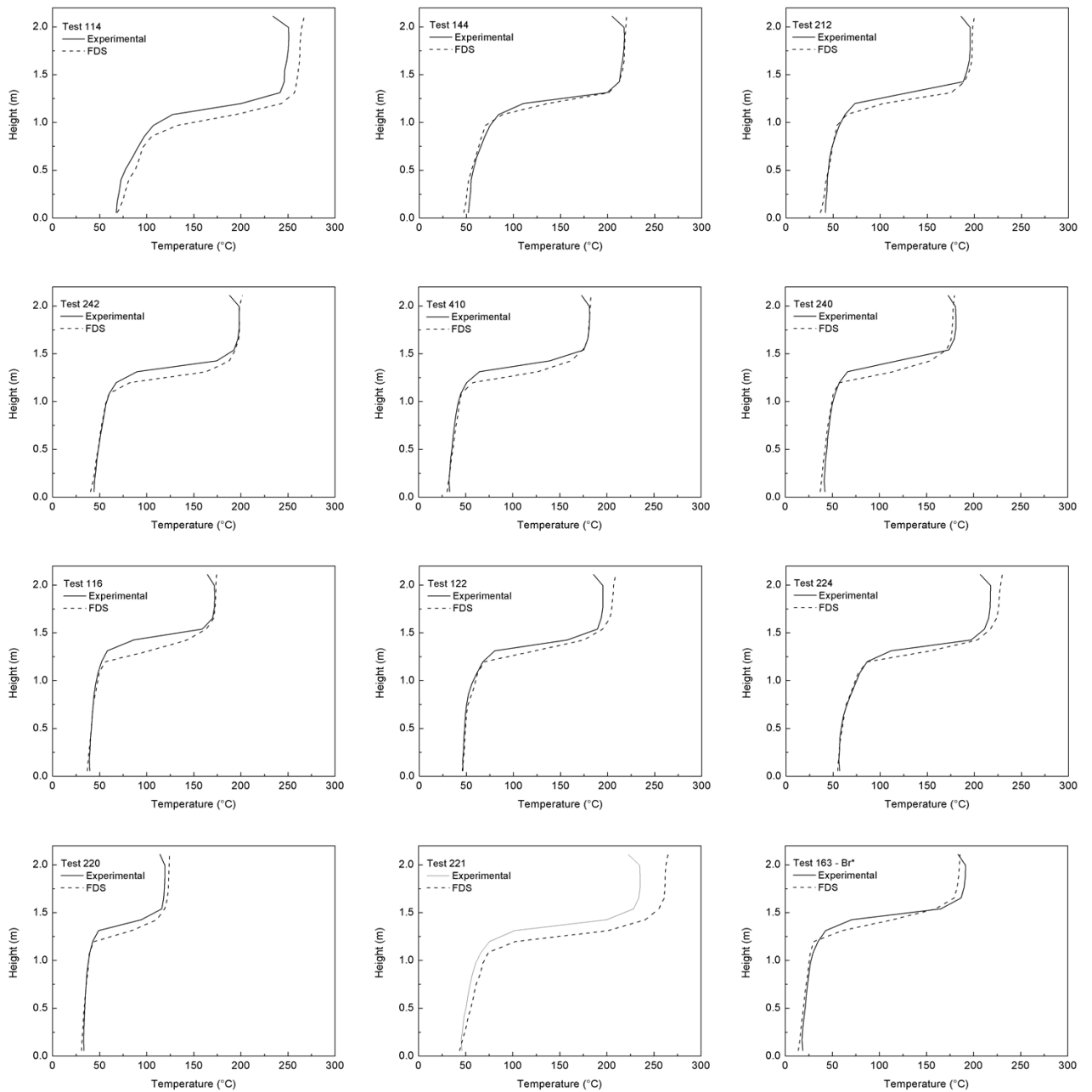


Figure 5.8 - Temperature profiles for fire source at the corner of the room (position B)

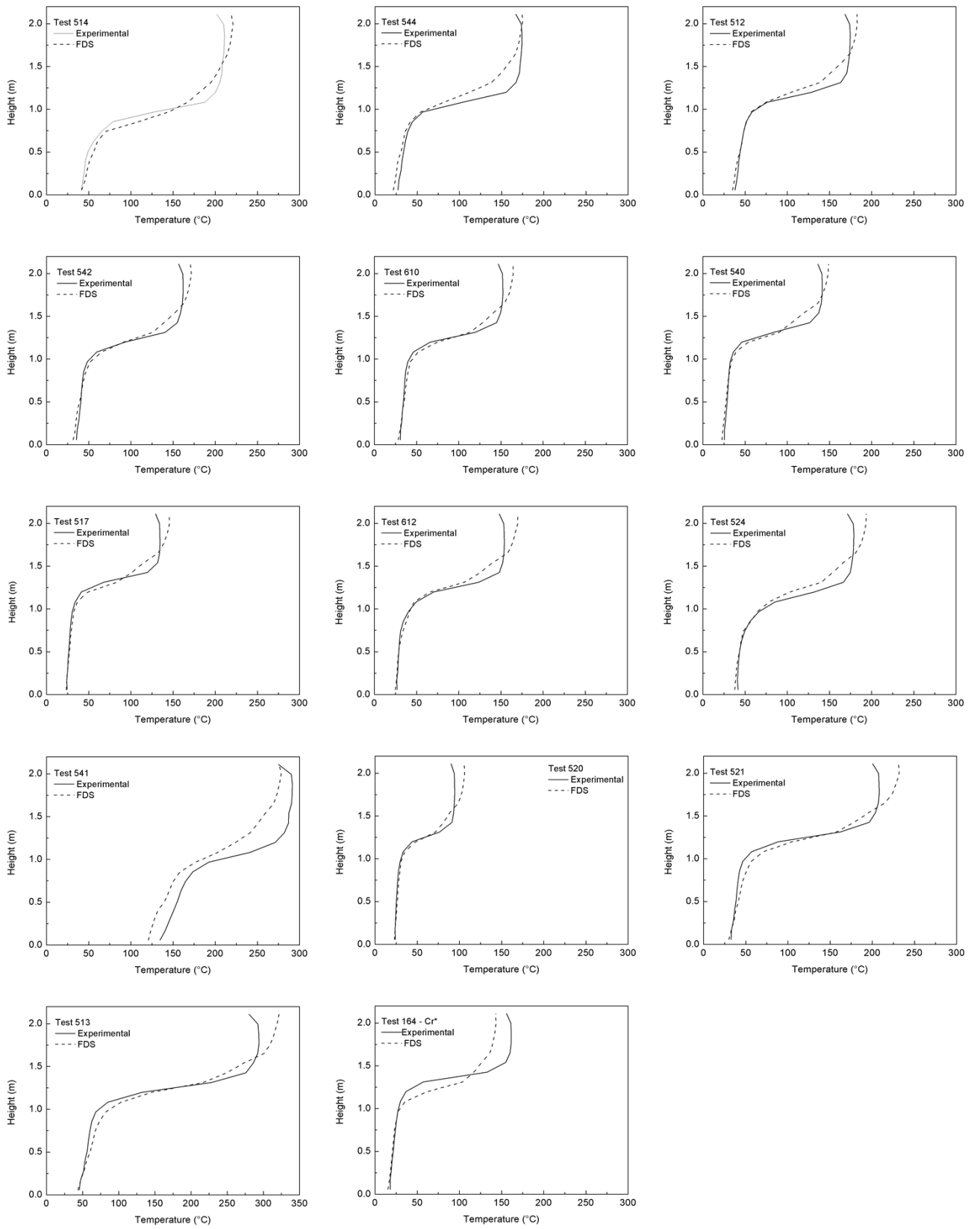


Figure 5.9 - Temperature profiles for fire source at the back wall of the room (position C)

Figures 5.7-5.9 also show a good agreement between experimental data and numerical results. So, it can be concluded that the mathematical model employed on FDS was verified and can be applied to generate reliable data for compartment fire scenarios.

5.5 Data Correlation

As well as the MQH correlation, the present correlations were derived from an energy balance on the well-stirred gas layer in the upper portion of the room.

Equation 3.13 can be represented in two dimensionless groups and since the height of the neutral plane, Z_n , depends mostly on \dot{Q} , T_U and geometric factors (H_0 and W_0), \dot{m}_g may be replaced by $\sqrt{g}\rho_\infty A_0 \sqrt{H_0}$. So the dependence is given by:

$$\frac{\Delta T}{T_\infty} = f \left(\frac{\dot{Q}}{\sqrt{g}C_p\rho_\infty T_\infty A_0 \sqrt{H_0}}, \frac{h_k A_T}{\sqrt{g}C_p\rho_\infty A_0 \sqrt{H_0}} \right) \quad (5.7)$$

The first variable represents the ratio of the energy released to the energy convected, and the second, the energy lost divided by the energy convected.

A power law relationship can be observed, so:

$$\frac{\Delta T}{T_\infty} = C \left(\frac{\dot{Q}}{\sqrt{g}C_p\rho_\infty T_\infty A_0 \sqrt{H_0}} \right)^A \cdot \left(\frac{h_k A_T}{\sqrt{g}C_p\rho_\infty A_0 \sqrt{H_0}} \right)^B \quad (5.8)$$

where the constant C and the exponents A and B will be determined from a best fit of the data from each group of fire positions (center, wall and corner) at the ground level, once we observed a great influence of these fire positions. This means that 3 different correlations will be obtained for the upper layer temperature, one for each position of the fire.

As it will be shown later in this work, the elevations influence did not show a power law relation, but a linear tendency instead, so it was decided to include this information as a correction term in the correlations.

These are the same dimensionless variables employed in the MQH correlation, however the MQH correlation was correlated only considering fires at the center of the room, and do not include a term for correction of the temperature as a function of the fire source height.

The fitting of the data was obtained through the software SPSS applying a multiple linear regression. To do that, first the data had to be linearized, through its logarithm.

6 RESULTS AND DISCUSSIONS

This chapter presents the results of the fire source position influence on the ground level (transversal and longitudinal positions) and in different vertical positions, the influence of important parameters, such as HRR and ventilation factor, the influence of the distance between the fire source and walls and corners, the correlations obtained to predict the hot gas layer temperature for center, wall and corner positions, with a correction term for the vertical position and the validation of these correlations, comparing the correlation results to experimental and numerical data.

6.1 Fire Source Position Influence (ground level)

Firstly, it is analyzed the influence of the fire source location at the ground level (transversal and longitudinal positions), varying the fire position along the axis x and y . The 13 studied cases have been simulated in 15 different positions, as can be seen in Figure 5.3, given 195 different scenarios.

Figures 6.1a-6.1m show the upper layer temperature (T_U) obtained through FDS simulations for each one of the studied ground level positions (Figure 5.3) for all the 13 cases (Table 5.2). This figure condenses the results of all the 195 simulations, each square represent the room geometry for each studied case and the upper layer temperature (T_U) results were placed on the position inside the room where the fire occurred (these temperatures must be assumed as homogeneous over all the HGL), so each square (plots a to m) presents the results of the 15 tested fire positions (Figure 5.3) for each case (Table 5.2).

As can be observed, the highest upper layer temperature was found on the corner fire location (positions B and N) followed by the near wall fire location (positions C, D, E, H, K and P). The positions away from the wall (positions A, F, G, J, L, M and Q) are the ones which produced the lowest upper layer temperatures, especially those near the opening doorway. This behaviour is expected, once in corner and wall fires the air entrainment is reduced.

Zukoski et al.,1981, observed that the rate of air entrainment in the plume can be related to the heat release rate, in accordance to Equation 6.1:

$$\dot{m}_p \propto \dot{Q}^{\frac{1}{3}} \quad (6.1)$$

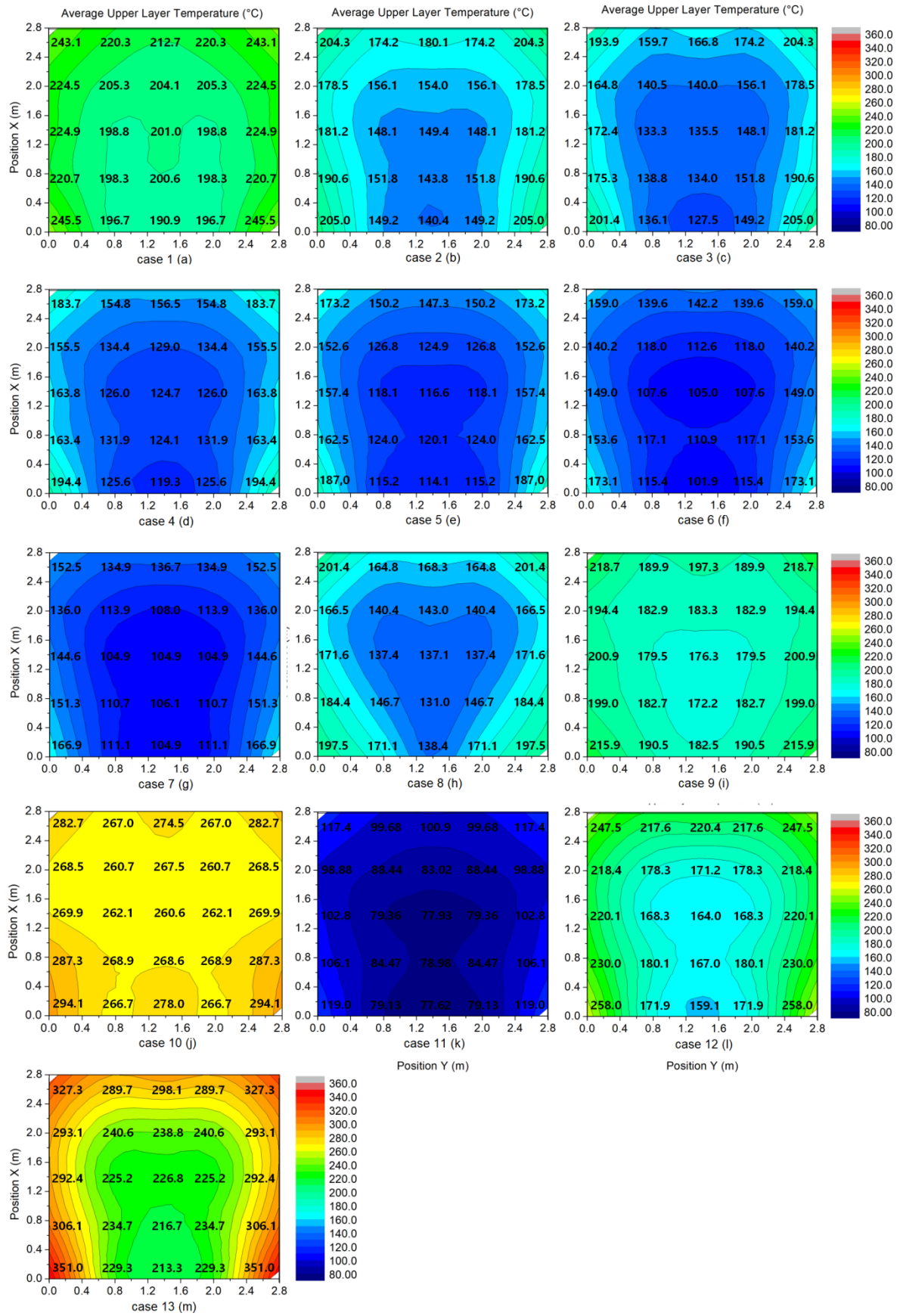


Figure 6.1 - Average upper layer temperature in each fire source position on the ground level

According to Zukoski et al., 1981, in the early stages of a fire (pre-flashover) in a building, the rate of production of hot gas by a fire and the temperature of this gas will depend very strongly on the rate of entrainment in the fire plume and in the flame itself.

The plume theory proposed by Zukoski et al., 1981, suggests that a pseudo-HRR four times the real HRR can be used to represent the effect in the reduction of the air entrainment when the fire source is located in a corner, and two times the real HRR for fires located along walls. However, the entrainment only occurs around one quarter of the perimeter of this pseudo-Fire for fires in corner and around one half for fires along walls. So, the actual air entrainment can be calculated according to Equations 6.2 and 6.3 for corners and wall, respectively [Mowrer and Williamson, 1987]:

$$\dot{m}_{p_{corner}} \sim \frac{(4\dot{Q})^{\frac{1}{3}}}{4} \approx 0.4\dot{Q}^{\frac{1}{3}} \quad (6.2)$$

$$\dot{m}_{p_{wall}} \sim \frac{(2\dot{Q})^{\frac{1}{3}}}{2} \approx 0.63\dot{Q}^{\frac{1}{3}} \quad (6.3)$$

The plume theory also indicates that the excess temperature over ambient in the plume is inversely proportional to the air entrainment rate, for a given HRR. This dependence is expressed by Equation 6.4.

$$\Delta T_p \propto \frac{\dot{Q}}{m_p} \quad (6.4)$$

where ΔT_p represents the excess temperature over ambient in the plume, \dot{Q} is the HRR and m_p is the rate of air entrainment in the plume.

According to Mowrer and Williamson, 1987, the fire plume temperature will significantly increase for corner and near wall fire plumes. It is important to highlight the direct proportionality between the upper layer temperature and the plume temperature, so the upper layer temperature is also inversely proportional to the air entrainment rate. As a conclusion of this dependence, Mowrer and Williamson, 1987, stated that the convective energy flux through the openings would not depend on the fire source location in the room. This statement was confirmed by the results shown on Figures 6.1a-6.1m, once fire source

position in the same group of interest (away from walls, along walls or near corners) showed small variations.

Based on the theory, the expected temperatures would be, respectively, for corners and walls [Mowrer and Williamson, 1987]:

$$\Delta T_{pcorner} \sim \frac{\dot{Q}^{\frac{1}{3}} \Delta T_{pcenter}}{0.4 \dot{Q}^{\frac{1}{3}}} \approx 2.5 \Delta T_{pcenter} \quad (6.5)$$

$$\Delta T_{pwall} \sim \frac{\dot{Q}^{\frac{1}{3}} \Delta T_{pcenter}}{0.63 \dot{Q}^{\frac{1}{3}}} \approx 1.6 \Delta T_{pcenter} \quad (6.6)$$

However, Mowrer and Williamson (1987) noticed that the reduced entrainment rates that occur for corner and wall fires cause the layer height to move upward in the room, and this in turn results in entrainment over a greater height. Thus, the excess temperature of the plume as it enters the layer would be less than the factors calculated before.

These theoretical results agreed qualitatively with the analysis of the fire source influence in the ground level (Figure 6.1a-6.1m), which showed that fires in corners would provide the highest temperatures, followed by fires along walls and then in center positions.

An interesting observation can be made through Figures 6.1h, 6.1i and 6.1j. These Figures represent cases 8, 9 and 10, which have window openings, so when the fire source is right below the opening (position Q – see Figure 5.3), the upper layer temperature becomes higher than when the opening is a doorway. This again is explained by the reduction of air entrainment, once a lower airflow rate is reaching the flame.

Another pattern can be easily observed, once the ventilation factor (opening size) is augmented, lower become the upper layer temperature.

This previous analysis confirmed the weak influence of the fire source location when the same level (floor level) is considered, except when the fire source is placed near a wall or corner (or even a piece of furniture), which reduces the air entrainment into the flame.

6.2 The Heat Release Rate Influence

The influence of the HRR on the average hot gas layer temperature has been analyzed based on 60 simulations. Four HRR values were tested (31.6, 62.9, 105.3 and 158 kW),

represented by the cases 5, 11, 12 and 13. All the simulations had the same geometry and ventilation factor. All the four cases have been simulated considering the 15 different ground positions ($z = 0$ m) studied.

Figure 6.2 presents the average HGL temperature as a function of the HRR, being the results divided into the three groups of interest (regarding fire positions: away from wall, near corner and near wall).

As can be observed, as the HRR is augmented, higher becomes the HGL temperature. A power dependence between the HRR and the temperature can be observed. This dependence is well-known in compartment fires, being the HRR one of the most important parameters considered on the hand-calculation methods to predict HGL temperatures.

As expected the results away from wall (center) showed the lowest results, while the ones near a corner presented the higher ones. An exception can be observed for the near wall position, which presented results similar to the ones away from the wall. These results represent cases 5, 11, 12 and 13 (Table 5.2) simulated at position P (Figure 5.3), and might be explained by the proximity to the doorway opening, so even being near a wall, the air entrainment rate is still high and consequently the temperatures are lower.

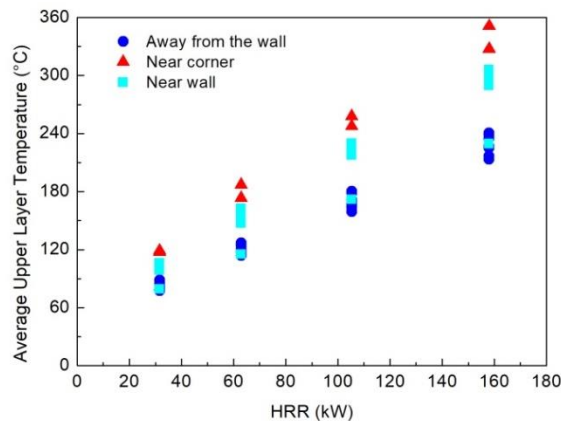


Figure 6.2 - Heat Release Rate influence on the upper layer temperature

6.3 Ventilation Factor Influence

The ventilation factor is another important parameter applied to correlations. Figure 6.3 shows the influence of the ventilation factor, considering a fixed geometry and HRR (62.9 kW) and only door openings, which is represented by the cases 1 to 7 (Table 5.2), tested for all 15 positions on ground level (Figure 5.3), with a total of 105 numerical experiments.

Figure 6.3 presents the average HGL temperature as a function of the ventilation factor, being the results divided into the three groups of interest (regarding fire positions: away from wall, near corner and near wall).

This parameter showed a less important influence over the HGL temperature, when comparing with the HRR. As the ventilation factor is augmented, the hot gas layer temperature decreases, which indicates an inversely proportional relation between these parameters. It can be explained again by the rate of air entrainment. Once a larger ventilation factor allows a greater quantity of air to enter the room and reach the plume, the plume temperature becomes lower, as well as the hot gas layer temperature.

Once again the exception presented on position P (close to the doorway) can be observed.

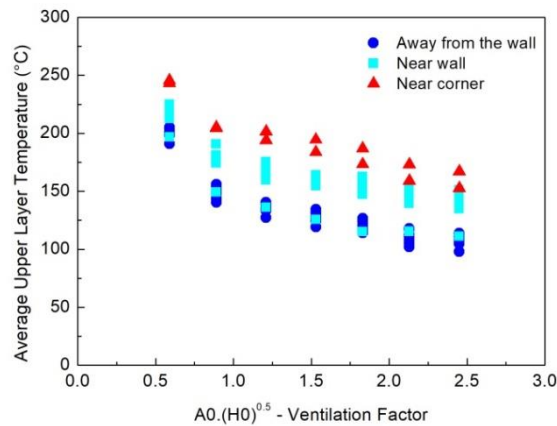


Figure 6.3 - Ventilation factor influence on the upper layer temperature

6.4 Fire Source Position Influence (vertical position)

For analysing the influence of the vertical position of the fire source on the upper layer temperature, it was simulated 19 elevations (ranging from $z = 0$ m to $z = 1.8$ m) for positions A (center), B (corner) and C (wall), as can be seen in Figure 5.3. These simulations were conducted only for case 5 (fixed opening and HRR, cf. Table 5.2), generating data for 57 numerical experiments.

Tables 6.1, 6.2 and 6.3 show the results of the upper layer temperature for each elevation and the difference on HGL temperature between elevations for positions A (center), B (corner) and C (wall), respectively. Figures 6.4, 6.5 and 6.6 present the relation between the upper layer temperature and the fire source elevation (z) for the same positions.

Table 6.1 - Upper layer temperature as a function of the vertical position (ground position A)

Elevation (z) (m)	Opening	HRR	Position	Upper layer temperature (T_U) (°C)	Difference from the previous level (°C)	Difference from the ground level (°C)
0.00	6/6	62.9	A	116.58	-	0.00
0.10	6/6	62.9	A	122.63	6.05	6.05
0.20	6/6	62.9	A	136.00	13.37	19.42
0.30	6/6	62.9	A	149.16	13.16	32.58
0.40	6/6	62.9	A	162.99	13.83	46.41
0.50	6/6	62.9	A	176.81	13.82	60.23
0.60	6/6	62.9	A	185.18	8.37	68.60
0.70	6/6	62.9	A	196.74	11.56	80.16
0.80	6/6	62.9	A	205.96	9.22	89.38
0.90	6/6	62.9	A	223.94	17.98	107.36
1.00	6/6	62.9	A	237.57	13.63	120.99
1.10	6/6	62.9	A	254.39	16.82	137.81
1.20	6/6	62.9	A	270.60	16.21	154.02
1.30	6/6	62.9	A	295.96	25.36	179.38
1.40	6/6	62.9	A	309.03	13.07	192.45
1.50	6/6	62.9	A	317.63	8.60	201.05
1.60	6/6	62.9	A	325.13	7.50	208.55
1.70	6/6	62.9	A	339.50	14.37	222.92
1.80	6/6	62.9	A	359.53	20.03	242.95

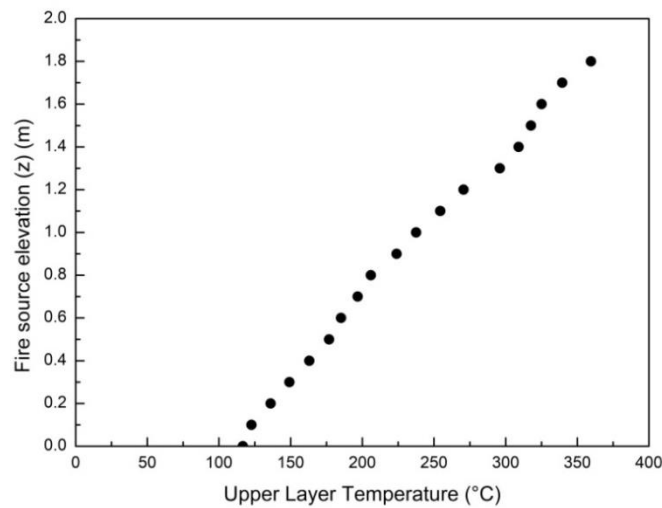


Figure 6.4 - Relation between fire source elevation and upper layer temperature for fires away from walls (ground position A)

Table 6.2 - Upper layer temperature as a function of the vertical position (ground position B)

Elevation (z) (m)	Opening	HRR	Position	Upper layer temperature (T_U) (°C)	Difference from the previous level (°C)	Difference from the ground level (°C)
0.00	6/6	62.9	B	178.82	-	0.00
0.10	6/6	62.9	B	185.73	6.91	6.91
0.20	6/6	62.9	B	196.81	11.08	17.99
0.30	6/6	62.9	B	201.09	4.28	22.27
0.40	6/6	62.9	B	210.51	9.42	31.69
0.50	6/6	62.9	B	219.69	9.18	40.87
0.60	6/6	62.9	B	223.82	4.13	45.00
0.70	6/6	62.9	B	232.55	8.73	53.73
0.80	6/6	62.9	B	237.22	4.67	58.40
0.90	6/6	62.9	B	244.89	7.67	66.07
1.00	6/6	62.9	B	258.15	13.26	79.33
1.10	6/6	62.9	B	265.15	7.00	86.33
1.20	6/6	62.9	B	269.42	4.27	90.60
1.30	6/6	62.9	B	277.24	7.82	98.42
1.40	6/6	62.9	B	280.5	3.26	101.68
1.50	6/6	62.9	B	282.12	1.62	103.30
1.60	6/6	62.9	B	288.02	5.90	109.20
1.70	6/6	62.9	B	285.6	-2.42	106.78
1.80	6/6	62.9	B	288.75	3.15	109.93

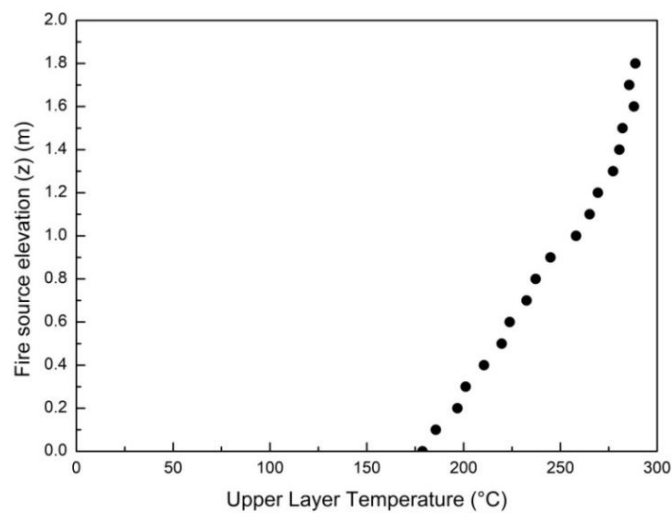


Figure 6.5 - Relation between fire source elevation and upper layer temperature for fires near corner (ground position B)

Table 6.3 - Upper layer temperature as a function of the vertical position (ground position C)

Elevation (z) (m)	Opening	HRR	Position	Upper layer temperature (T_U) (°C)	Difference from the previous level (°C)	Difference from the ground level (°C)
0.00	6/6	62.9	C	149.26	-	0.00
0.10	6/6	62.9	C	152.14	2.88	2.88
0.20	6/6	62.9	C	153.6	1.46	4.34
0.30	6/6	62.9	C	155.23	1.63	5.97
0.40	6/6	62.9	C	161.15	5.92	11.89
0.50	6/6	62.9	C	167.65	6.50	18.39
0.60	6/6	62.9	C	179.04	11.39	29.78
0.70	6/6	62.9	C	197.07	18.03	47.81
0.80	6/6	62.9	C	205.8	8.73	56.54
0.90	6/6	62.9	C	220.03	14.23	70.77
1.00	6/6	62.9	C	236.3	16.27	87.04
1.10	6/6	62.9	C	250.26	13.96	101.00
1.20	6/6	62.9	C	271.01	20.75	121.75
1.30	6/6	62.9	C	280.96	9.95	131.70
1.40	6/6	62.9	C	296.11	15.15	146.85
1.50	6/6	62.9	C	310.33	14.22	161.07
1.60	6/6	62.9	C	319.04	8.71	169.78
1.70	6/6	62.9	C	324.81	5.77	175.55
1.80	6/6	62.9	C	329.71	4.90	180.45

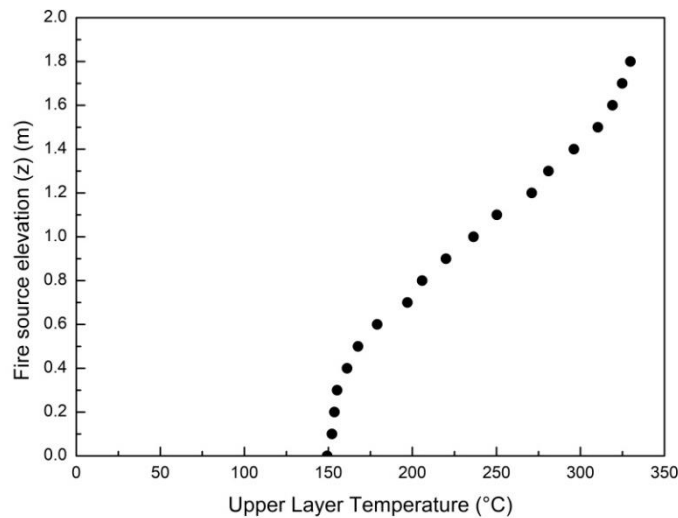


Figure 6.6 - Relation between fire source elevation and upper layer temperature for fires along walls (ground position C)

As can be observed, as the height of the fire source location was augmented, so was the upper layer temperature. This behaviour was observed for all positions (center, wall and corner). However, the influence of the elevation was greater for fires in the center of the room, followed by fires along walls, and finally fire near corners. This can be explained by the reduction of the air entrainment rate. When the fire source is elevated it becomes closer to the hot gas layer interface and its plume and flame have a smaller region to entrain fresh air

(Figures 6.7a-6.7c). With the reduction of air entrainment the upper layer temperature rises. However, fires in corners and along wall already have an air entrainment of approximately one quarter and one half (as a consequence of the walls restriction in the perimeter of the flame/plume), respectively. For this reason, when elevated they suffer less influence than the ones away from walls.

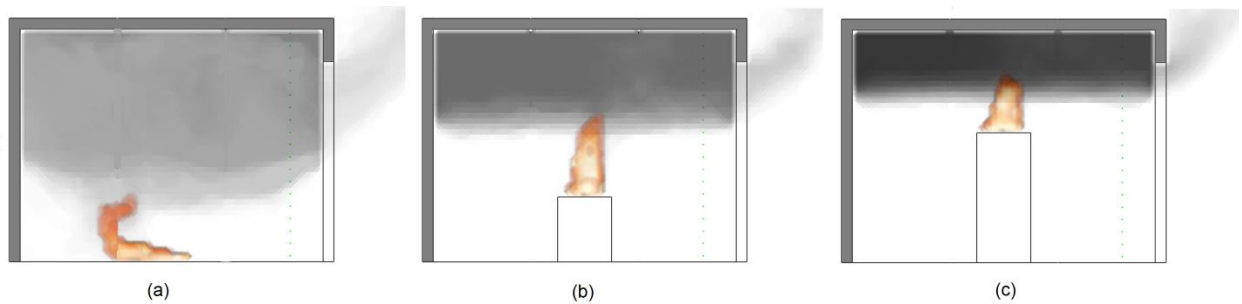


Figure 6.7 - Reduction on the air entrainment area when the fire source is elevated (a) $z=0\text{m}$ (b) $z=0.6\text{m}$ (c) $z=1.2\text{m}$

Significant differences in the upper layer temperature between subsequent levels can be seen, being most of them of the order of 10-20 °C (considering the steps of 0.1 m between elevations), while when comparing T_U for the fire source at the floor level and at the highest level, the difference in T_U was of more than 100 °C in all cases, reaching 242 °C in some cases.

Although the influence of the elevation on the upper layer temperature is not perfectly linear, a linear dependence can be considered to correlate the upper layer temperature and the elevation of the fire source.

To have a better understanding of the temperature behaviour, Figure 6.8, 6.9 and 6.10 present the temperature profiles for each elevation in positions A, B and C, respectively. As can be noticed, as the fire source was elevated, the hot gas layer depth was reduced, which means the layer interface height becomes higher. The maximum temperature (near the ceiling) also increased. This increase in upper layer temperature and maximum temperature is also explained by the air entrainment. Once the fire source is elevated, the top of the flame and plume enter the HGL (see Figures 6.7a-6.7c), so less air reaches the flame/plume and the entrainment rate is reduced increasing the plume temperature.

Therefore, it can be concluded that the z position of the fire source (elevation) has an extremely important influence on the upper layer temperature. It also importantly influences the temperature profile and interface layer height.

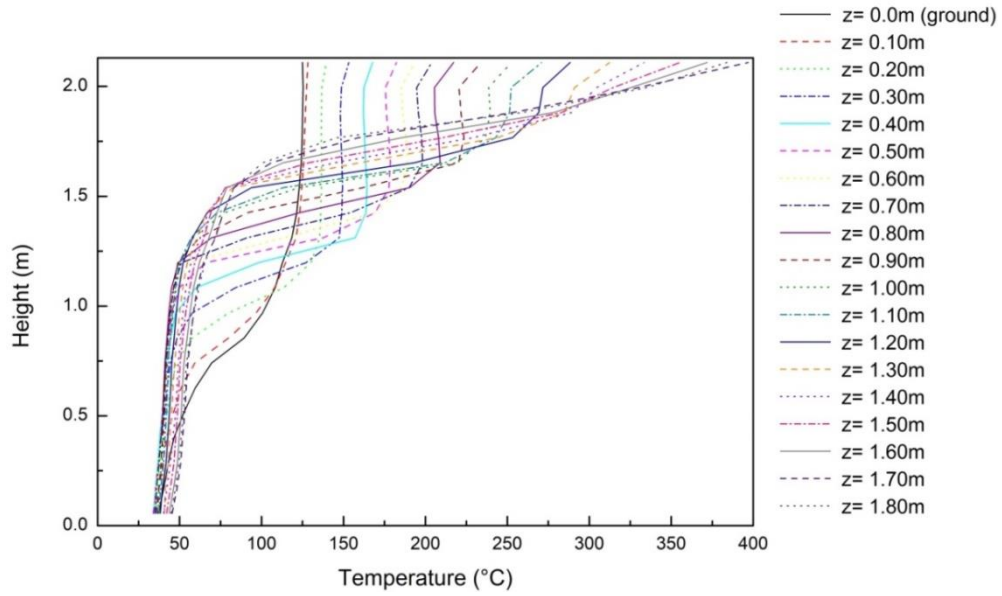


Figure 6.8 - Temperature profiles for different fire source elevation in ground position A (center)

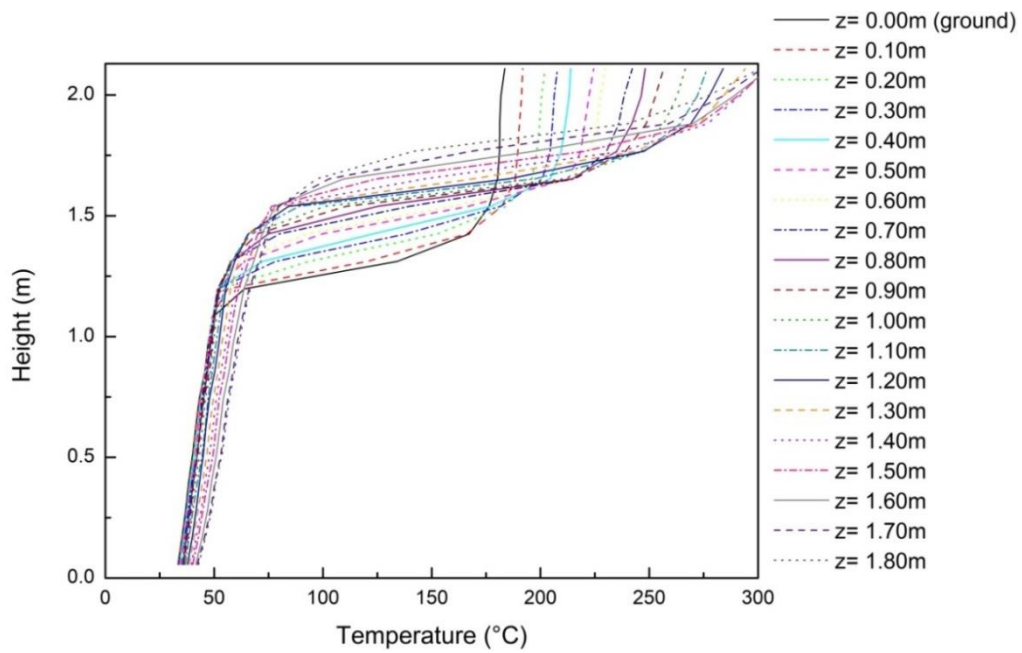


Figure 6.9 - Temperature profiles for different fire source elevation in ground position B (corner)

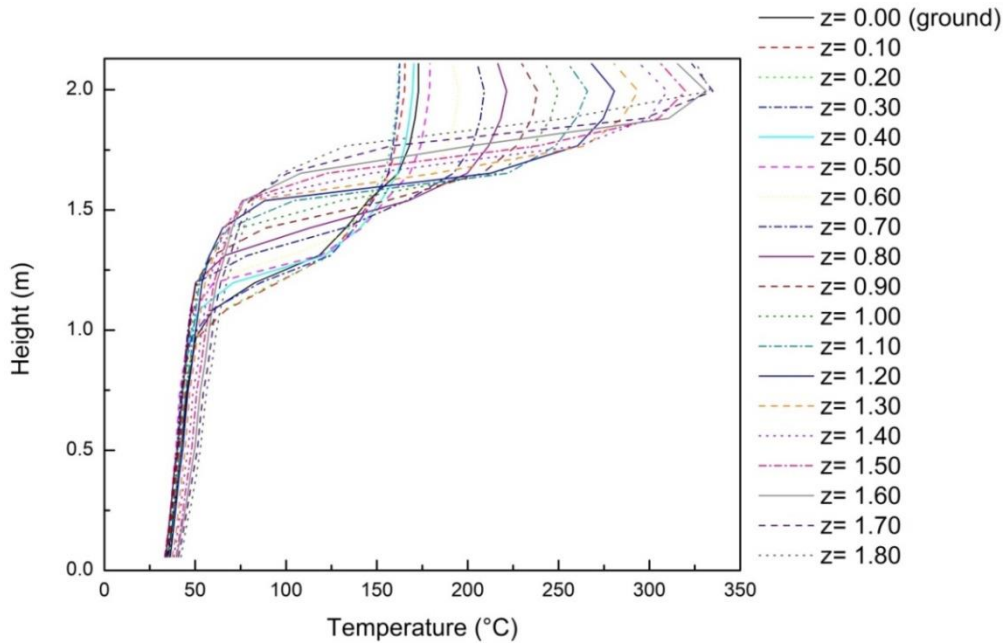


Figure 6.10 - Temperature profiles for different fire source elevation in ground position C (wall)

6.5 Wall and Corner Vicinity Influence

To better understand how the vicinity of a wall affects the upper layer temperature results, a study has been carried out. We started analysing the influence of the back wall, with the pool fire tangent to this wall ($x = 2.8$ m, $\Delta x = 0$ m) and it was increased the distance from the wall in steps of $\Delta x = 0.05$ m, see Figure 6.11. This method was applied to determine when the fire stops to behave as a wall fire and starts to behave as a center fire.

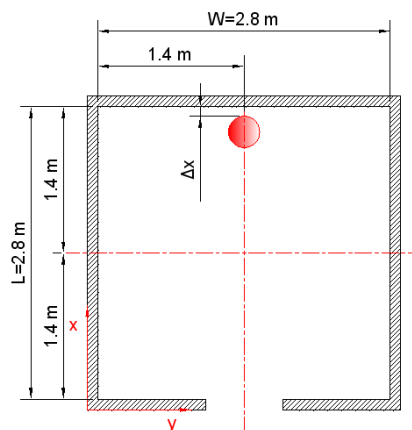


Figure 6.11 - Wall vicinity influence on HGL temperature analysis scheme.

A similar analysis was employed to verify the influence of two perpendicular walls (corner). At first the fire source was placed at the corner with its tangents touching the

sidewall ($y = 0 \text{ m}$, $\Delta y = 0 \text{ m}$) and back wall ($x = 2.8 \text{ m}$, $\Delta x = 0 \text{ m}$) simultaneously, and it was moved along the back wall in steps of $\Delta y = 0.05 \text{ m}$. See Figure 6.12. This method was applied to determine when the fire stops to behave as a corner fire and starts to behave as a wall fire.

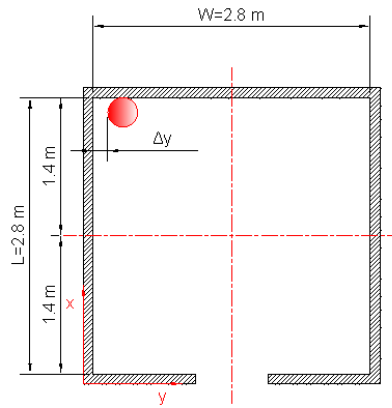


Figure 6.12 - Corner vicinity influence on HGL temperature moving along the backwall analysis scheme.

A posterior analysis was made, starting at the corner, and moving the fire source in both directions, x and y , with the same steps of $\Delta x = \Delta y = 0.05 \text{ m}$. See Figure 6.13. This analysis was used to determine when the fire loses the corner fire characteristics and starts to behave as a center fire source.

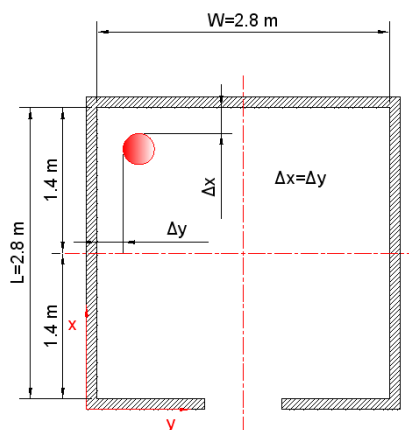


Figure 6.13 - Corner vicinity influence on HGL temperature moving away from both walls analysis scheme.

Two dimensionless parameters are presented to help these analyses:

$$x^* = \frac{\Delta x}{L} \quad (6.7)$$

$$y^* = \frac{\Delta y}{W} \quad (6.8)$$

where Δx is the distance between the pool fire tangent and the back wall (m), L is the length of the room (m), Δy is the distance from the sidewall (m), and W is the width of the room (m), as can be seen in Figures 6.11 to 6.13.

As it can be observed in Figure 6.14, the upper layer temperature stops to suffer the influence of the wall when the pool fire tangent is approximately 0.45 m from the wall, which corresponds to approximately 16% of the room length. It can be concluded through Figures 6.15a-6.15d, that the upper layer temperature stops suffering the influence of the wall when the flame do not touch it anymore, so the fire source can be considered as a center fire source.

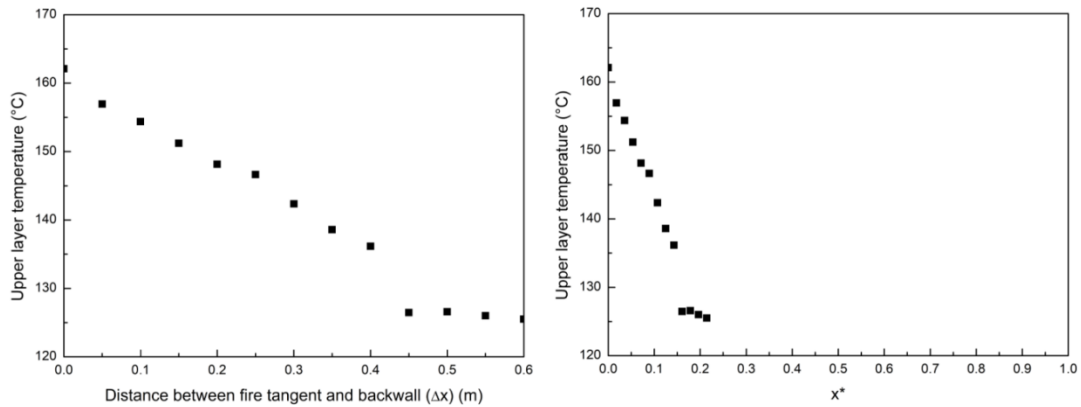


Figure 6.14 - Influence of the wall vicinity in the upper layer temperature.

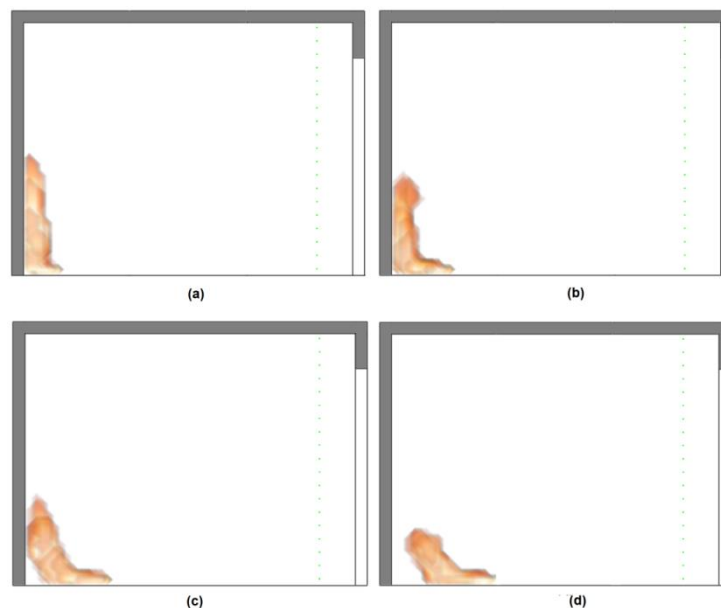


Figure 6.15 - Lateral view of flame and backwall interaction (a) $\Delta x = 0cm$ (b) $\Delta x = 20cm$ (c) $\Delta x = 40cm$ and (d) $\Delta x = 60cm$

A similar behaviour is observed when the fire source is initially at the corner and then it is moved away from the corner, but touching the back wall. The influence of the corner stopped approximately 0.50 m from the sidewall, which corresponds to approximately 18% of the room width, at this point the fire started to present upper layer temperatures of a wall fire (see Figure 6.16). Figures 6.17a-6.17d show that the upper layer temperature stops suffering the influence of the corner when the flame does not touch or interact with the sidewall anymore, so the fire source can be considered as a wall fire source.

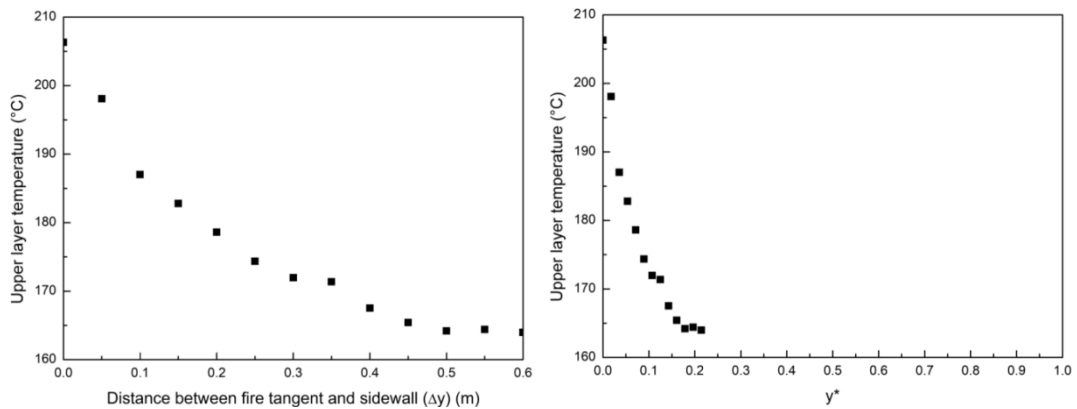


Figure 6.16 - Influence of the corner vicinity moving the fire source along the back wall

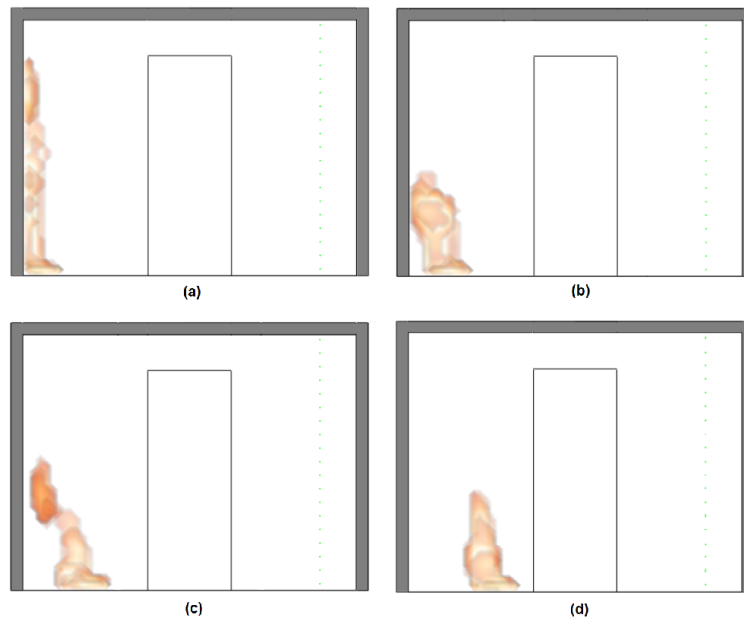


Figure 6.17 - Front view of flame and sidewall interaction (a) $\Delta y = 0\text{cm}$ (b) $\Delta y = 20\text{cm}$ (c) $\Delta y = 40\text{cm}$ and (d) $\Delta y = 60\text{cm}$

When the source fire was moved simultaneously the same distance in directions x and y the influence of the corner stopped approximately 0.70 m from the walls, which corresponds

to approximately 25% of the room width and length (once they have the same value), at this point the fire started to present upper layer temperatures of a center fire (Figure 6.18). As can be seen in Figures 6.19a-6.19h, that is the distance where the flame does not touch or interact with none of the walls. As it can be observed in Figures 6.19e and 6.19f, when the flame is at 0.40 m from both walls it does not touch the sidewall anymore, but it still interacts with the backwall, so at this point it still cannot be considered a center fire source.

By this way, it can be concluded that the flame-wall (or flame-obstruction) interaction is the responsible by the reduction on the air entrainment and consequently the rise on the temperature. Even when the pool fire is not tangent to the wall, the wall may interact with the flame, once the air flux into the room causes a flame inclination towards back and side walls.

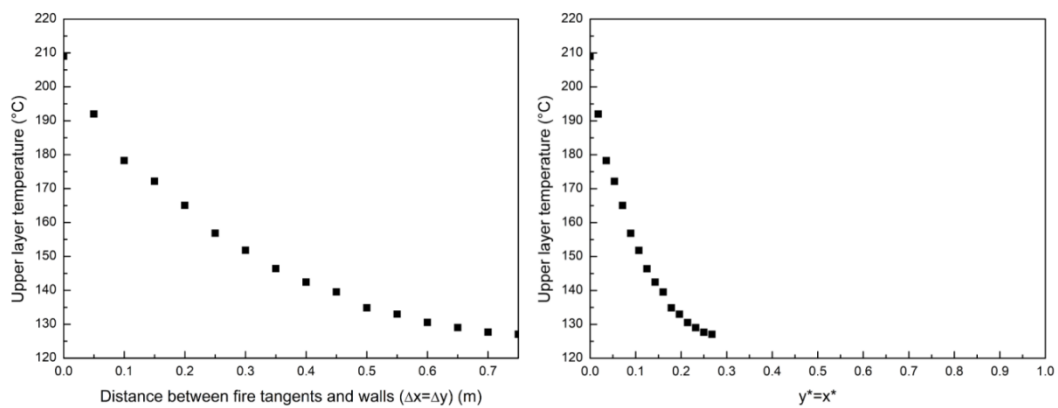


Figure 6.18 - Influence of the corner vicinity moving the fire source diagonally to the center of the room

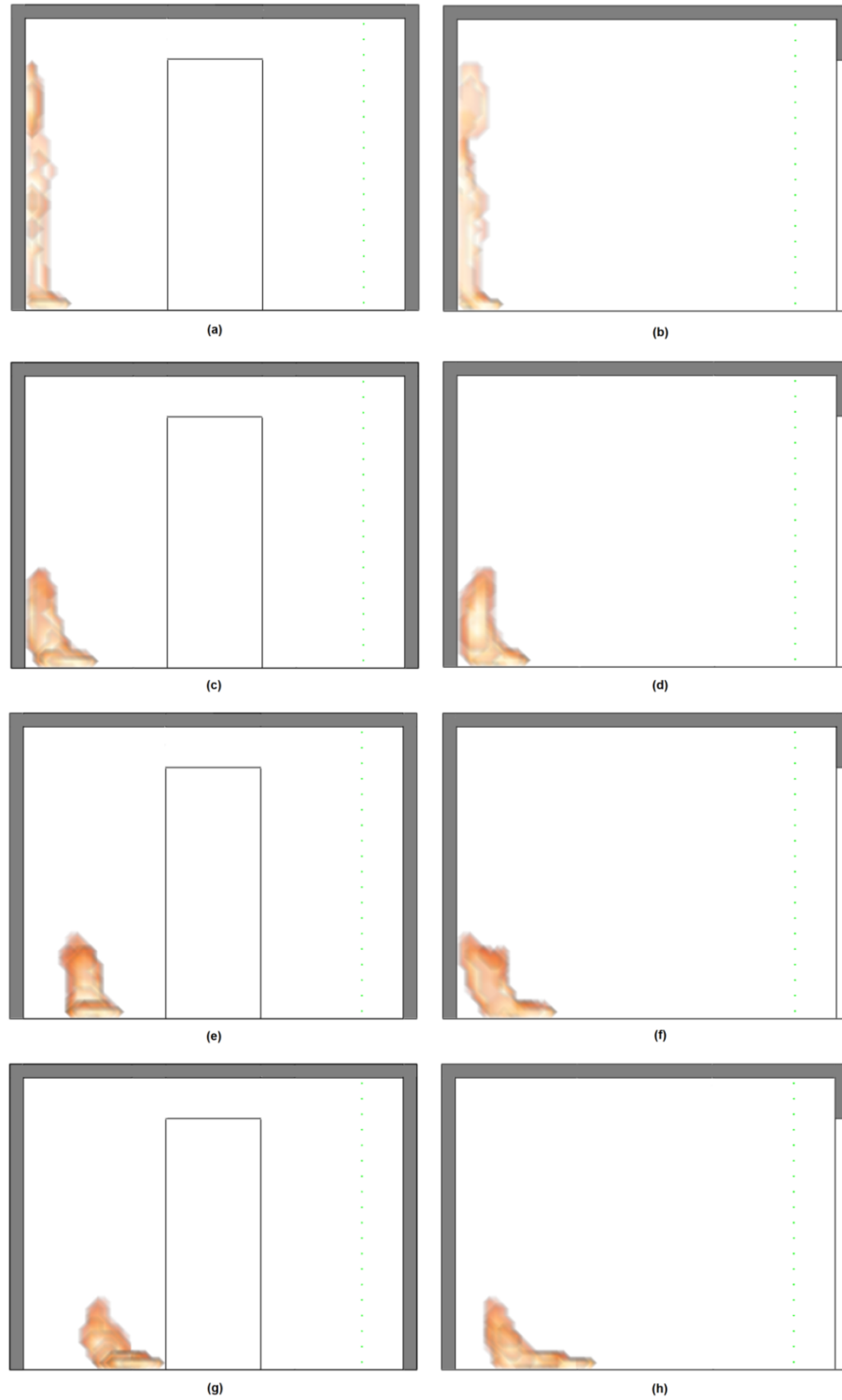


Figure 6.19 - Flame and walls interaction (a) front view $\Delta x = \Delta y = 0\text{cm}$ (b) lateral view $\Delta x = \Delta y = 0\text{cm}$ (c) front view $\Delta x = \Delta y = 20\text{cm}$ (d) lateral view $\Delta x = \Delta y = 20\text{cm}$ (e) front view $\Delta x = \Delta y = 40\text{cm}$ (f) lateral view $\Delta x = \Delta y = 40\text{cm}$ (g) front view $\Delta x = \Delta y = 70\text{cm}$ and (h) lateral view $\Delta x = \Delta y = 70\text{cm}$

6.6 Correlations to Predict Upper Layer Temperature at the Ground Level

As it can be observed in the previous analysis, the fire source location has an extremely important influence on the upper layer temperature. It is noticed that walls and other objects that can restrict the air entrainment rate in the fire plume/flame will cause an augmentation on the plume temperature, and consequently in the upper layer temperature.

It is also noticed the great influence that the vertical fire source position has on the HGL temperature in a quite linear relation.

As the available correlations do not take into account properly the fire source location, it was developed three improved correlations to predict the upper layer temperature in pre-flashover compartment fires, depending on the fire position at the ground level (center, wall or corner), or in other words, according to the air entrainment restriction imposed by walls or furniture.

Starting from the two dimensionless groups ($X1$ and $X2$) obtained through the energy balance (Equations 5.7 and 5.8), it can be plotted the results obtained by FDS and verify a power relationship (see Figure 6.20) :

$$\frac{\Delta T}{T_{\infty}} = f(X1, X2) \quad (6.9)$$

where

$$X1 = \frac{\dot{Q}}{\sqrt{g} C_p \rho_{\infty} T_{\infty} A_0 \sqrt{H_0}} \quad (6.10)$$

and

$$X2 = \frac{h_k A_w}{\sqrt{g} C_p \rho_{\infty} A_0 \sqrt{H_0}} \quad (6.11)$$

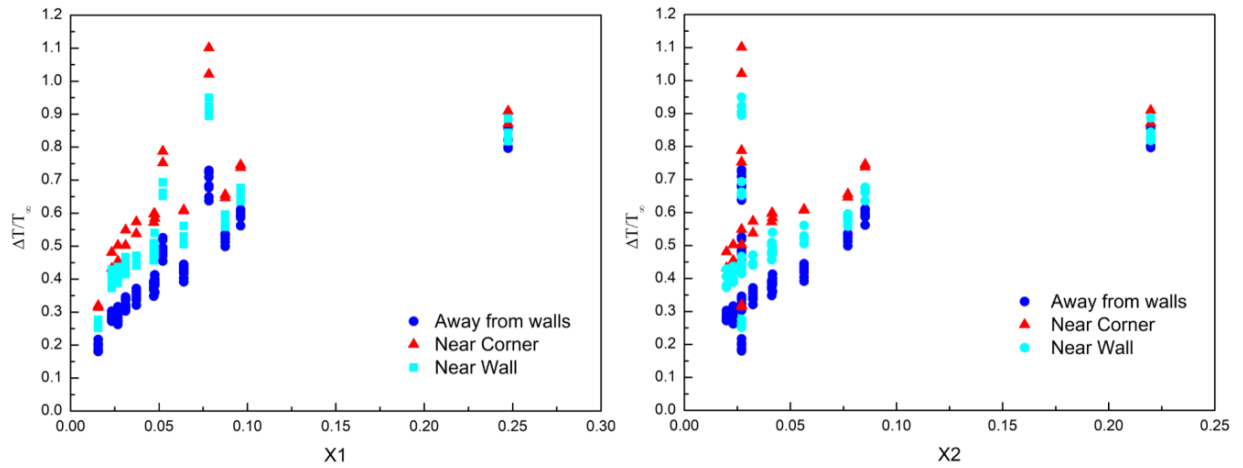


Figure 6.20 - Dimensionless temperatures as a function of the dimensionless groups (X1 and X2) showing a power relation

Therefore, the following power relation can be applied:

$$\frac{\Delta T}{T_{\infty}} = C(X1)^A \cdot (X2)^B \quad (6.12)$$

The fitting of the data for Equation 6.12 was obtained through the software SPSS applying a multiple linear regression. To do that, first the data had to be linearized, through its logarithm. Figure 6.21 show the linearized data for each term (X1 and X2).

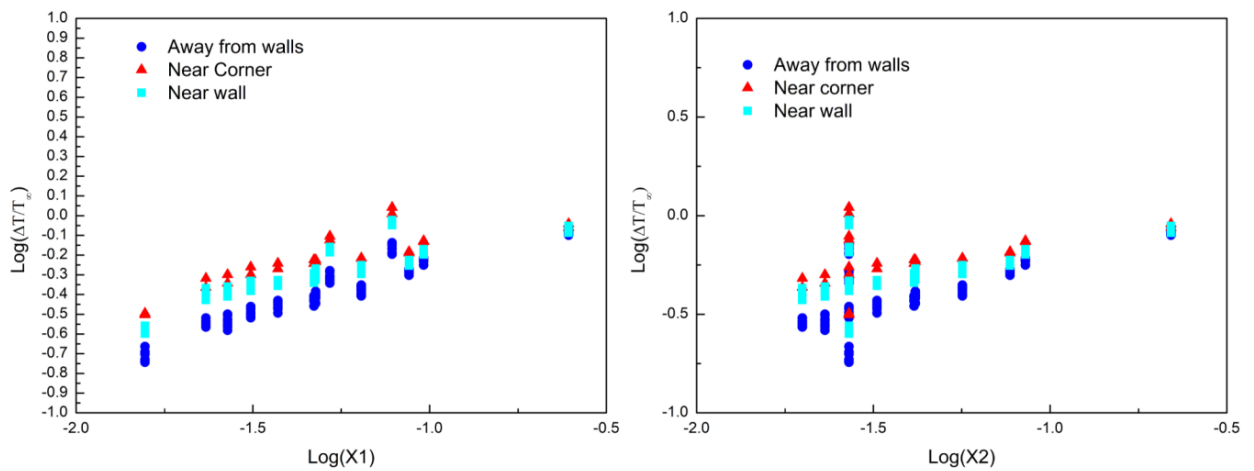


Figure 6.21 - Dimensionless temperature logarithm as a function of the dimensionless groups logarithm showing a linear behaviour (linearized data applied to the multiple linear regression)

Three different correlations were designed, one for each interest group position (away from walls, near wall and near corner).

For fire sources away from walls (center fires) or obstructions at the ground level, Equation 6.13 was obtained:

$$\frac{\Delta T}{T_{\infty}} = 1.55 \left(\frac{\dot{Q}}{\sqrt{g} C_p \rho_{\infty} T_{\infty} A_0 \sqrt{H_0}} \right)^{0.80} \cdot \left(\frac{h_k A_w}{\sqrt{g} C_p \rho_{\infty} A_0 \sqrt{H_0}} \right)^{-0.33} \quad (6.13)$$

Figure 6.22, presents the comparison between the predicted values of the upper layer temperature applying Equation 6.13 and the numerical data for fire sources away from walls or obstructions. The dashed lines represent a 10% tolerance. As can be observed in Figure 6.22 a good fitting was obtained with Equation 6.13.

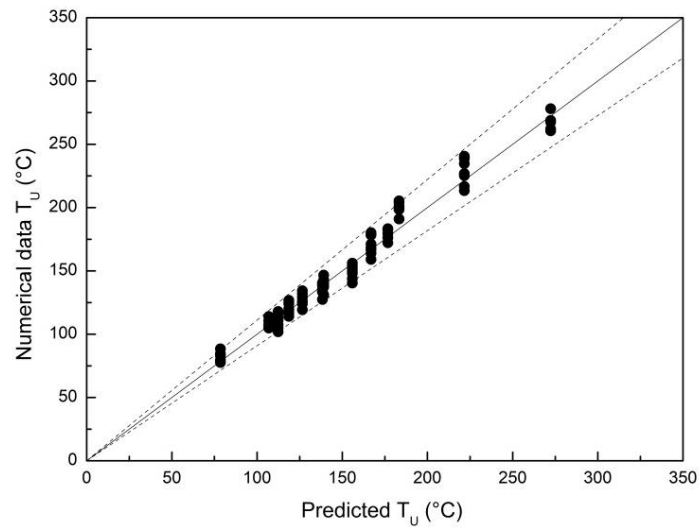


Figure 6.22 - Comparison between predicted upper layer temperature and numerical data for fire sources away from walls.

For fire sources near a wall or obstruction at the ground level, Equation 6.14 must be applied:

$$\frac{\Delta T}{T_{\infty}} = 1.26 \left(\frac{\dot{Q}}{\sqrt{g} C_p \rho_{\infty} T_{\infty} A_0 \sqrt{H_0}} \right)^{0.79} \cdot \left(\frac{h_k A_w}{\sqrt{g} C_p \rho_{\infty} A_0 \sqrt{H_0}} \right)^{-0.47} \quad (6.14)$$

Figure 6.23 presents the comparison between the predicted values of the upper layer temperature applying Equation 6.14 and the numerical data for fire sources positioned near

walls or obstructions. The dashed lines represent a 10% tolerance. As can be observed in Figure 6.23 an excellent fitting was obtained with Equation 6.14.

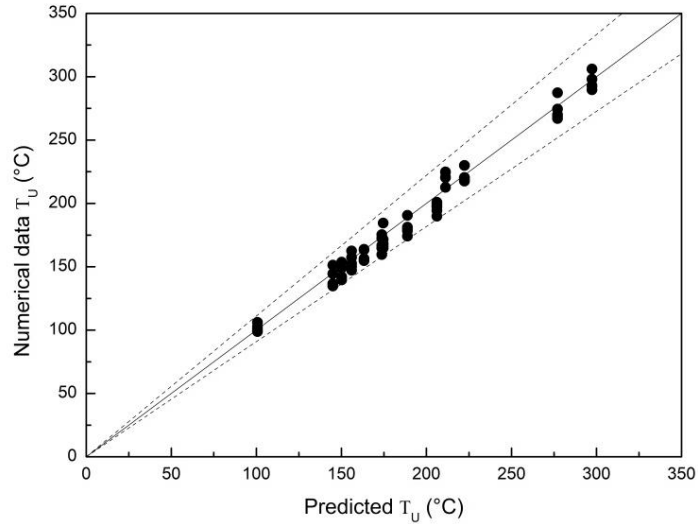


Figure 6.23 - Comparison between predicted upper layer temperature and numerical data for fire sources along walls

For fire sources near a corner at the ground level, it is recommended the appliance of Equation 6.15:

$$\frac{\Delta T}{T_{\infty}} = 1.26 \left(\frac{\dot{Q}}{\sqrt{g} C_p \rho_{\infty} T_{\infty} A_0 \sqrt{H_0}} \right)^{0.76} \cdot \left(\frac{h_k A_w}{\sqrt{g} C_p \rho_{\infty} A_0 \sqrt{H_0}} \right)^{-0.48} \quad (6.15)$$

Figure 6.24 presents the comparison between the predicted values of the upper layer temperature applying Equation 6.15 and the numerical data for fire sources positioned near corners. The dashed lines represent a 10% tolerance. As can be observed in Figure 6.24 an excellent fitting was obtained with Equation 6.15.

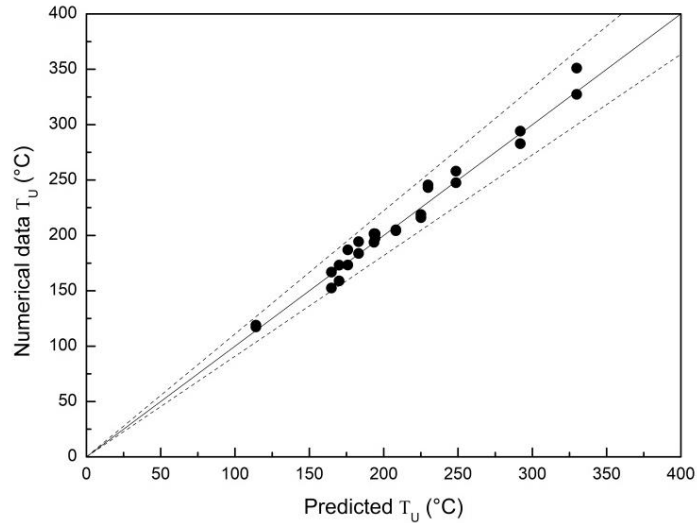


Figure 6.24 - Comparison between predicted upper layer temperature and numerical data for fire sources near corners

The correlations presented in Equations 6.13, 6.14 and 6.15 must be applied only for fires at the ground level. Once it was noticed an important influence of the fire source vertical position on the upper layer temperature, when the fire location is elevated from the ground, these correlations must be corrected. That is the subject of the next section.

6.7 Correction Term for Elevated Fire Sources

As the elevation does not present a power relation, but a quite linear one (as shown in Figures 6.4 to 6.6), it was decided to deal with it as a correction term, that should be summed to the correlation when the elevation is different from zero.

This correction term is defined by the dimensionless parameter z^* :

$$z^* = \frac{z}{H} \quad (6.16)$$

where z is the vertical fire position (m) and H is the height of the room (m).

The correlation for Equation 6.16 was obtained through a simple linear regression of the difference between the dimensionless temperature of each level $(\Delta T/T_\infty)_{level}$ and of the ground level $(\Delta T/T_\infty)_{ground}$. As can be observed in Figures 6.25, 6.26 and 6.27 for the fire source away from walls, near a wall and near a corner, respectively, the squares represent the value of the difference of the dimensionless temperature of each level and of the ground level

as a function of the dimensionless height of the fire source obtained through numerical simulations, while the continuous line represent the correlation obtained.

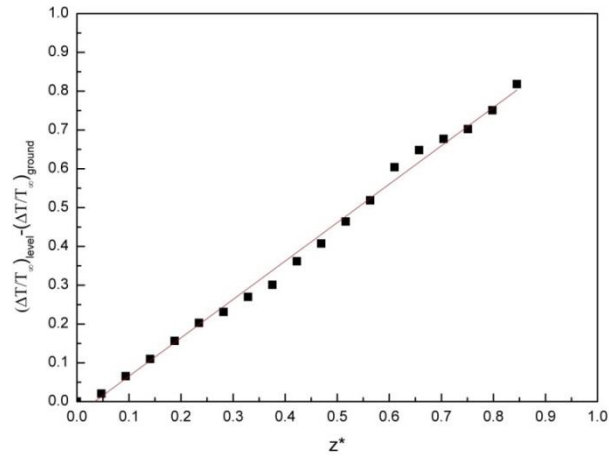


Figure 6.25 - Fitting of the correction term for elevated fire sources away from walls (center).

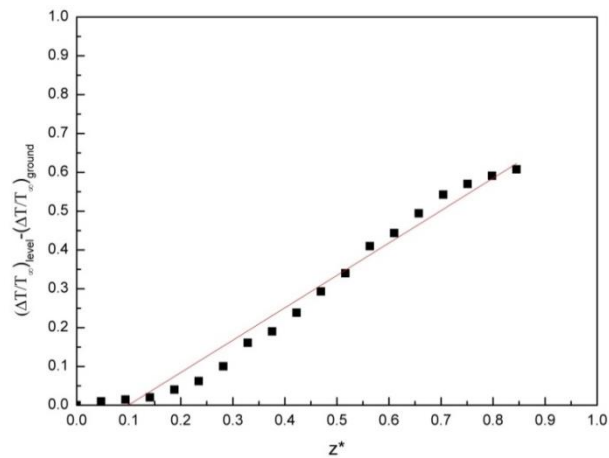


Figure 6.26 - Fitting of the correction term for elevated fire sources near a wall.

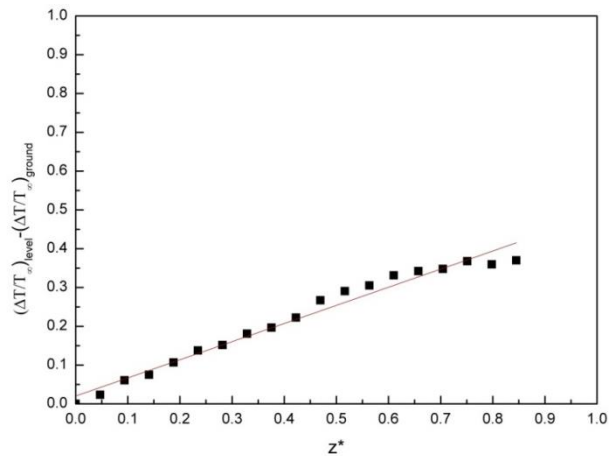


Figure 6.27 - Fitting of the correction term for elevated fire sources near a corner.

So, for elevated fire sources ($z > 0$) away from walls or obstructions, Equation 6.18 contains the correction term for the elevation:

$$\frac{\Delta T}{T_{\infty}} = 1.55 \left(\frac{\dot{Q}}{\sqrt{g} C_p \rho_{\infty} T_{\infty} A_0 \sqrt{H_0}} \right)^{0.80} \cdot \left(\frac{h_k A_w}{\sqrt{g} C_p \rho_{\infty} A_0 \sqrt{H_0}} \right)^{-0.33} + 0.99 \cdot \left(\frac{z}{H} \right) - 0.03 \quad (6.18)$$

Figure 6.28 presents the comparison between the predicted values of the upper layer temperature applying Equation 6.18 and the numerical data for elevated fire sources away from walls or obstructions. The continuous line represents the correlation and the dashed lines represent a 10% tolerance. As can be seen, an excellent fitting was found with Equation 6.18.

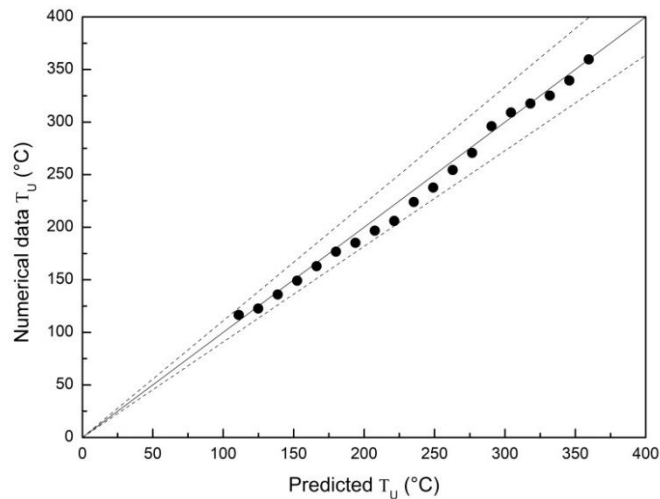


Figure 6.28 - Comparison between predicted upper layer temperature and numerical data for elevated fire sources away from walls.

For elevated fire sources ($z > 0$) near a wall or obstruction, Equation 6.19 is recommended:

$$\frac{\Delta T}{T_{\infty}} = 1.26 \left(\frac{\dot{Q}}{\sqrt{g} C_p \rho_{\infty} T_{\infty} A_0 \sqrt{H_0}} \right)^{0.79} \cdot \left(\frac{h_k A_w}{\sqrt{g} C_p \rho_{\infty} A_0 \sqrt{H_0}} \right)^{-0.47} + 0.83 \cdot \left(\frac{z}{H} \right) - 0.08 \quad (6.19)$$

Figure 6.29 presents the comparison between the predicted values of the upper layer temperature applying Equation 6.19 and the numerical data for elevated fire sources along walls. The continuous line represents the correlation and the dashed lines represent a 10% tolerance. As can be seen, a good fitting was found with Equation 6.19.

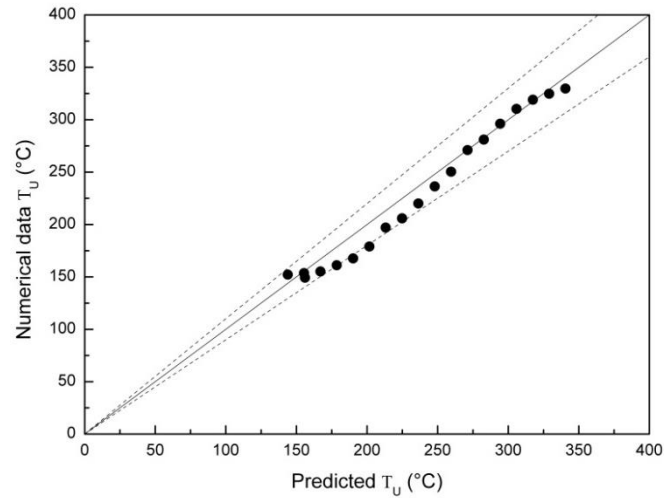


Figure 6.29 - Comparison between predicted upper layer temperature and numerical data for elevated fire sources near a wall.

For elevated fire sources ($z > 0$) near a corner, Equation 6.20 is here recommended:

$$\frac{\Delta T}{T_{\infty}} = 1.26 \left(\frac{\dot{Q}}{\sqrt{g} C_p \rho_{\infty} T_{\infty} A_0 \sqrt{H_0}} \right)^{0.76} \cdot \left(\frac{h_k A_w}{\sqrt{g} C_p \rho_{\infty} A_0 \sqrt{H_0}} \right)^{-0.48} + 0.47 \cdot \left(\frac{z}{H} \right) + 0.02 \quad (6.20)$$

Figure 6.30, presents the comparison between the predicted values of the upper layer temperature applying Equation 6.20 and the numerical data for elevated fire sources near corners. The continuous line represents the correlation and the dashed lines represent a 10% tolerance. As can be seen, an excellent fitting was found.

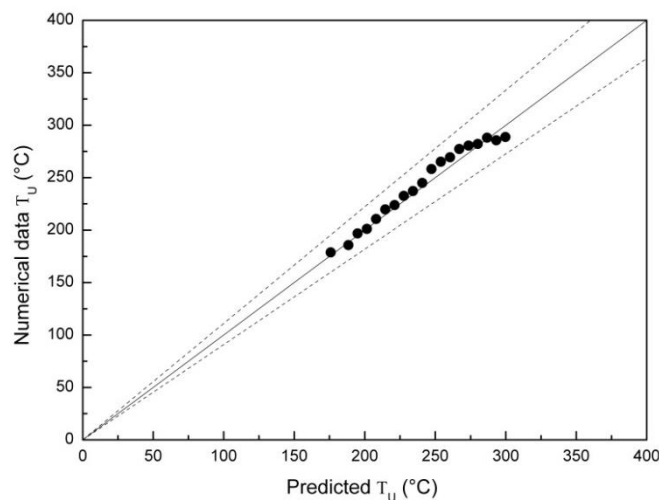


Figure 6.30 - Comparison between predicted upper layer temperature and numerical data for elevated fire sources near a corner.

6.8 Comparison Between Experimental Data and Correlation Predictions

To ensure the quality and applicability of the obtained correlations, the predictions obtained through each correlation were compared to different sets of experimental data, to represent several fire scenarios.

Table 6.4 describe the characteristics of each data set employed in the comparisons, for more information the references must be consulted.

Table 6.4 - Experimental data sets compared to correlation results

Experimental Data Set	Multi-room	Fire room size (W x L x H) [m]	Openings (Wo x Ho) [m]	HRR	Fire location
Hamins et al. (2006) ¹	No	7.04 × 21.7 × 3.82	Door (2.0 × 2.0)	1 MW	Center at ground
Johansson et al. (2015)	Yes	Conf. 1 - 1.2 × 1.2 × 0.8 Conf. 2 - 0.6 × 0.9 × 0.6	Door (0.2 × 0.5) Door (0.3 × 0.5)	10 kW 20 kW	Center at ground
Quintiere et al. (1984)	No	2.8 × 2.8 × 2.13	Door (0.23 × 1.83) Door (0.49 × 1.83) Door (0.74 × 1.83) Door (0.99 × 1.83) Window (0.74 × 1.37) Window (0.74 × 0.91) Window (0.74 × 0.46)	From 30 to 120 kW	Wall at ground
Dembsey et al. (1995)	No	2.5 × 3.7 × 2.5	Door (0.76 × 2.0)	From 330 to 980 kW	Center elevated 0.61 m Wall elevated 0.61 m
Li and Hertzberg (2015)	No	2.4 × 2.4 × 3.6	Door (0.8 × 2.0)	100 kW 300 kW	Center elevated 0.3 m Corner elevated 0.3 m
McCaffrey and Rockett (1977)	No	3.0 × 3.0 × 2.3	Door (0.73 × 1.93)	62 kW 140 kW 340 kW 459 kW	Center elevated 0.3 m Corner elevated 0.3 m Wall elevated 0.3 m
Mowrer and Williamson (1987)	No	2.44 × 3.66 × 2.44	Door (0.76 × 2.03)	40 kW 80 kW 160 kW	Center elevated 0.3 m Corner elevated 0.3 m Wall elevated 0.3 m
Steckler's experiment	No	2.8 × 2.8 × 2.13	See Figure 5.2	31.6 kW 62.9 kW 105.3 kW 158 kW	Center at ground Corner at ground Wall at ground Center elevated 0.3 m Corner elevated 0.3 m Wall elevated 0.3 m

6.8.1 Comparison of the Results

Figure 6.31 shows the comparison of the predicted upper layer temperatures for fire away from walls at the ground level obtained through Equation 6.13. The continuous line

represents the correlation, the dashed lines represent a 10% tolerance and the dotted lines a 20% tolerance, this is also valid for Figures 6.31-6.36.

As can be observed an excellent agreement was obtained for experimental data from Hamins et al., 2006, and Steckler's experiments. A good agreement was also found to Johansson et al., 2015, however the experimental results were found to be a bit higher than those predicted. This may be explained by the fact that this data results were obtained from a multi-room experiment, where the fire room opening was connected to another room instead of being connected to the exterior. This usually reduces the flow of air into and out the room, which in turns, increases the upper layer temperature.

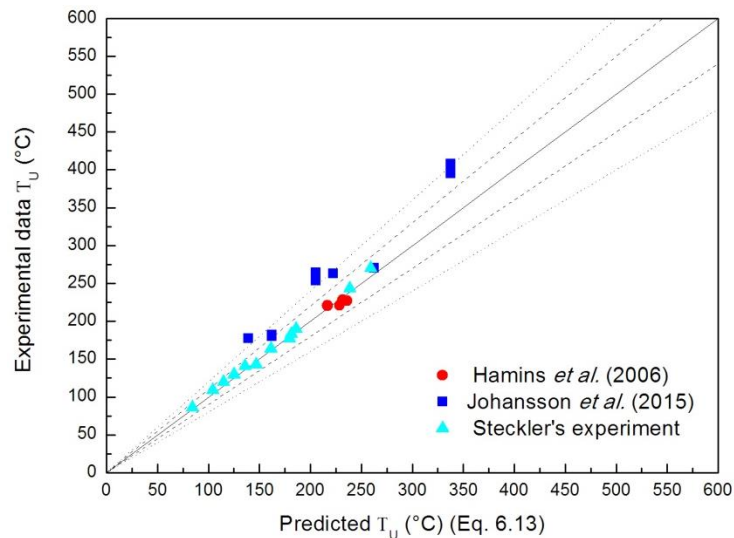


Figure 6.31 - Comparison between upper layer temperature for fire away from walls at the ground level predicted by Equation 6.13 and experimental data

Figure 6.32 shows the comparison of the predicted upper layer temperatures for fire along walls or near obstructions at the ground level obtained through Equation 6.14.

As can be observed an excellent agreement was obtained for experimental data from Quintiere et al., 1984, and Steckler's experiments. Most of the results have differences smaller than 10%. The highest differences were found for very wide line fire source, which may be expected, once the correlation was designed with data from circular burners.

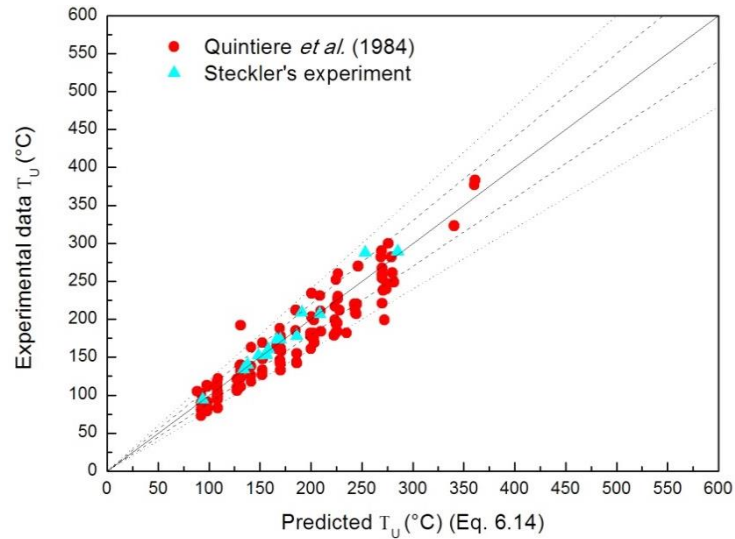


Figure 6.32 - Comparison between upper layer temperature for fire along walls or near obstructions at the ground level predicted by Equation 6.14 and experimental data

Figure 6.33 show the comparison of the predicted upper layer temperatures for fire near corners at the ground level obtained through Equation 6.15.

As can be observed an excellent agreement was obtained for experimental data from Steckler's experiment, being all differences less than 10%.

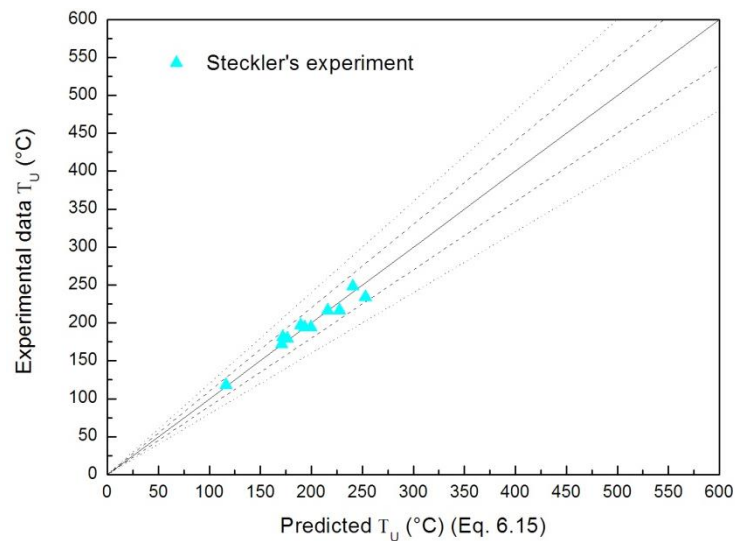


Figure 6.33 - Comparison between upper layer temperature for fire near corners at the ground level predicted by Equation 6.15 and experimental data

Figure 6.34 show the comparison of the predicted upper layer temperatures for fires away from walls or obstructions and above the ground level ($z > 0$), obtained through Equation 6.18

As can be observed, even with a great variety of fire scenarios, an excellent agreement was obtained for all experimental data, being all differences close to 10% or less.

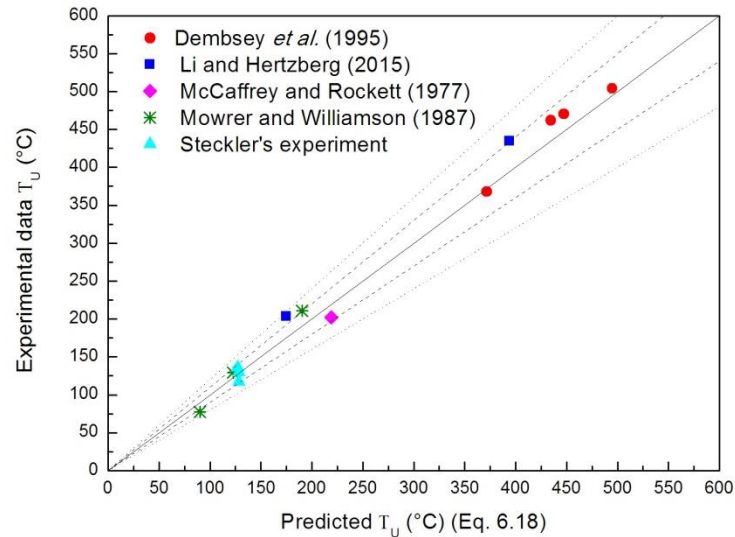


Figure 6.34 - Comparison between upper layer temperature for fires away from walls or obstructions and above the ground level ($z > 0$) predicted by Equation 6.18 and experimental data

Figure 6.35 shows the comparison of the predicted upper layer temperatures for fires along walls or obstructions and above the ground level ($z > 0$), obtained through Equation 6.19.

As can be observed a very good agreement was obtained for experimental data from McCaffrey and Rockett, 1977, Dembsey *et al.*, 1995, and Steckler's experiments. The data from Mowrer and Williamson, 1987, again shown a variation of the order of 20%, which can be result of the experiment uncertainty or of the lack of information about the ambient temperature during experiments and precise wall and linen material properties to apply in the correlation.

Figure 6.36 shows the comparison of the predicted upper layer temperatures for fires near corners and above the ground level ($z > 0$), obtained through Equation 6.20.

As can be observed a very good agreement was obtained for experimental data from McCaffrey and Rockett, 1977, Li and Hertzberg, 2015, and Steckler's experiments. The data from Mowrer and Williamson, 1987, showed a slight higher variation, but still of the order of 20%, which is still a very reasonable agreement, considering that experimental data always present some uncertainty.

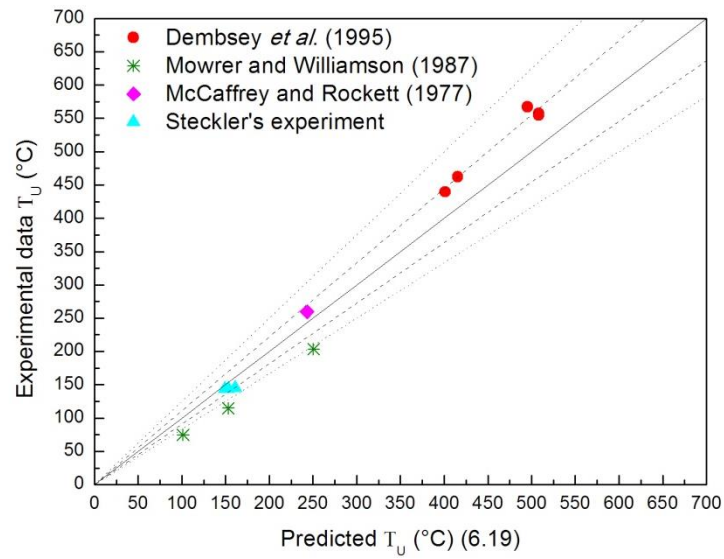


Figure 6.35 - Comparison between upper layer temperature for fires along walls or obstructions and above the ground level ($z > 0$) predicted by Equation 6.19 and experimental data

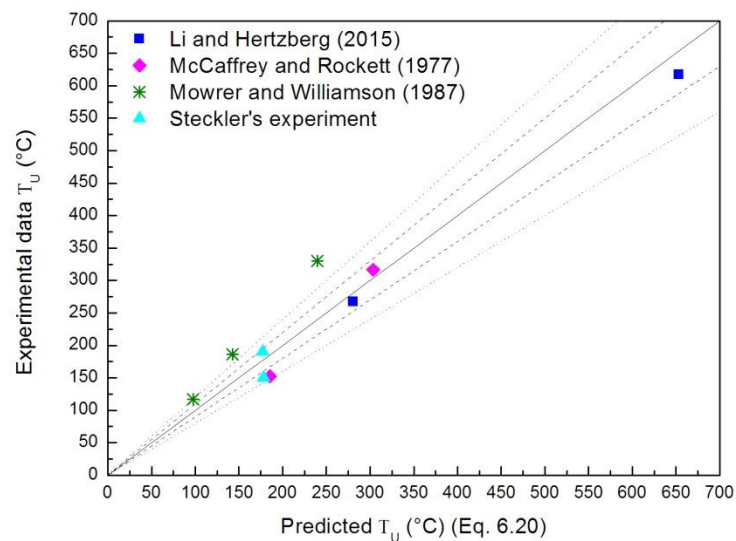


Figure 6.36 - Comparison between upper layer temperature for fires near corners and above the ground level ($z > 0$) predicted by Equation 6.20 and experimental data

Although the numerical results applied to develop the correlations presented small heat release rates, which would represent the maximum heat release rate of a small pool fire (31.6 and 62.9 kW) or small wood furniture (105.3 and 158 kW) (eg. a wood framed chair with Polyurethane foam and cover), the comparison to other sets of experiments showed that these correlations stand for higher heat release rates.

7 CONCLUSIONS

This work studied the influence of the fire source position (transversal, longitudinal and vertical positions) on the upper layer temperature of a pre-flashover compartment fire. Based on the findings six improved correlations have been designed to predict the HGL temperature considering the fire source position.

Nowadays the correlations designed to determine the upper layer temperature in pre-flashover compartment fire do not take into account the fire source location. For example, the well-established correlation MQH concerns only centered fire sources at the floor level. Although, Mowrer and Williamson, 1987, concerned by this limitation, developed modification factors to adapt the MQH correlation to wall and corner fire positions at the ground level with a reasonable agreement.

This study confirmed that the HGL temperature does not depend on the fire source position when the fire occurs away from walls or obstructions (i.e. pieces of furniture), and that the air entrainment reduction is the responsible for the augmentation on those temperatures when the fire occurs at corners or walls (at the ground level). Ground fires near corners presented the highest temperatures, followed by fires near wall and the lowest temperatures were observed for fire sources away from walls.

This work also showed a great influence of the fire source elevation on the HGL temperature, temperature profile and interface layer height. An increase in the upper layer temperature mostly on the range of 10-20 °C was observed between subsequent vertical levels (0.1 m), while when comparing the HGL temperature for the fire source at the floor level ($z = 0$ m) and at the highest level ($z = 1.8$ m) the difference in T_U was of more than 100 °C in all cases, reaching 242 °C for the fire in the center of the room. It was also observed that fires away from obstructions or walls suffered more influence from the elevation of the fire source, followed by fires near wall and the lowest influence was presented by fires near corners. It was noted that for fires occurring near the ceiling (above 50-55% the room high) the behaviour was the opposite than for fires on the floor, presenting the highest temperatures for fires at the center and the lowest for fires near corners.

A wall and corner vicinity analysis was also conducted, and it was concluded that the fire stops to behave as a wall or corner fire when the flame stops to interact with the walls or obstructions. This interaction may occur even when the fire pool is not tangent to the wall, once the air flux into the room deflects the flame towards the walls. It was observed that, for

the studied fire scenario, the fire stopped to be influenced by the wall when the pool fire rim was placed in a distance of 15-25% the length of the room from the walls (0.45-0.70 m).

Based on the previous findings six improved correlations were designed to assess the upper layer temperature for pre-flashover compartment fires taken into account the fire source position. Three for fires at the ground level (away from walls, near walls and near corners) and another three for fires above the ground level.

The correlations were developed based on numerical data generated by the CFD code called FDS and a good agreement between the predicted upper layer temperatures and the numerical data have been found.

The predictions of the designed correlations were also compared to experimental data from different sets of experiments showing a good agreement. So, the designed correlations can be considered as validated for pre-flashover compartment fires and are capable to predict the upper layer temperature considering the fire source location. This is an important achievement once it was observed that fires near corner or at higher levels produce higher upper layer temperatures than those at the ground and away from walls, which are the ones predicted by the conventional correlations.

7.1 Future Works

Some suggestions for future works are:

1. Conduct a more extensive study on the wall vicinity is suggested to identify how the shape, size and power of the fire source, the ventilation factor and the room geometry can affect these results;
2. Produce a similar study applied to post-flashover compartment fires;
3. Develop similar correlation to be applied to adjacent rooms in multi-room compartment fires;

REFERENCES

Alpert, R. L. Turbulent Ceiling-Jet Induced by Large-Scale Fires. **Combustion Science and Technology**, vol. 11(5–6), p. 197–213, 1975.

Azhakesan, M. A., Shields, T. J., Silcock, G. W. H., and Quintiere, J. G. An interrogation of the MQH correlation to describe centre and near corner pool fires. **Fire Safety Science**, p. 371–382, 2003.

Cooper, L. Y. Compartment Fire-Generated Environment and Smoke Filling. In **SFPE Handbook of Fire Protection Engineering** (Third Edit). Quincy, Massachuse: National Fire Protection Association, 2002.

De Ris, J. Fire radiation—A review. **Symposium (International) on Combustion**, vol. 17(1), p. 1003–1016, 1979.

Deardorff, J. W. Stratocumulus-capped mixed layers derived from a three-dimensional model. **Boundary-Layer Meteorology**, vol. 18(4), p. 495–527, 1980.

Delichatsios, M. A., Lee, Y. P., and Tofilo, P. A new correlation for gas temperature inside a burning enclosure. **Fire Safety Journal**, vol. 44(8), p. 1003–1009, 2009

Dembsey, N. A., Pagni, P. J., and Williamson, R. B. Compartment fire experiments: Comparison with models. **Fire Safety Journal**, vol.25(3), p. 187–227, 1995.

Drysdale, D. **An Introduction to Fire Dynamics**. Chichester, UK: John Wiley and Sons, Ltd, 2011.

Dusso, A., Grimaz, S., and Salzano, E. Quick assessment of the hot gas layer temperature and potential fire spread between combustible items in a confined space. **Chemical Engineering Transactions**, vol. 53(2012), p. 37–42, 2016.

Gaitonde, U. **Quality Criteria for Large Eddy Simulation**. University of Manchester, 2008.

Gao, Z. H., Ji, J., Fan, C. G., Sun, J. H., and Zhu, J. P. Influence of sidewall restriction on the maximum ceiling gas temperature of buoyancy-driven thermal flow. **Energy and Buildings**, vol. 84, p. 13–20, 2014.

Gao, Z. H., Liu, Z. X., Ji, J., Fan, C. G., Li, L. J., and Sun, J. H. Experimental study of tunnel sidewall effect on flame characteristics and air entrainment factor of methanol pool fires. **Applied Thermal Engineering**, vol. 102, p. 1314–1319, 2016.

Gross, D., and Robertson, A. F. Experimental fires in enclosures. **Symposium (International) on Combustion**, vol. 10(1), p. 931–942, 1965.

Hamins, A., Maranghides, A., Johnsson, R., Donnelly, M., Yang, J., Mulholland, G.

and Anleitner, R. L. **Report of Experimental Results for the International Fire Model Benchmarking and Validation exercise # 3**. NIST Special Publication, 1013(June), 2006.

Hansell, G. O. **Heat and mass transfer processes acting smoke control in atrium buildings**. South Bank University, London, 1993.

Hasemi, Y., and Tokunaga, T. Some Experimental Aspects of Turbulent Diffusion Flames and Buoyant Plumes from Fire Sources Against a Wall and in a Corner of Walls. **Combustion Science and Technology**, vol. 40(1–4), p. 1–18, 1984

Heskestad, G. Fire Plumes, Flame Height, and Air Entrainment. In **SFPE Handbook of Fire Protection Engineering** (Third Edit). Quincy, Massachuse: National Fire Protection Association, 2002.

Heskestad, G., and Delichatsios, M. A. The initial convective flow in fire. **Symposium (International) on Combustion**, vol. 17(1), p 1113–1123, 1979.

Heskestad, G., and Delichatsios, M. A. Short Communication - Update : The Initial Convective Flow in Fire, **Fire Safety Journal**. vol. 15, p. 471–475, 1989.

Hottel, H. C., and Hawthorne, W. R. In **3rd Symposium (International) on Combustion**, p. 255–266. Baltimore, MD: Williams and Wilkins, 1949.

Janssens, M., and Tran, H. C. Data Reduction of Room Tests for Zone Model Validation. **Journal of Fire Sciences**, vol. 10(6), p. 528–555, 1992.

Ji, J., Fu, Y., Li, K., Sun, J., Fan, C., and Shi, W. Experimental study on behavior of sidewall fires at varying height in a corridor-like structure. **Proceedings of the Combustion Institute**, vol. 35(3), p. 2639–2646, 2015.

Johansson, N. The pre-flashover compartment fire and fire safety engineering – a review of hand-calculation methods, In **Proceedings 11th Conference on Performance-based Codes and Fire Safety Design Methods**. p. 84-95, 2016

Johansson, N., Svensson, S., and Van Hees, P. An evaluation of two methods to predict temperatures in multi-room compartment fires. **Fire Safety Journal**, vol. 77, p. 46–58, 2015.

Karlsson, B., and Quintiere, J. G. **Enclosure fire dynamics**. Boca Raton, Florida: CRC Press LLC, 2000.

Kawagoe, K. **Fire Behavior in Rooms - Report 27**. Tokyo, Japan, 1958.

Lee, S. L., and Emmons, H. W. A study of natural convection above a line fire. **Journal of Fluid Mechanics**, vol. 11(03), 1961.

Li, Y. Z., and Hertzberg, T. Scaling of internal wall temperatures in enclosure fires. **Journal of Fire Sciences**, vol. 33(2), p. 113–141, 2015.

Ludwig, C. B., Malkmus, W., Reardon, J. E., and Thomson, J. A. L. **Handbook of Infrared Radiation From Combustion Gases**, 1973.

Matsuyama, K., Fujita, T., Kaneko, H., Ohmiya, Y., Tanaka, T., and Wakamatsu, T. Simple predictive method for room fire behaviour. **Fire Science and Technology**, vol. 18(1), p. 23–32, 1998.

McCaffrey, B. J., Quintiere, J. G., and Harkleroad, M. F. Estimating room temperatures and the likelihood of flashover using fire test data correlations. **Fire Technology**, vol. 17(2), p. 98–119, 1981.

McCaffrey, B. J., and Rockett, J. A. Static pressure measurements of enclosure fires. **Journal of Research of the National Bureau of Standards**, vol. 82(2), p. 107–117, 1977.

McDermott, R. J., Forney, G. P., McGrattan, K., and Mell, W. E. Fire Dynamics Simulator version 6: complex geometry, embedded meshes, and quality assessment. In **V European Conference on Computational Fluid Dynamics ECCOMAS CFD**, p. 14–17. Lisbon, Portugal, 2010.

McGrattan, K., Hostikka, S., McDermott, R., Floyd, J., Vanella, M., Weinschenk, C., and Overholt, K. **Fire Dynamics Simulator Technical Reference Guide Volume 1: Mathematical Model** (Sixth Edit). NIST Special Publication. Gaithersburg, MD, 2017a

McGrattan, K., Hostikka, S., McDermott, R., Floyd, J., Vanella, M., Weinschenk, C., and Overholt, K. **Fire Dynamics Simulator User's Guide** (Sixth Edit). NIST Special Publication. Gaithersburg, MD, 2017b.

McGrattan, K., Hostikka, S., McDermott, R., Floyd, J., Vanella, M., Weinschenk, C., and Overholt, K. **Fire Dynamics Simulator Technical Reference Guide Volume 3: Validation** (Sixth Edit). NIST Special Publication. Gaithersburg, MD, 2017c.

Morton, B. R., Taylor, G., and Turner, J. S. Turbulent Gravitational Convection from Maintained and Instantaneous Sources. **Proceedings of the Royal Society A: Mathematical, Physical and Engineering Sciences**, vol. 234(1196), p. 1–23, 1956.

Mowrer, F. W., and Williamson, R. B. Estimating room temperatures from fires along walls and in corners. **Fire Technology**, vol. 23(2), p. 133–145, 1987.

Petersen, R. E., and Emmons, H. W. Stability of Laminar Flames. **Physics of Fluids**, vol. 4(4), p. 456, 1961.

Pope, S. B. **Turbulent Flows**. Cambridge University Press, 2000.

Pope, S. B. Ten questions concerning the large-eddy simulation of turbulent flows. **New Journal of Physics**, vol. 6, 2004.

Poreh, M., and Garrad, G. Study of wall and corner fire plumes. **Fire Safety Journal**,

vol. 34(1), p. 81–98, 2000

Prahl, J., and Emmons, H. W. Fire induced flow through an opening. **Combustion and Flame**, vol. 25(C), p. 369–385, 1975.

Quintiere, J. G. Compartment Fire Modeling. In **SFPE Handbook of Fire Protection Engineering** (3rd ed.). Quincy, Massachuse: National Fire Protection Association, 2002

Quintiere, J. G. **Fundamentals of Fire Phenomena. Fundamentals of Fire Phenomena**. Chichester, UK: John Wiley and Sons Ltd, 2006.

Quintiere, J. G., Steckler, K., and Corley, D. An assessment of fire induced flows in compartments. **Fire Science and Technology**, 1984.

Quintiere, J. G., and Wang, L. A general formula for the prediction of vent flows. **Fire Safety Journal**, vol. 44(5), p. 789–792, 2009.

Rehm, R. G., and Baum, H. R. The equations of motion for thermally driven, buoyant flows. **Journal of Research of the National Bureau of Standards**, vol. 83(3), p. 297, 1978.

Rockett, J. A. Fire Induced Gas Flow in an Enclosure. **Combustion Science and Technology**, vol. 12(4–6), p. 165–175, 1976.

Ryder, N. L., Sutula, J. A., Schemel, C. F., Hamer, A. J., and Brunt, V. Van. Consequence modeling using the fire dynamics simulator. **Journal of Hazardous Materials**, vol. 115(1–3 SPEC. ISS.), p. 149–154, 2004.

Steckler, K. D., Baum, H. R., and Quintiere, J. G. Fire induced flows through room openings-flow coefficients. **Symposium (International) on Combustion**, vol. 20(1), p. 1591–1600, 1984a.

Steckler, K. D., Baum, H. R., and Quintiere, J. G. **Fire Induced Flows Through Room Openings - Flow Coefficients**. NBS Publications, Washington, DC, 1984b.

Steckler, K. D., Quintiere, J. G., and Rinkinen, W. J. **A Flow Induced by Fire in a Compartment**. NBS Publications, Washington, DC, 1982a.

Steckler, K. D., Quintiere, J. G., and Rinkinen, W. J. Flow induced by fire in a compartment. In **Nineteenth Symposium (International) on Combustion/The Combustion Institute**. p. 913–920, 1982b

Stroup, D., and Lindeman, A. **Verification and Validation of Selected Fire Models for Nuclear Power Plant Applications**. NUREG-1824, supplement 1. Washington, DC, 2013

Takahashi, W., Tanaka, H., Sugawa, O., and Ohtake, M. Flame and Plume Behavior in and near a Corner of Walls. **Fire Safety Science—Proceedings of the Fifth International Symposium**, p. 261–271, 1997.

Thomas, P. SFPE classic paper review: Fire behavior in rooms by Kunio Kawagoe. **Journal of Fire Protection Engineering**, vol. 14(1), p. 5–8, 2004.

Thomas, P. H., Bullen, M. L., Quintiere, J. G., and McCaffrey, B. J. Flashover and instabilities in fire behavior. **Combustion and Flame**, vol. 38, p. 159–171, 1980.

Tlili, O., Mhiri, H., and Bournot, P. Airflow induced by a room fire: Effect of roof shape and source location. **International Journal of Thermal Sciences**, vol. 90, p. 135–149, 2015.

Tlili, O., Mhiri, H., and Bournot, P. Empirical correlation derived by CFD simulation on heat source location and ventilation flow rate in a fire room. **Energy and Buildings**, vol. 122, p. 80–88, 2016.

Tran, H. C., and Janssens, M. L. Wall and Corner Fire Tests on selected Wood Products. **Journal of Fire Sciences**, vol. 9(2), p. 106–124, 1991.

Tran, H. C., and Janssens, M. L. Modeling the Burner Source Used in the ASTM Room Fire Test. **Journal of Fire Protection Engineering**, vol. 5(2), p. 53–66, 1993.

Walton, W. D., and Thomas, P. H. Estimating Temperatures in Compartment Fires. In **SFPE Handbook of Fire Protection Engineering** (3rd ed.). Quincy, Massachuse: National Fire Protection Association, 2002.

Wang, L., Lim, J., and Quintiere, J. G. On the prediction of fire-induced vent flows using FDS. **Journal of Fire Sciences**, vol. 30(2), p. 110–121, 2012.

Wang, L., and Quintiere, J. G. An analysis of compartment fire doorway flows. **Fire Safety Journal**, vol. 44(5), p. 718–731, 2009.

Węgrzyński, W., and Konecki, M. Influence of the fire location and the size of a compartment on the heat and smoke flow out of the compartment. **AIP Conference Proceedings 1922**, 2018

Xiaojun, C., Lizhong, Y., Zhihua, D., and Weicheng, F. A multi-layer zone model for predicting fire behavior in a fire room. **Fire Safety Journal**, vol. 40(3), p. 267–281, 2005.

Zeinali, D., Verstockt, S., Beji, T., Maragkos, G., Degroote, J., and Merci, B. Experimental study of corner fires—Part I: Inert panel tests. **Combustion and Flame**, vol. 189, p. 472–490, 2018.

Zhang, J., Lu, S., Li, Q., Li, C., Yuan, M., and Yuen, R. Experimental study on elevated fires in a ceiling vented compartment. **Journal of Thermal Science**, vol. 22(4), p. 377–382, 2013.

Zhang, J., Lu, S., Li, Q., Yuen, R. K. K., Chen, B., Yuan, M., and Li, C. Smoke filling in closed compartments with elevated fire sources. **Fire Safety Journal**, vol. 54, p. 14–23,

2012.

Zhiyin, Y. Large-eddy simulation: Past, present and the future. **Chinese Journal of Aeronautics**, vol. 28(1), p. 11–24, 2015.

Zukoski, E. E. Development of a stratified ceiling layer in the early stages of a closed room fire. **Fire and Materials**, vol. 2(2), p. 54–62, 1978.

Zukoski, E. E., Kubota, T., and Cetegen, B. Entrainment in fire plumes. **Fire Safety Journal**, vol. 3(3), p. 107–121, 1981